DESIGN AND OPTIMIZATION OF A DURABLE GOLD-BASED MICROELECTRODE FOR DOPAMINE DETECTION

A THESIS SUBMITTED TO

THE GRADUATE SCHOOL OF

ENGINEERING AND NATURAL SCIENCES

OF ISTANBUL MEDIPOL UNIVERSITY

IN PARTIAL FULFILLMENT OF THE REQUIREMENTS FOR

THE DEGREE OF

MASTER OF SCIENCE

IN

BIOMEDICAL ENGINEERING AND BIOINFORMATICS

By

Bashir Bwogi

August, 2021

DESIGN AND OPTIMIZATION OF A DURABLE GOLD-BASED MICROELECTRODE FOR DOPAMINE DETECTION

By Bashir Bwogi

23 August 2021

We certify that we have read this dissertation and that in our opinion it is fully adequate, in scope and in quality, as a dissertation for the degree of Master of Science.

_____

Assoc. Prof. Dr. Yasemin Yüksel Durmaz (Advisor)

_____

Assist. Prof. Dr. Mehmet Kocatürk (Co-Advisor)

_____

Assist. Prof. Dr. Hasan Kurt

_____

Assist. Prof. Dr. Ömer Aydın

Approved by the Graduate School of Engineering and Natural Sciences:

_____

Assoc. Prof. Dr. Yasemin Yüksel Durmaz

Director of the Graduate School of Engineering and Natural Sciences

I hereby declare that all information in this document has been obtained and presented in accordance with the academic rules and ethical conduct. I also declare that, as required by these rules and conduct, I have fully cited and referenced all material and results that are not original to this work.

Signature :

Name, Surname: BASHIR BWOGI

ACKNOWLEDGEMENT

This work was made easier by the relentless advice and unwavering support from my advisor Assoc. Prof. Dr. Yasemin Yüksel Durmaz throughout my entire graduate studies and designing of the project. I would also like to thank Assist. Prof. Dr. Mehmet Kocatürk for his work in helping me with various characterization studies, it would not have been to this level of success without his effort. I want to send a special appreciation to Assist. Prof. Dr. Ömer Aydın for his fundamental role of seconding me to take the position on this project under my supervisor, it was an honor to get his confidence.

In addition, a special thanks goes to Mr. Erhan Demirel who helped me with the orientation phase of the laboratory and kickstarted my speed in using specific laboratory devices. Also, I thank Ms. Shazia Iqbal, Mr. Waleed Mustafa, and Mr. Ahsan Ayyaz for the continued support given during the different laboratory experiments and data analysis, it was a pleasure working alongside them.

Extended gratitude goes to my parents and family who have supported me with love and motivation throughout my study period.

This work was supported by the Scientific and Technological Research Council of Turkey (TUBITAK) Grant #118S072.

Bashir Bwogi

August, 2021

CONTENTS

Page

ACKNOWLEDGEMENT ..... **iv**
CONTENTS ..... **v**
LIST OF FIGURES ..... **vii**
LIST OF TABLES ..... **ix**
LIST OF SYMBOLS ..... **x**
ABBREVIATIONS ..... **xi**
ÖZET ..... **xiii**
ABSTRACT ..... **xv**
1. INTRODUCTION **1**
2. THEORETICAL PART **6**
2.1. Neurotransmission Pathways of Dopamine 6
2.2. Treatment of Parkinson's Disease 9
2.3. Dopamine Detection Techniques 10
2.3.1. Micro-dialysis 11
2.3.2. Positron emission tomography (PET) 12
2.3.3. Functional magnetic resonance imaging (fMRI) 12
2.3.4. Fast-scan cyclic voltammetry (FSCV) 14
2.4. Different Systems and Microelectrodes for Dopamine Detection 16
2.4.1. Carbon-based electrodes 16
2.4.2. Metal and metal oxide nanoparticles 17
2.4.3. Metal organic frameworks (MOFs) 19
2.4.4. Gold electrodes 20
2.4.5. Inorganic modifiers 20
2.4.6. Ionic liquids 21
2.4.7. Polymeric modifiers 22
3. EXPERIMENTAL PART **24**
3.1. Materials 24
3.2. Software 24
3.3. Characterization 25
3.4. Electrochemical Graphene Deposition on Copper Electrode (Cu-GO) 25
3.5. Electrochemical Graphene Deposition on Gold Electrode (Au-GO) 27
3.6. Sulfonation of poly(ether ether ketone) (PEEK) - SPEEK 27
3.7. Electrochemical SPEEK Deposition on Graphene-Coated Gold Electrode (Au-GO-SPEEK) 27
3.8. Dip Coating of SPEEK on Graphene-Coated Gold Electrode (Au-GO-SPEEK) 28
3.9. Electrochemical Pyrrole Deposition on Graphene and SPEEK Coated Gold Electrode (Au-GO-SPEEK-ppy) 28
3.9.1. Measurements 28
4. RESULTS AND DISCUSSION **31**
4.1. Electrochemical Graphene Deposition on Gold Electrode (Au-GO) 38
4.1.1. Effect of supporting electrolytes 43
4.1.2. Effect of GO concentration 48
4.1.3. Effect of deposition time 51
4.2. Sulfonation of Poly(ether ether ketone) (PEEK) - SPEEK 54
4.3. Electrochemical SPEEK Deposition on Graphene-Coated Gold Electrode (Au-GO-SPEEK) 58

4.4. Dip Coating of SPEEK on Graphene-Coated Gold Electrode (Au-GO-SPEEK) 62
4.5. Electrochemical Pyrrole Deposition on Graphene and SPEEK Coated Gold Electrode (Au-GO-SPEEK-ppy) 65
5. CONCLUSIONS AND FUTURE WORK 79
BIBLIOGRAPHY 83
APPENDIX A 95
APPENDIX B 100
CURRICULUM VITAE 101

LIST OF FIGURES

Figure 1.1: Summary of coating procedures for the biocompatible materials onto the gold surface……..…….…….....4
Figure 2.1: The process of neurotransmission across the neural network…….....6
Figure 2.2: Dopaminergic pathways…..…….....…….....8
Figure 2.3: A breakdown of the DBS system…..…….……...….10
Figure 2.4: Micro-dialysis procedure…..……..……...……...11
Figure 2.5: PET image of a normal person (**a)** and PD patient (**b)**……..…….....12
Figure 2.6: Use of molecular fMRI for dopamine detection in the ventral striatum ...13
Figure 2.7: Applied waveform during dopamine detection…….…..…..…..….14
Figure 2.8: Redox reaction of dopamine…….……..…..……..…15
Figure 2.9: Simplified system circuit of FSCV…….…….……..……15
Figure 2.10: Conventional carbon-fiber microelectrode…...…….……17
Figure 3.1: Illustration of electrochemical setup for GO deposition……..….26
Figure 3.2: A summary of the fabrication and characterization of the electrode…….29
Figure 4.1: a) Appearance of GO solution and electrodes before application of a DC potential. **b)** Upon application of a constant voltage, the electrically reduced GO sheets collect at the copper anode. **c)** Appearance of rGO coated copper electrode……..….32
Figure 4.2: a) Bare Cu electrode surface **b)** Cu electrode surface appearance obtained as a result of coating with chemically reduced GO, **c)** Cu electrode surface with GO plates collected but not reduced chemically, **d)** Cu electrode surface view where GO sheets after electrocoating are then reduced with $NaBH_4$, **e)** Cu_2O cubic crystals formed by Cu^{2+} ions leaving the electrode surface accumulated on the electrode surface again……...….33
Figure 4.3: Graphical representation of obtained results after stabilization (**a)** and **b)**) and after addition of 10 μM dopamine (**c)** and **d)**)…….……..…...36
Figure 4.4: Detection of dopamine at different concentrations using bare gold electrode……...……...39
Figure 4.5: Uncoated gold wire and graphene coated electrode. **a)** 76.2 µm thick, 3 meters long gold wire. **b)** Graphene coated gold wire…….…….40
Figure 4.6: SEM images (0.5 mg/mL, 1 hour, in distilled water) of GO coated Au electrode at different voltage values **a)** Bare Au, **b)** 2 V, **c)** 5 V, **d)** 10 V, and **e)** 30 V. EDX results of surface atomic composition (bottom right corner)……..…...….41
Figure 4.7: DLS results of GO in different supporting electrolytes of different pH....44
Figure 4.8: SEM images showing the effect of supporting electrolyte. **a)** Bare Au, **b)** Only distilled water, **c)** 0.5 M NaCl neutralized by 0.5 M KOH, and **d)** 0.067 M PBS made basic with 0.5 M KOH ..……..…….……..46
Figure 4.9: FSCV analysis using 10 μM dopamine solution showing the effect of supporting electrolyte. Only distilled water (green), 0.5 M NaCl neutralized by 0.5 M KOH (blue), and 0.067 M PBS made basic with 0.5M KOH (red) coated for 15 min……..47
Figure 4.10: Different GO concentrations. SEM images of Au-GO coated electrode at **a)** Bare Au, **b)** 0.02, **c)** 0.1, and **d)** 0.3 mg/mL GO concentration (10 V, 15 mins)…49
Figure 4.11: Voltammogram obtained with FSCV in 10 μM dopamine solution for Au electrodes coated for 15 mins at different GO concentration values. Deposition potential of 10 V…….……...……..……..……..50
Figure 4.12: SEM images of Au-GO coated microelectrodes at different coating times. **a)** Bare Au, **b)** 7, **c)** 15, **d)** 30, and **e)** 60 min ……..……..52

Figure 4.13: FSCV voltammogram obtained at different coating times with 10 μM dopamine solution of Coated Au electrodes at 0.1 mg/mL GO concentration (10V deposition potential)…….....……..….53
Figure 4.14: Schematic for the sulfonation of PEEK to form SPEEK ……..……54
Figure 4.15: Solubility of SPEEK in water **a)** 100 kDa and **b)** 10 kDa at 700 rpm 24 h of stirring at 37 ℃……...……..……...55
Figure 4.16: FTIR analysis for PEEK and SPEEK…….…..……...……..56
Figure 4.17: ^{1}H-NMR spectrum of **a)** 100 kDa and **b)** 10 kDa SPEEK……...……57
Figure 4.18: Thermogravimetric Analysis of SPEEK……...…58
Figure 4.19: SEM images of microelectrodes coated with both GO and SPEEK using electrodeposition. **a)** Bare Au, **b)** Au-GO coated consecutively with 10 kDa SPEEK, **c)** Au-GO coated consecutively with 100 kDa SPEEK, **d)** Au coated simultaneously with GO and 10 kDa SPEEK, and **e)** Au coated simultaneously with GO and 100 kDa SPEEK.…….……..60
Figure 4.20: FSCV analysis of the Au microelectrode electrically coated with GO and SPEEK using 10 μM dopamine ……..…...…...……...…...61
Figure 4.21: SEM images of SPEEK dip-coated Au-GO microelectrodes at 25 ℃. **a)** Bare Au, **b)** 10 kDa SPEEK (15 mins), **c)** 10 kDa SPEEK (130 min), **d)** 100 kDa SPEEK (15 min), and **e)** 100 kDa SPEEK (130 min)……...…..……63
Figure 4.22: FSCV study using 10 μM dopamine for Au-GO microelectrodes dip-coated with SPEEK …….…….…..64
Figure 4.23: FSCV study using 10 μM dopamine to compare the optimal SPEEK coating…….65
Figure 4.24: FSCV graph of Au microelectrode coated with py for 30 s. 10 μM dopamine…….66
Figure 4.25: SEM images of the Au microelectrode coated with GO, SPEEK and py to show the effect of ppy on the surface morphology. **a)** Bare Au, **b)** Au-ppy, **c)** Au-GO-ppy, **d)** Au-GO-SPEEK-ppy, and **e)** Au/GO/SPEEK/ppy..…….68
Figure 4.26: FSCV study of Au-GO-SPEEK-ppy consecutively coated microelectrode to analyze the optimal deposition time for the py layer. 10 μM dopamine……. 70
Figure 4.27: FSCV analysis using 1 μM of dopamine to compare the sensitivity of the carbon fiber (C) electrode with bare gold (Au). 50 μm gold disc and a 7 μm diameter by 150 μm length carbon fiber microelectrode…….....……..……...72
Figure 4.28: SEM image of a gold electrode coated with the optimal conditions of the GO, SPEEK and py biomaterial coatings. **a)** Bare Au, **b)** Au-GO, **c)** Au-GO-SPEEK, and **d)** Au-GO-SPEEK-ppy……..……...……...73
Figure 4.29: SEM image showing the durability of the surface coating before and after running the electrode in the FSCV for 2 and 5 h at 10 Hz. Consecutive electrodeposition of GO (30 min) and 100 kDa SPEEK (15 min) (Au-GO-SPEEK) followed by 10 s ppy coating…….…….75
Figure 4.30: SEM image showing the durability of the surface coating before and after running the electrode in the FSCV for 5 h at 50 Hz. Consecutive dip coating of 10kDa SPEEK for 130 minutes on Au-GO (30 min) (Au-GO-SPEEK) followed by 3 s ppy coating...……..……..……..77

LIST OF TABLES

Table 4.1: Different supporting electrolytes to apply in the FSCV as dopamine carrier……...……...35
Table 4.2: Arrangement of electrodes upon change of solution pH and varying supporting electrolytes mixed to make 50 mL solutions……...…...…….....……..43
Table 4.3: Electrical properties of the materials ……..……..……..…67
Table 4.4: Coat thickness after deposition of the biomaterials……..……..…..…74
Table 4.5: EDX results of microelectrodes before the FSCV study, after running the electrode in the FSCV for 2h, and for 5h at 10 Hz……..…76

LIST OF SYMBOLS

$\mathbf{V_0}$: Output voltage
G : System gain
$\mathbf{R_f}$: Feedback resistor
i : Current
$\boldsymbol{D^s}$: Degree of sulfonation
A : Area
(aq) : Aqueous
(g) : Gas
$\mathbb{\Gamma}$: Concentration of adsorbed electrolyte
$\boldsymbol{i_p}$: Peak current
$\boldsymbol{v}$: Scan rate
R : resistance
r : input resistance
Δ : intensity
$\boldsymbol{w}$: coated weight
$\boldsymbol{f}$: efficiency factor
$\boldsymbol{\mu}$: electrophoretic mobility
$\boldsymbol{E}$: deposition potential
$\boldsymbol{C}$: concentration
$\boldsymbol{\rho}$: resistivity
L : length
$\mathbf{D_c}$: Diffusion coefficient

ABBREVIATIONS

CNS : Central Nervous System
ATP : Adenosine Triphosphate
GABA : Gamma Amino Butyric Acid
PD : Parkinson's Disease
DBS : Deep Brain Stimulation
IPG : Implantable Pulse Generator
STN : Subthalamic Nucleus
RF : Resonance Frequency
PET : Positron Emission Topography
FSCV : Fast Scan Cyclic Voltammetry
fMRI : functional Magnetic Resonance Imaging
L-DOPA : Levodopa
hTAAR1 : human Trace Amine-Associated Receptor 1
VTA : Ventral Tegmental Area
NAc : Nucleus Accumbens
PFC : Pre-Frontal Cortex
BBB : Blood-Brain Barrier
Ag/AgCl : Silver/Silver Chloride electrode
CNT : Carbon Nanotube
PEDOT : Poly(3,4-ethylenedioxythiophene)
PEEK : poly(ether ether ketone)
SPEEK : sulfonated poly(ether ether ketone)
SEM : Scanning Electron Microscopy
GO : Graphene Oxide
rGO : reduced Graphene Oxide
erGO : electrically reduced Graphene Oxide
py : pyrrole
ppy : polypyrrole
kDa : kilo Dalton
rpm : rotations per minute
FTIR : Fourier Transform Infra-Red Spectroscopy
EDX : Energy-Dispersive X-ray Spectroscopy
DC : Direct Current
M_w : Molecular Weight
TGA : Thermogravimetric Analysis
^{1}H-NMR : Proton Nuclear Magnetic Resonance
DLS : Dynamic Light Scattering Analysis
DNA : Deoxyribonucleic Acid
DMF : Dimethylformamide
CPs : Carbon Polymers
PCA : Polycinnamic Acid
CPE : Carbon Paste Electrode
GCE : Glassy Carbon Electrode
Au : Gold
NP : Nanoparticle
P_2NO : Poly 2-Napthol Orange
PIGE : Paraffin Wax-Impregnated Graphite Electrode
LOQ : Limit of Quantification
LOD : Limit of Detection

4ABSA : 4-Amino Benzene Sulfonic Acid
GPLE : Graphite Pencil Lead Electrode
LSG : Laser Scribe Graphene
SWCNT : Single-Wall Carbon Nanotube
SPCE : Screen-Printed Carbon Electrodes

DOPAMİN TESPİTİ İÇİN DAYANIKLI ALTIN-TABANLI MİKROELEKTRODUN TASARIMI VE OPTİMİZASYONU

ÖZET

Bashir Bwogi

Biyomedikal Mühendisliği ve Biyoenformatik, Yüksek Lisans

Tez Danışmanı: Doç. Dr. Yasemin Yüksel Durmaz

Eş Danışmanı: Dr. Öğr. Üyesi Mehmet Kocatürk

Ağustos, 2021

Dopamin, motor kontrol ve ödül aracılı öğrenme/bağımlılık konusunda önemli bir rol oynar. Dopamin konsantrasyonunun değiştirilmesi nörolojik hastalıklara, örneğin şizofreni, bağımlılık, ve Parkinson hastalığına yol açar. Günümüzde dopamini tespit etmek için kullanılan mikroelektrotlar zayıf duyarlılığa, düşük zamansal çözünürlüğe ve implantasyondan sonra gliyal hücrelerin büyümesine yol açan daha az biyolojik uyumluluğa sahiptir. Dopamin konsantrasyonunu izlemek ticari olarak bulunan karbon (C) mikroelektrotlara alternatif olarak kolay üretilebilen, yüksek iletkenliğe sahip ve biyouyumlu elektrotlar geliştirilmesi önem taşımaktadır. Bu ihtiyacı gidermek amacıyla, mevcut çalışmada altın bazlı bir elektrot geliştirilmiştir. Pürüzsüz altın yüzeyi, elektro kimyasal olarak grafen oksit (GO) tabakası ile kaplanmıştır. Bu şekilde duyarlılığı arttırılan yüzeyin mekanik mukavemetini ve biyouyumluluğu arttırmak için daldırıp kaplama yöntemi ile sülfonlanmış poli (eter eter keton) (SPEEK) ikinci bir yüzey olarak kaplanmıştır. Poli (eter eter keton) (PEEK) sülfonlanması ayrıca ıslanabilirliği ve iyon transferini arttırmaya yardımcı olmaktadır. Son olarak elektropolimerizasyon yolu ile polipirol tabakası biriktirilerek biyouyumluluğu kronik implantasyona daha uygun hala getirilmesi hedeflenmiştir. Mikroelektrotların yüzey morfolojisi ve yüzey analizi taramalı elektron mikroskobu yardımı ile incelenmiştir. Mikroelektrotların dopamin ölçümüne karşı duyarlılıkları elektriksel duyarlılık hızlı taramalı döngüsel voltametri (FSCV) kullanılarak en etkin kaplamanın belirlenmesi hedeflenmiştir. Elde edilen sonuçlar GO, SPEEK ve polipirol tabakalarının aynı anda karıştırılarak kaplanması yerine tabaka tabaka sırasıyla kaplanmasının daha etkin duyarlılık sağladığı görülmüştür. Üretilen elektrot, voltametrik dalga biçiminde sırasıyla -0,2 V ve +0,6 V iken, GO ve SPEEK tabakaları ile kaplandığında dopamin duyarlılığını dopaminin *in-vivo* tespiti için geleneksel olarak kullanılan karbon fiber mikroelektrotlardan 50 kattan fazla artırırken, polipirol tabakasının eklenmesi ile sadece yaklaşık 2 kat daha fazla artırmıştır. 5 saat süreyle FSCV döngülerine maruz bırakılan elektrotların dayanıklığı yüzey kaplama bileşimi ve morfolojisi incelendiğinde dayanıklılık ve dopamin duyarlılığının bu süreçten etkilenmediği görülmüştür. Oksidasyon potansiyeli uzun süre sağladığında, pirol katyon değişim tabakası oldukça yüksek biyouyumluluk ve yüksek yüzey korozyon direncine sahiptir. Bu sonuç, elektrotun genel yüzey hassasiyetini azaltsa bile gelecekteki kronik implantasyonlarda (> 1 yıl) kullanılabileceğini göstermektedir.

Anahtar sözcükler: Dopamin, voltametri, altın, grafen oksit, SPEEK, polipirol.

DESIGN AND OPTIMIZATION OF A DURABLE GOLD-BASED MICROELECTRODE FOR DOPAMINE DETECTION

ABSTRACT

Bashir Bwogi

MSc in Biomedical Engineering and Bioinformatics

Advisor: Assoc. Prof. Dr. Yasemin Yüksel Durmaz

Co-Advisor: Assist. Prof. Dr. Mehmet Kocatürk

August, 2021

Dopamine plays a vital role in motor control and reward-mediated learning/addiction. Disorders of the dopamine system lead to neurological diseases such as schizophrenia, addiction, depression, and Parkinson's disease. Currently used microelectrodes to detect dopamine have poor sensitivity, low temporal resolution, and less durability, leading to microglial reactivity after implantation. Tracking the concentration of dopamine is vital using a reproducible, highly conductive, and durable option as compared to the conventional carbon (C) fiber electrodes. To address this need, in the present work, a gold-based electrode has been developed. The smooth gold surface is electro-coated with a highly sensitive graphene oxide (GO) layer. In addition, a polymer poly (ether ether ketone) (PEEK) through the sulfonation process have charged groups introduced, to help enhance its wettability and ion transfer. This sulfonated poly (ether ether ketone) (SPEEK), deposited by dip-coating mainly improves the thin electrode's mechanical strength and biocompatibility. The third layer of pyrrole is electrodeposited. Microelectrodes were characterized for electrical sensitivity (using the fast-scan cyclic voltammetry (FSCV)), surface morphology and composition, durability, and the effect of the deposition thickness. Layer-by-layer deposition in the order GO, SPEEK then polypyrrole gave optimal results unlike simultaneous deposition of the mixture. The sensitivity of the electrode depended on the electric conductivity and the morphology of the outer surface. The fabricated electrode improved dopamine sensitivity by over 50 folds when using GO and SPEEK whereas the addition of a polypyrrole layer reduces this to just about 2 folds more than the carbon fiber microelectrodes conventionally used for *in-vivo* detection of dopamine when the holding and peak potentials in the voltammetric waveform are -0.2 V and +0.6 V, respectively. Studies on durability showed that the composition and morphology of the surface coatings were not affected after 5 hours of FSCV runs at 10 Hz whilst maintaining a high degree of sensitivity. The pyrrole cation exchange layer is biocompatible and highly resists surface corrosion when supplied with an oxidizing potential in a long term. This result indicates that the electrode may be utilized in chronic implantations (> 1 year) even if it reduced the overall surface sensitivity.

Keywords: Dopamine, voltammetry, gold, graphene oxide, SPEEK, polypyrrole

CHAPTER 1

1. INTRODUCTION

The desire for this work stems from the continued urgency of highly effective sensing platforms in implantable devices that surpass the need to change them over time due to degradation in surface functionality. As the disease (Parkinson's disease) from which the motivation of the study was got, affects over 1% the elderly above 60 years, complications due to repeated surgeries to replace the microelectrodes of the system to detect dopamine, become more evident. In this work, therefore, is an elaboration of a better solution with comparable efficiency to the existing microelectrodes.

The central nervous system (CNS) comprises of the brain and the spinal cord. The brain is the most sophisticated organ made up of the cerebellum, brainstem, and cerebrum. It can be simply described as the body's central processing unit for all activities. It integrates the information from the sensory organs around the body and coordinates it into responses that can be interpreted by other target organs for actuation. Memory, self-control, language, learning and hormonal-release control are some of the notable functions of the brain. The entire brain tissue is made up of more than 100 billion cells of two varieties namely, the protective glial cells and the information transmitting neuron cells [1]. Nerve impulses incite neurons to release neurotransmitters through the network system. This network forms neural circuits through complex neural pathways that enable brain activity under a process called neurotransmission.

Besides adenosine triphosphate (ATP) and noradrenaline which are co-transmitters, there are various neurotransmitters that include: serotonin, acetylcholine, glutamate, gamma amino butyric acid (GABA), adrenaline, oxytocin, and dopamine. These are known to have many vital physiological functions like blocking some signals, feeling of joy, relaxation, fear, decision making, uterus contractions, building human connections and sleep [2]. The concentrations of these neurotransmitters must be kept in check otherwise

an imbalance can result in dangerous health complications mainly in the behavioral and mental condition. Dopamine, which is secreted from the basal ganglia plays a major role in the coordination of many physiological responses i.e., motivation, addiction, sexual satisfaction, reward-based reactions, and motor control [2], [3]. A progressive degeneration of the regions of the CNS that control release of dopamine leads to neurological diseases e.g., schizophrenia, addiction, depression, and Parkinson's Disease (PD) mainly displayed in the elderly of above 60 years, which displays symptoms like muscle rigidity, limb tremors, paralysis, slow movement, and cognitive problems such as apathy, stress, depression, and some issues of anxiety. In the advanced stages, the patients exhibit insomnia and memory gaps. Various methods of treatment for PD have been in use which include both surgical and non-surgical options.

To decide the favorable diagnosis method, concentrations of dopamine are monitored using both invasive and non-invasive methods such as positron emission topography (PET), micro dialysis, functional magnetic resonance imaging (fMRI) and fast scan cyclic voltammetry (FSCV). It is possible to measure the changes in dopamine concentration in brain structures with high temporal resolution (100 ms intervals) using the FSCV technique. For decades, carbon-fiber microelectrodes have been utilized in the detection of various neurotransmitters. Their poor sensitivity efficiency was shown to be improved further by various advanced techniques like pyrolyzing through 3D-printing or through the process of nanolithography [4]. The effect of the material used in fabrication i.e., carbon nanotubes (CNT), nano diamond or graphene elevate the surface characteristics by introducing surface oxides that improve adsorption of dopamine on the carbon-fiber microelectrode surface [5].

In 2020, it was shown that microelectrodes made of ultra-flexible materials (i.e., SU8) offer seamless biocompatibility in chronic implantations and enable reliable extracellular action potential recordings [6]. In the present work, our goal was to develop a gold-based microelectrode for the detection of dopamine using FSCV technique. The present approach, based on use of gold as recording site, has the potential to be applied onto ultra-flexible microelectrode arrays (presented in [7]) so that seamless biocompatibility and reproducibility might be achieved in future *in-vivo* sensor applications. The work done analyzes the different surface conditions at which a gold microelectrode can be used to detect dopamine. Besides the high electrical conductivity of gold (44.2 S/m) and the ability to resist corrosion, it is also ductile [8] allowing ease to reshape it into fine

electrodes that do not resist the minor micro-movements of the brain tissue hence reducing the possible growth of glial cells. This ductility advantage is also seen in the conventional thin 7 μm diameter carbon fiber microelectrodes where chronic implantations are possible [9]. Irrespective of sitting third in ranks of metal electric conductivities behind silver (62.1 S/m) and copper (58.7 S/m) [10], gold was a preferred choice because it resists corrosion that can be a result of reaction with elements in the brain's local environment. This can be attributed to the small atomic radius of 135 pm compared to silver of 160 pm and copper of 140 pm hence a weaker nuclear attraction for the free electron in the outer orbital. As a novelty, in this project, the surface of the microelectrode was coated with biocompatible materials which can be suitable for durable application of FSCV technique and enable the detection of dopamine with high sensitivity and high temporal resolution. Thus, a highly sensitive gold microelectrode compared to the conventional thin (7 μm diameter, 150 μm length) carbon fiber microelectrodes in the limited -0.2 to +0.6 V potential range at a 100 Vs^{-1} scan rate. This has potential to enable real-time detection of dopamine was developed.

Three different materials were used to improve the gold sensitivity, temporal resolution and reduce possible growth of glial cells due to interaction with the microelectrode surface. These are, GO, SPEEK and pyrrole (py) using two fabrication procedures namely, electrochemical deposition and dip coating as summarized in **Figure 1.1** below.

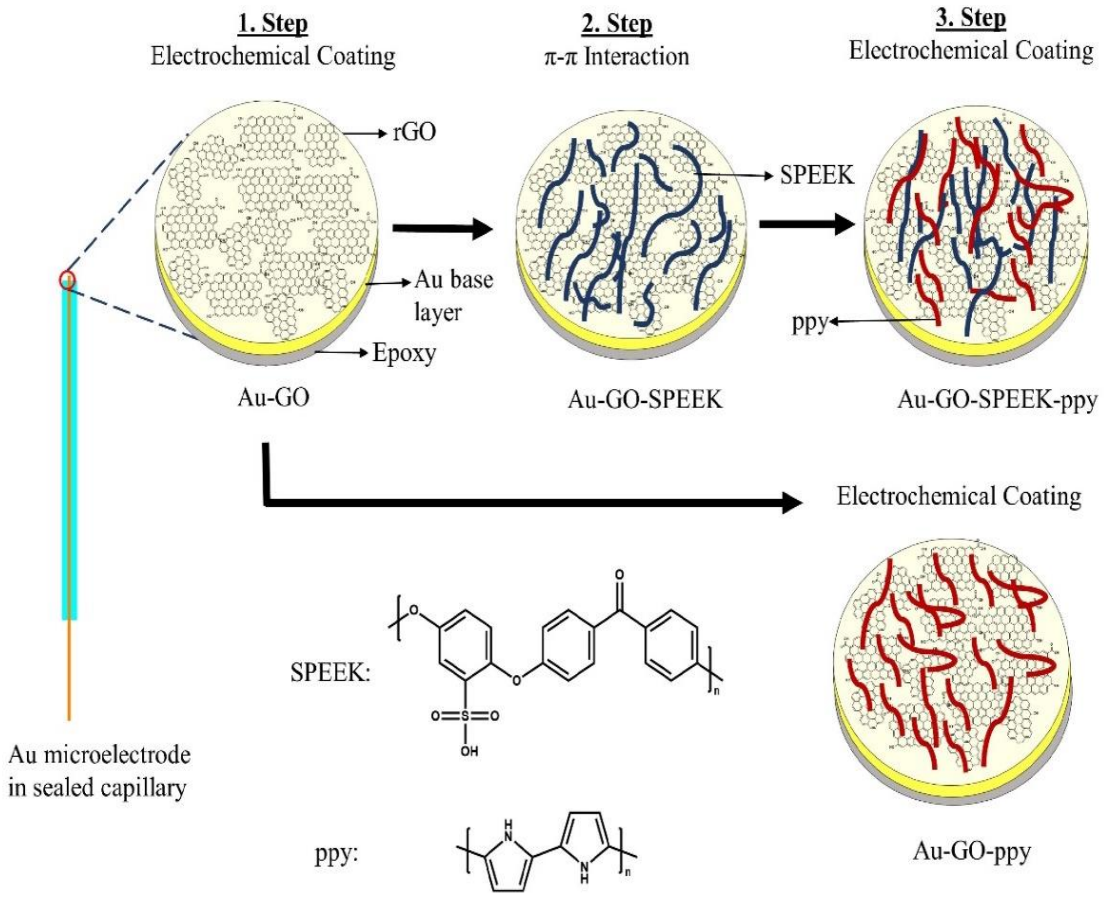


Figure 1.1: Summary of coating procedures for the biocompatible materials onto the gold surface.

Altering the 3D surface of the gold microelectrode enhances electroconductivity by increasing the surface area. Scanning electron microscopy (SEM) studies have shown that the coatings introduce surface roughness or curving/pores of micrometer sizes [4]. These pores enable the characterized surface to behave as thin-layer cells, momentarily having the dopamine analyte trapped as the redox reaction occurs in the FSCV studies. The gold disc-shaped microelectrode surface was first coated with graphene oxide (GO) to increase the surface sensitivity. Additional SPEEK coating was performed via dip coating on the graphene-coated Au surface through $\pi - \pi$ interaction to increase bio-inertness of the electrode. A final layer of polypyrrole that influences selectivity and biocompatibility, was electrochemically introduced to test whether it contributes towards durability (**Figure 1.1**). Not only does GO increase electrical conductivity [11], [12] but also elevates stabilization of organic solvents [13] and forms a strong anti-corrosion layer upon coating on conducting surfaces [14]. It was also illustrated that polymer coatings such as poly (3,4-ethylenedioxythiophene) (PEDOT) or sometimes nafion greatly influence the selectivity and sensitivity of particularly dopamine functional groups and ascorbic acid

[15], [16]. Recent studies have shown that a new polymer; sulfonated poly (ether ether ketone) (SPEEK) has comparable results whilst providing higher biocompatibility for the microelectrode [17], [18]. A better understanding of the design importance at the micron scale enables utilization of further conductive as well as non-toxic polymers such as pyrrole, which allow formation of an inert microelectrode surface that prevents local cellular reactions upon implantation; a problem that has been the main cause of growth of glial cells in existing sensing systems.

Characterization studies were performed for each surface coating when applied at different conditions of time, concentration, applied potential, coating techniques used, and consecutive vs. simultaneous material deposition. Upon obtaining the optimal conditions for coating each layer, a final electrode with these conditions was fabricated. The area of the recording site is 600 μm^2 to additionally enable the recordings of the action potential from neighboring neurons. For viability characterization of the microelectrode, the modification in the surface morphology and composition after several runs in the FSCV analysis will be investigated using the SEM technique. To increase the performance effectiveness and surface area of dopamine detection regions, the study optimized the surface conditions that will be used in future studies to design a microelectrode array having at least eight recording sites.

CHAPTER 2

2. THEORETICAL PART

2.1. Neurotransmission Pathways of Dopamine

What happens during neurotransmission? With the presence of a threshold action potential, the axon terminal of the presynaptic neuron releases the signaling molecules (neurotransmitters) which attach to the postsynaptic neuron across the interconnection via neuroreceptors on the dendrites. The reaction at the postsynaptic neuron induces an inhibitory or excitatory by the postsynaptic potentials (short term effects) or signaling cascades (long terms effects). The process is a result of both chemical and electrical transmission as shown below in **Figure 2.1.**

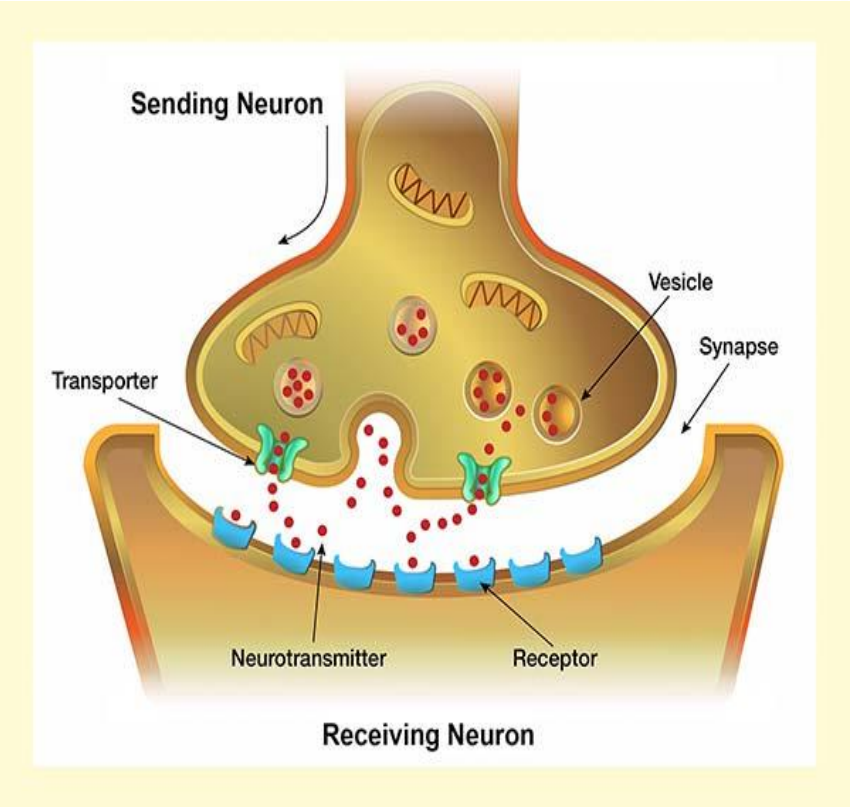


Figure 2.1: The process of neurotransmission across the neural network [19].

The likeliness of neuro-excitation depends on the difference between the action potential and the membrane potential as the presynaptic neuron's input bring it further from the required threshold level. Through a process called summation, the neuron integrates both the inhibitory and excitatory impulses received and if the outcome is excitatory then the neuron will most likely generate a graded electrical potential causing it to "fire". At that point, a good number of potential-dependent sodium channels open so that an influx of sodium into the postsynaptic cell causes a net inward current greater than the outward current. The opposite is true in case the total effect is inhibitory.

3,4-dihydroxyphenethylamine (also called dopamine) is a vital amino-based neurotransmitter that makes up 80% of the catecholamine chemical family (which also constitute epinephrine and norepinephrine). It is primarily a result of decarboxylation of levodopa (L-DOPA), a chemical produced in the brain and kidneys (cells within the medulla of adrenal glands). L-DOPA can also be synthesized from L-tyrosine or L-phenylalanine [20]. The primary role of dopamine is to convey signals received and interpreted by the brain, to other neurons along dopaminergic pathways. Within the CNS, these pathways modulate functions of hormonal release [21], motor control [22], [23] and reward-stimulated behavior [24]. Around the body, dopamine is noticed to influence various other physiological functions as seen:- in the kidneys, increasing sodium elimination and urine production; in the blood vessels, acting as vasodilators, in the intestines, protecting the mucosa and in the immune system, regulating the dynamics of the lymphocytes. The major effect of excessive dopamine release is seen in the created reward-demanding loops and aligning them with addictive behavior as the pleasure [25], [26].

Dopamine binds and exerts its effect on the receptors of the target cells called dopamine receptors and human trace amine-associated receptor 1 (hTAAR1), which are metabotropic G-protein coupled receptors, implying a second-messenger system is required to initiate their functionality [27]. These receptors fall in two main categories namely, D1-resembling and D2-resembling receptors [28]. The presynaptic D1-like receptors (D5 and D1) activate excitation by opening the Na^+ channels or inhibition by opening the K^+ channels. The postsynaptic D2-like receptors (D4, D3 and D2) mainly inhibit "firing" at the target neuron. In that case, a combination of which receptors are present at the target neuron and the response to the second-messenger, cAMP (cyclic

adenosine monophosphate); determines whether dopamine will act as excitatory or inhibitory [28]–[30].

There are four dopaminergic pathways as shown in **Figure 2.2** below: Mesolimbic, Nigro-striatal, Mesocortical and Tuberoinfundibular pathway [31]. Each of these pathways have different functions and a malfunction can cause severe mental disorders and Parkinson's disease [32].

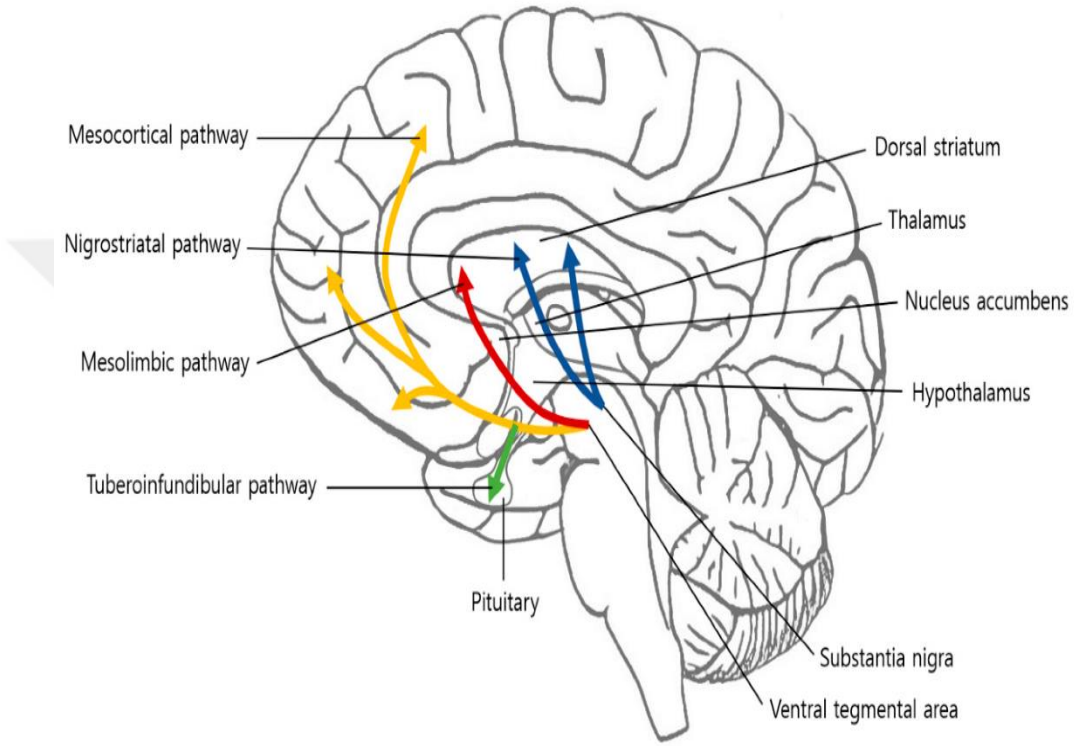


Figure 2.2: Dopaminergic pathways [33].

The mesolimbic pathway that originates from the ventral tegmental area (VTA) to the nucleus accumbens (NAc) plays the major role of dopamine i.e., reward stimulated pleasure. Stimulation at the terminal of this pathway (NAc) from stimuli such as food, drugs, sex, behavior etc. is vital in regulation of daily body activity [34]. However, overexcitation in this pathway causes unwavering demand leading to addiction and ultimately euphoria [35]. Like the mesolimbic pathway, the mesocortical pathway originates from the VTA and goes all way to the prefrontal cortex (PFC). This PFC region coordinates decision making, memory strength and cognition and thus effects such as amnesia, failure to concentrate or take decisions may occur in case an impairment is incurred along this pathway. An excess of dopamine in the region on the other hand cause mental illnesses like schizophrenia [36]. The nigro-striatal pathway is the basic role-

player in motor control [31]. The pathway goes directly from the substantia nigra to the putamen and caudate located in the basal ganglia regions constituting the largest amount of brain dopamine. From its named function, a reduction of functional neurons in this pathway leads to motor impairment causing major conditions of focus in this thesis such as parkinsonism, dyskinesia, tremors, spasms, and uncontrolled muscle contractions [37]. Finally, the tuberoinfundibular pathway starts from the hypothalamus in its arcuate and periventricular nuclei. It terminates in the infundibular hypothalamic region. This pathway is more eminent in females as it inhibits secretion of prolactin [38]. Functional failure of this pathway leads to over release of prolactin which affects menstrual cycles, bone health, libido, and fertility [39].

As noted from above, the functions of dopamine are so vast and a lot of research on this neurotransmitter has increased in the past decade. Our work will mainly address the nigro-striatal pathway in which concentration depreciation leads to PD.

2.2. Treatment of Parkinson's Disease

The main disease in focus (PD) can be treated using both surgical and non-surgical procedures. The latter involves administration of levodopa, monoamine oxidopaminese B inhibitors and dopamine agonists. Surgical treatment is applied for patients who display negative responses to medical therapeutics. Formerly, pallidotomy and thalamotomy (heat-destruction of a minute portion of the globus pallidus and thalamus respectively) where used to eliminate these parts of the brain responsible for inhibiting dopamine release. Since the 1990s, advanced technique for the above life-threatening consequences, deep brain stimulation (DBS) systems have been produced to keep track of the concentration of dopamine in suspected patients. A DBS system is made up of the clinician programmer, charger, implantable pulse generator (IPG), remote control and the microelectrode leads as shown in **Figure 2.3.**



Figure 2.3: A breakdown of the DBS system [40].

The DBS leads are implanted in the subthalamic nucleus (STN) of the brain to cause stimulation by the delivered electrical pulses from the IPG, of generally low intensity. These pulses are controlled with variations in frequency, amplitude, and pulse-width from the programmer. A non-invasive remote control helps to run the stimulator at required settings by the patient themselves or a health personnel. Without secondary surgery after every period, the system's battery can be charged by a radiofrequency (RF) dependent charging tool kit [40]. The main drawback is that after some time, glial cells develop around the DBS leads in response to protection from the foreign non-inert material used, which lowers efficiency of the system [41]. There are also recorded cases of post-surgery tissue inflammation [42], [43].

2.3. Dopamine Detection Techniques

There are majorly two electrochemical methods used in detection and monitoring of the action of various neurotransmitters i.e., micro-dialysis and FSCV. Other advanced procedures include fMRI, and PET.

2.3.1. Micro-dialysis

Micro-dialysis is a sampling technique of minor-invasive nature in which the concentration of any free and unbound organic compounds (neurotransmitters, glucose, hormones, glycerol etc.), within the extracellular environment are continuously measured. A tiny micro-dialysis catheter/probe containing a low concentrated viscous solution (perfusate) of laboratory-produced dopamine solution, is injected firmly into the target tissue region and minute solutes cross the semi-permeable membrane in a process called passive diffusion. The collected dialysate is delivered into the insight autosampler to measure the analyte properties after a preselected volume and time as shown below in **Figure 2.4**.

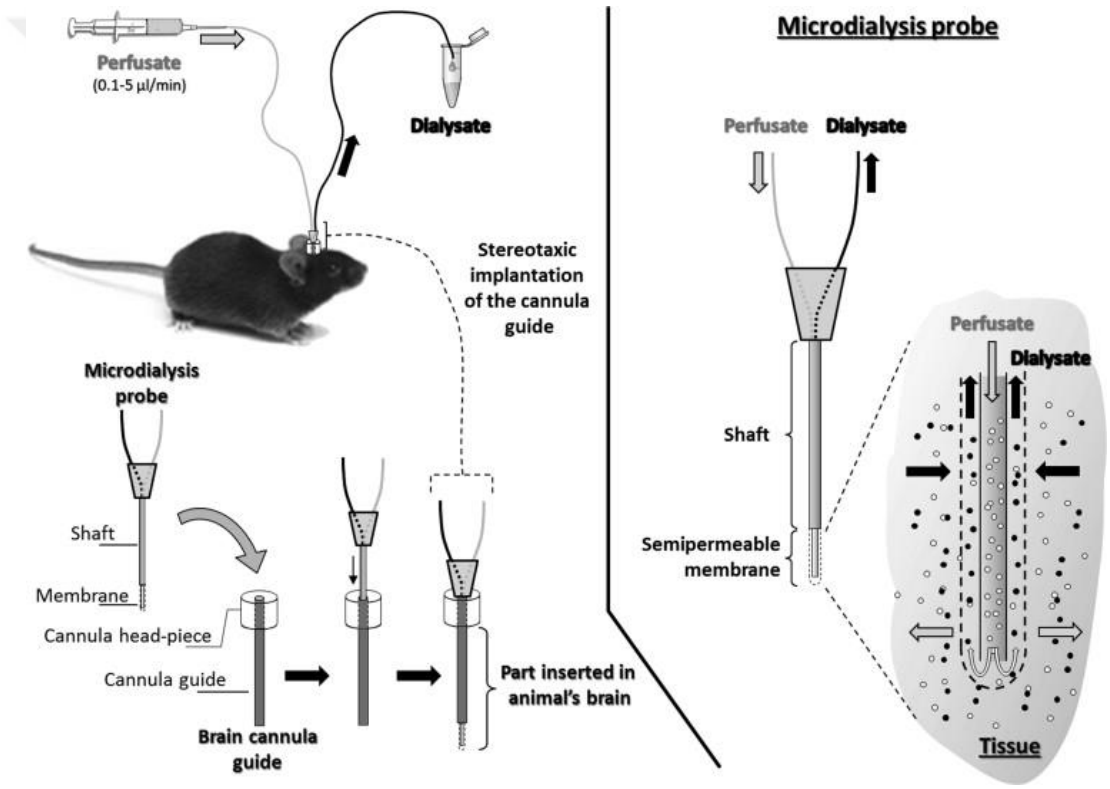


Figure 2.4: Micro-dialysis procedure [44].

There has been work on reducing the probe size and improving permeability efficiency, but the technique faces negative reviews from the ethical point of view. It is also reported to hinder micro-movements in the brain leading to alteration of tissue morphology, reduced metabolic rates and vast damage to the blood-brain barrier (BBB) [45]. The technique also exhibits relatively low temporal resolution (a few minutes) and spatial resolution (the probe covers a few millimeters of the area) [46], [47].

2.3.2. Positron emission tomography (PET)

PET is a very expensive non-invasive functional imaging procedure that employs radioactive materials (radiotracers) to map and quantify variations in metabolic processes, chemical composition, blood flow, and regional chemical load. Various radiotracers are injected in the intravenously depending on the targeted analyte prior to the imaging for example [^{11}C] McN 5652 and [^{11}C] DASB for serotonin transporters, [^{11}C] raclopride and [^{18}F] desmethoxyfallypride, and [^{18}F] mefway for serotonin 5HT1A receptors. These tracers are used during electroencephalogram (EEG) neuro feedbacks so that they attach to and allow visibility of the targeted brain region containing the dopamine pool in plurality [48]. Neuro feedbacks induce dopamine release as the brain is trained to control their cortical oscillations using the EEG's real-time audio or video feedback [49]. **Figure 2.5** below shows an example for a PET for a normal person (a) and one with PD (b).

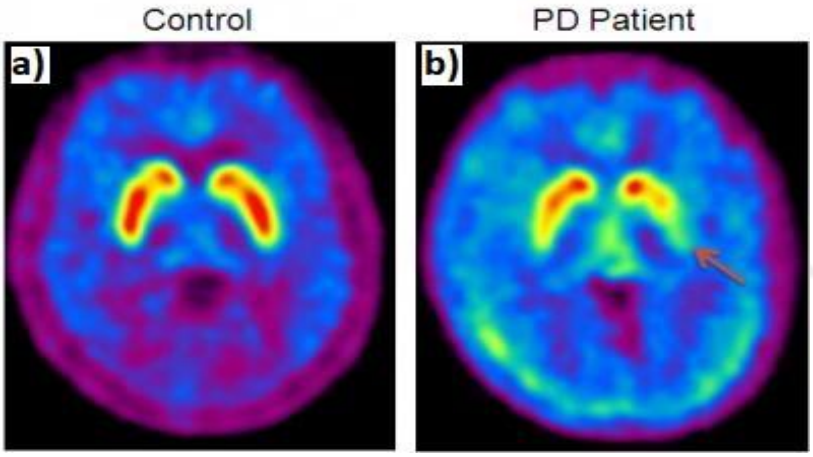


Figure 2.5: PET image of a normal person (**a)** and PD patient (**b)** (modified from [50]).

The hot colors imply increased brain activity of the regions that release dopamine as seen in the normal brain in **Figure 2.5a** above. In PD patients, these dopamine releasing regions deteriorate in activity as seen in **Figure 2.5b** hence eventually get lost in the advanced stages of the disease. This technique is however hindered by the inability to show micro- and macroscopic aberrations of white and gray mater structures and with high concerns of radiation risks [51].

2.3.3. Functional magnetic resonance imaging (fMRI)

This technique basically relies on the blood flow kinetics that can be followed up by marker molecules [52]. The idea is that neuronal activity and cerebral blood flow function

coherently implying that when a given nervous system's region is stimulated then blood going to the region is increased [53]. fMRI maps this brain's activation (ventral striatum for dopamine) by combining spatial coverage and molecular specificity with the help of a magnetically detectable neurotransmitter sensor. Studies on reward-based hypothalamic brain stimulation of the mice injected with the dopamine sensor give time-resolved voltametric calculations with peak dopamine concentrations mainly seen in the nucleus accumbens [54]. **Figure 2.6** below shows a brief description of applying fMRI in detecting dopamine. The stimulating electrode (in red) is inserted into the lateral hypothalamus (LH) and the cannula in NAc enabled the dopamine sensor infusion (blue) allowing the MRI data to be obtained from the surrounding brain slices as seen in **Figure 2.6a**. The infusion of the dopamine sensor causes a medial forebrain bundle (MFB) stimulation (**Figure 2.6b**) with the real-time MRI image seen in **Figure 2.6c**. After five successive stimulations noted by the red ticks in **Figure 2.6d**, region of interest (ROI)-averaged MRI signals are noted [54].

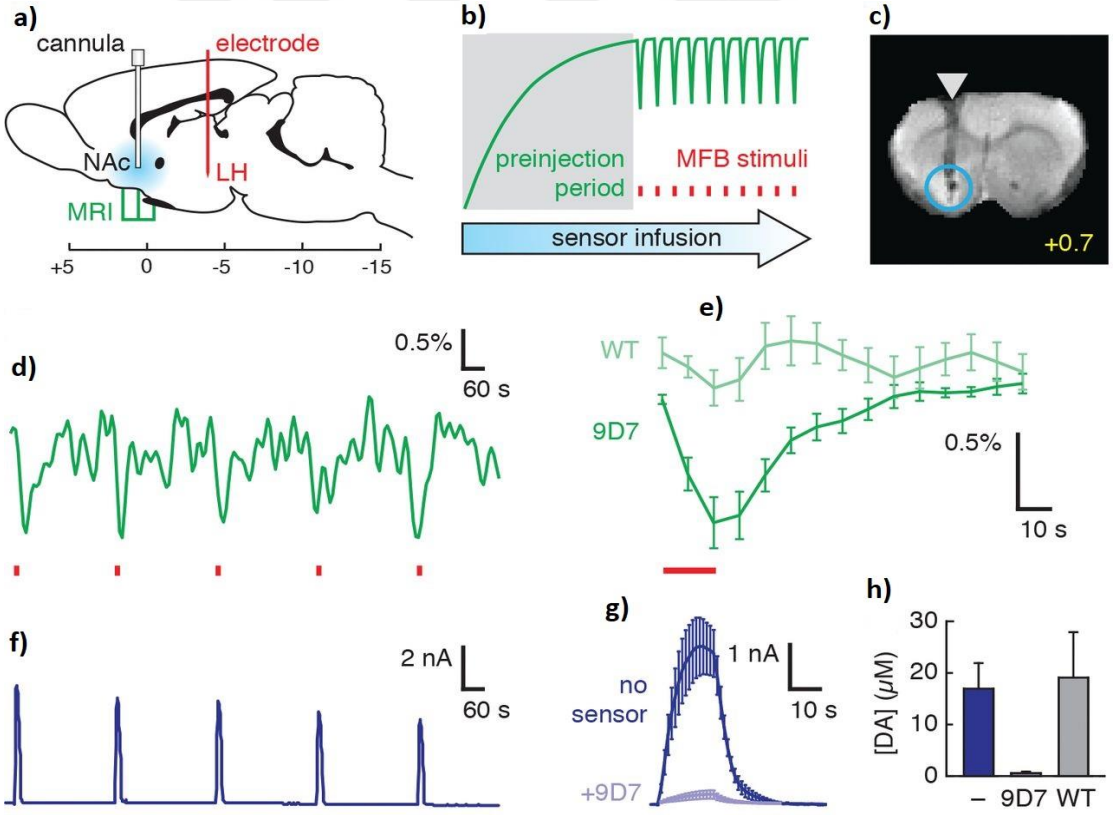


Figure 2.6: Use of molecular fMRI for dopamine detection in the ventral striatum (modified from [54]).

Mean peristimulus impulse response function (IRF) gained through the ROI from rats injected with BM3h-9D7 or the control material BM3h-WT (dopamine non-sensitive

protein) are shown in **Figure 2.6e** above. Amperometric measurements of the release of dopamine by NAc initiated by the five MFB stimuli are given in **Figure 2.6f** with the amperometric transient responses before and after infusion of the dopamine sensitive material, BM3h-9D7 indicated in **Figure 2.6g**, dark blue and light blue, respectively. A comparative study on the efficiency of the sensor is given in **Figure 2.5h** for the calibrated amplitudes of dopamine (without sensor infusion – dark blue, after infusion of BM3h-9D7 – middle, and after infusion of the control material BM3h-WT – grey) [54]. The advantage of fMRI is that it can also give both the dynamics and quantitative measurements of the concentrations of dopamine in the ventral striatum with ability to detect any rapid changes in the brain activity unlike PET, however, it usually faces an issue a very low limit of detection (LOD) for neurotransmitters in the brain [51].

2.3.4. Fast-scan cyclic voltammetry (FSCV)

FSCV, however, with a high scan rate of 100 Vs^{-1}, is an electroanalytical technique that allows fast recording of a voltammogram in just a few milliseconds. This ensures a high temporal resolution. A micrometer scale electrode is inserted into the brain, extracellular environment, or solution under study to rapidly raise and lower the ramp of the potential in a triangle form shown in **Figure 2.7**.

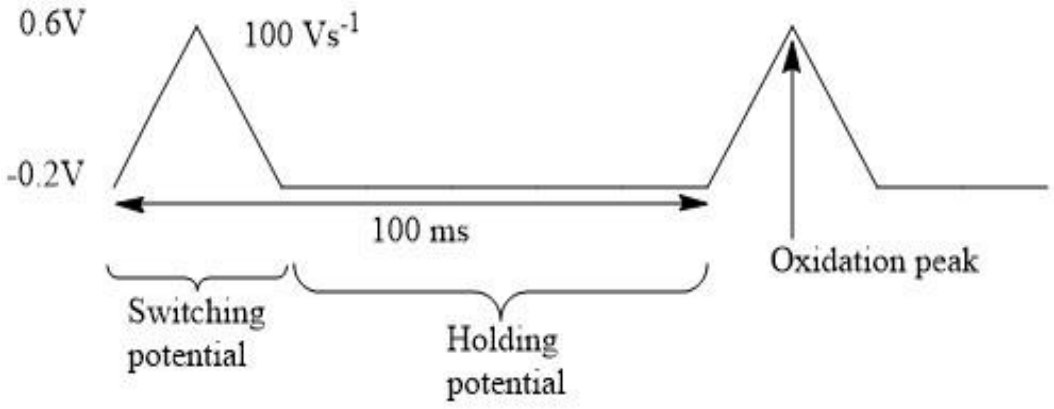


Figure 2.7: Applied waveform during dopamine detection.

The dopamine gets oxidized during the rising triangular ramp with loss of two electrons and the formed dopamine-o-quinone is reduced in the falling ramp by gaining two electrons as elaborated in **Figure 2.8** below. For dopamine detection using gold-based electrodes, a potential window of -0.2 V to +0.6 V was used.

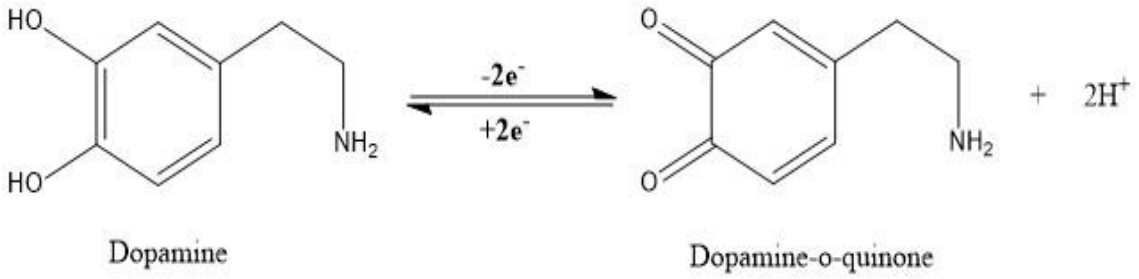


Figure 2.8: Redox reaction of dopamine.

The interchange between switching potential to holding potential continues after every 100ms continuously and the recorded oxidation peak spike corresponds to the level of dopamine concentration. The potential values (V_0), system gain (G) and used feedback resistor (R_f) in the system are used to obtain the current (i), and a cyclic voltammogram is plotted to show the relation of the applied potential to the current going through the fabricated microelectrode. A simplified version of the voltammetry circuit is shown in **Figure 2.9** below in which the designed electrode was the working electrode (WE) and the response to the input voltage ramp is recorded after systemic amplification as a voltage (V_0) at the output. By using the given formular for i in **Figure 2.9** below, the current response which is in inversely proportional to impedance and in direct proportionality to the sensitivity is obtained.

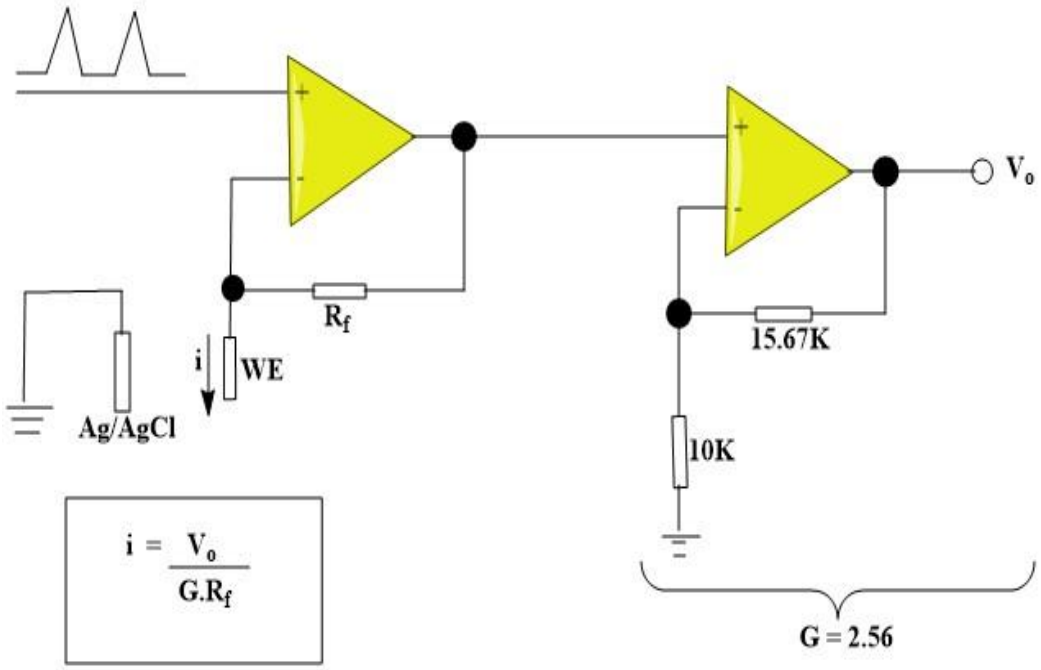


Figure 2.9: Simplified system circuit of FSCV.

The fabricated electrode was used as the working electrode inserted into the saline solution. After stabilization of the system, dopamine solution was added, against the

reference electrode of Ag/AgCl. The present microelectrode supports the recordings of extracellular action potentials during the time periods in which dopamine is realized in the system. The FSCV system was developed and optimized concurrently as the electrode design process was ongoing hence the results obtained in **chapter 4** underwent progressive adjustments accordingly.

2.4. Different Systems and Microelectrodes for Dopamine Detection

The implantable microelectrodes for application of the FSCV technique are generally manufactured manually and have a single recording channel. Since they are manufactured manually, their production is difficult, and their production reproducibility is poor. In the literature, there is no microelectrode which is designed for detection of dopamine concentration with high temporal resolution, ability to be used with multi-channels and is suitable for future chronic use. Various materials have been used in the detection of dopamine with consideration of a range of factors i.e., cost, electrocatalytic activity, stability of modification, ease and reproducibility synthesis of modifiers, sensitivity, selectivity, simplicity of fabrication, and the abundance of modifiers that can be used on the electrodes. These include carbon-based, metal and metal oxide nanoparticles and metal organic frameworks. The various previous studies on these dopamine detecting electrodes whose characteristics can be improved by ionic liquids, polymeric or inorganic modifiers; are discussed in the following sections.

2.4.1. Carbon-based electrodes

Utilization of the carbon nanotubes to analyze the oxidation of the dopamine neurotransmitter dates way back as early as 1996 [55].

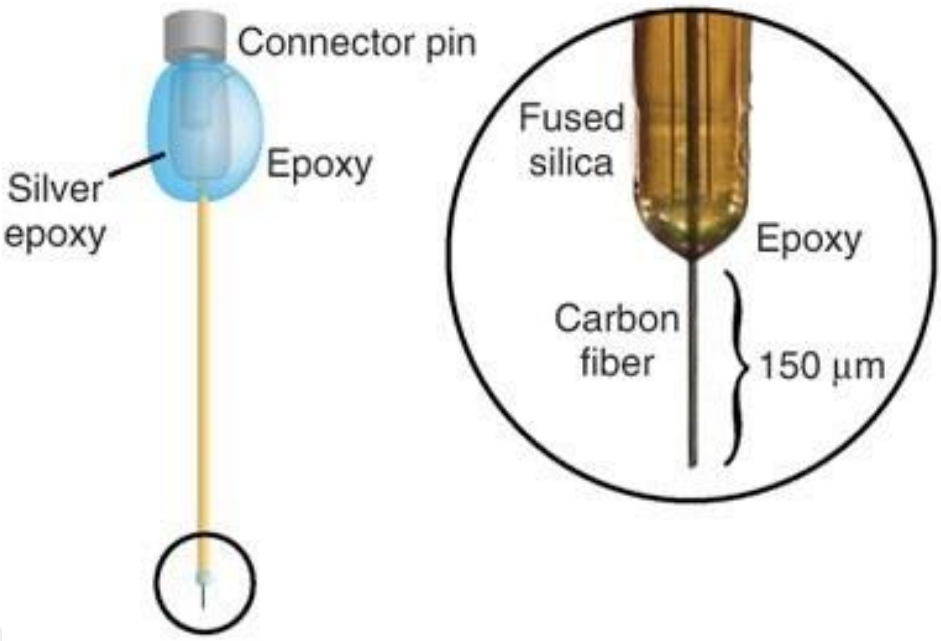


Figure 2.10: Conventional carbon-fiber microelectrode (modified from [9]).

Commercially produced carbon fibers have successfully been used to in different bio-applications to detect various neurotransmitters and organic compounds [56], [57]. The carbon fiber electrodes were also implemented in developing a reliable and less complex FSCV system utilized in the *in-vivo* detection of dopamine in mice [58]. Even with their relatively good sensitivity, these electrodes have posed various issues in chronical studies such as to growth of glial cells due to a low biocompatibility and poor ductility. On that note, a study was done to functionalize the carbon fiber surfaces to improve selective sensitivity towards only the desired neurotransmitter through coating with gold nanoparticles mixed with deoxyribonucleic acid (DNA) and various polymers [59]. Another study showed that dip-coating of carbon nanotubes dissolved in an organic solution of dimethylformamide (DMF) onto the carbon fiber surface greatly improved sensitivity possibly due to the increase in the surface area to volume ratio [60]. However, this process was not reproducible and led to a significant decline in the signal to noise ratio [60].

2.4.2. Metal and metal oxide nanoparticles

Superiorly, metal nanoparticles (MNPs) give better electrical, physical, and chemical properties than their bulk equivalents due to the increased surface area to volume ratio in the reactivity processes. Usually, chemical stabilizers are used during the synthesis

process of MNPs to control their charge, size, stability, and shape. These MNPs are usually used in various combinations to enhance the analytical sensitivity of the desired analytes. Dispensing of Au NPs (known for their good catalytic, electronic properties, and superior amperometric response during dopamine oxidation) on the highly porous $Ni(OH)_2$ (that is cheap, biocompatible, and chemically stable), gave good peak separation of the differential pulse voltammograms of uric acid (280 mV) and dopamine (260 mV) [61]. This lowered the interference during dopamine detection. Conversely, cellulose microfibers modified with Pd NPs have shown a relatively high oxidation ability of dopamine when low potentials are used [62].

Despite of their usability, it has been studied that the selectivity is low during biological experiments in which the ascorbic and uric acid concentrations are high thus incorporation of GO so that the negatively charged sheets increase attraction of the positively charged dopamine [62]. The several active sites and ready availability of p-type semiconductor Cu_2O nanoparticles having a small band gap (1.9 - 2.1 eV), enabled their solvothermal incorporation on graphene and the composite used to modify the surface of glassy carbon electrodes (GCEs) for high selective sensitivity of dopamine over ascorbic acid [63]. Another MNP is Fe_2O_3 which has good electrocatalytic characteristics, convincing bandgap, non-toxic, stable, cheap, and very abundant in nature. GO sheets modified with Fe_2O_3 NPs and deposited of GCEs gave broad linear ranges in electrochemical studies and a desirable LOD of 0.004 μM for differential pulse voltammetry (DPV) [64].

In recent years, utilization of GO has peaked due to its excellent electrical conduction property. Besides being considered the strongest material currently even with its minimum weight, GO exhibits a high thermal stability and resistivity to corrosion once deposited on surfaces which resist cracking and thus helps to develop very durable coatings for chronical studies. For these reasons, it was used to boost the gold's sensitivity furthermore. Preparation and application of GO coating to enhance surface properties for electrochemical applications have previously been shown to easily be performed in water [65], [66]. A study indicated how Au-GO nanocomposites upon coating on the gold surface improved both selectivity and sensitivity in a specific potential window as emphasized for gold [67]. Various other studies have shown the improved surface charge transfer properties obtained by utilizing GO [68]–[72].

As notably seen, GO plays a vital role as a chemical modifier but as well as an independent NP too. It has effectively been used in various other studies for detecting dopamine to modify the NPs such as in formation of a ZnO-rGO complex through a 1-pot approach at room temperature to modify functionality of GCEs [73], ultrafine Pt-Ni/rGO complex showed improved dopamine detection when used to modify GCEs in presence acetaminophen with a superiorly low LOD of 0.0026 μM for dopamine [74], and a quadruplet composite of Au NPs/C dots/GO/ferrocene derivative simultaneously detected uric acid, dopamine, ascorbic acid, and acetaminophen with elevated catalytic activity due to the synergistic effect of the combined NPs and chemical mediators even if the LOD for dopamine slightly raised to 0.05 μM [75].

2.4.3. Metal organic frameworks (MOFs)

These are also known as coordination networks/polymers with open metal sites, tunable pore sizes, ordered crystalline structures, and a desirable surface area; are used in various applications i.e., catalysis, sensing and adsorption [76]. These MOFs can readily be reacted with other materials i.e., GO or CNTs to further enhance their electrocatalytic activity. However, not much research on their performance in sensing platforms has been done yet with just a few examples in the past decade. For example, the electron-lacking bipyridinium moieties in the MOFs of UiO-67-DQ and UiO-67-MQ (DQ = N,N′-ethylene 2,2′-bipyridinium, MQ = N,N′-dimethyl-2,2′-bipyridinium) can link with the electron-rich dopamine to greatly improve voltametric detection of the analyte [77]. A copper terephthalate MOF-GO nanocomposite upon electrochemical treatment converts GO into rGO that allows the complex to disperse and stabilize well in water followed by drop-casting onto a GCE [76]. The modified GCE exhibited improved sensitivity of dopamine and acetaminophen as a result of the high electron mediation due to the MOF and the high conductivity of the erGO. Another such example of an MOF is the homogenous inter-grown nanocrystals of zeolitic imidazolate frameworks (ZIF-8) on the GO sheets' surface to prevent possible restacking of the GO sheets and allow and increased surface area as compared to the 3D GO [78]. On the side note, the LOD was quite high when detecting dopamine as much as 1 μM which is unfavorable thus more research on these materials needed.

2.4.4. Gold electrodes

The utilization of very fine gold of about 76 μm in diameter, as the base sensing surface ensures flexibility of the electrode such that there is limitation of the micro-movements of the brain during normal physiological functioning. This increases the robustness of the fabricated microelectrode for possible long-term implantation and effective sensitivity results over several surrounding neurons. It has also been shown in a study that the gold microelectrodes are selective for the dopamine neurotransmitter in the -0.2 V to +0.6 V potential window giving unique characteristic cyclic voltammograms [79]. Unfortunately, other oxidizable analytes like uric and ascorbic acid coexist with dopamine which will directly be oxidized by a high working potential [80]. A narrow working potential is therefore used. In terms of electrode materials, Au and Pt behave alike but the former is limited for use in the positive potentials since its surface undergoes oxidation but it gives superior sensitivity in electrodes modified with self-assembled monolayer coatings [81].

2.4.5. Inorganic modifiers

Various inorganic modifiers have been used in recent studies due to their profound characteristics in detection of dopamine. In this regards, nickel has been most utilized in examples like nitrogen-doped graphene (N-G)/nickel tetra sulfonated phthalocyanine (NiTsPc) with immobilization through $\pi - \pi$ interaction [82]. The N-G matrix gave a favorable condition for NiTsPc to improve electron transfer with a maintained electrocatalytic performance. Nickel foam (NF) was also used to grow a stable and reproducible 3D array consisting of a homogenous nanoneedle $NiCoS_4$ core and a $NiCoS_4$ nanosheet forming the shell with high selectivity over ascorbic and uric acid [83]. The only drawback of this nanoneedle is the potential interferents from tyramine. Crystalline 2D hexagonal boron nitride (2D-hBN) nanosheets can also be used to modify a number of commercially available dopamine sensing electrodes such as screen-printed graphitic electrodes (SPEs), glassy carbon electrodes (GCE), and boron-doped diamond (BDD) through drop-casting [84]. Anchoring of Bi_2S_3 on reduced graphene oxide (rGO/ Bi_2S_3) through a rapid 1-pot hydrothermal process provided a composite inorganic-enhanced modifier for GCE with good oxidation potential of dopamine and a favorably low LOD of 12.3 nM [85].

Perovskite-type (ABO_3) complexes exhibit unique physical and chemical characteristics, thus used in a wide range of energy and electrochemical catalytic processes. A rather rarely used element of lanthanum (La) has also been used in different compounds to improve selectivity of dopamine-detecting electrodes such as $LaCoO_3$ nanostructures synthesized with urea as the surfactant was used to modify GCE for the simultaneous detection of dopamine in solutions containing ascorbic acid and uric acid [86]. Comparatively, $LaMnO_3$ was used in a related study on GCE [87]. Metal complexes mediate and increase the catalytic effect towards dopamine detection through shifting the potential to vastly low values and reinforcing the electron transfer [88]. Copper complexes for example having N-N donor group ligands have been investigated to have catechol affinity (which is the group in which dopamine belongs) [89]. Other modifier metal complexes for dopamine detecting surfaces include manganese (II) Schiff-base compound coated on a gold electrode [90], and cobalt (II) complexes mixed with single-wall carbon nanotubes (SWCNTs) and nafion to enhance sensitivity of screen-printed carbon electrodes (SPCEs) [91]. Lastly, tin oxide doped with fluorine (FTO) has shown great acceleration in research due to its wide electrochemical window, low cost, and high thermal stability hence the graphene nanoplatelet (GNP)-modified FTO electrodes were designed for highly sensitive and selective detection of dopamine in solutions containing other organic compounds namely, ascorbic and uric acid [92]. The ease of dissociation and random reactivity of most of these inorganic compounds with the ionic cellular microenvironments in chronical implantations poses a potential great threat to their applications.

2.4.6. Ionic liquids

These are molten salts that melt at temperatures near or below the room temperature. Their structure is made up of two asymmetric ions of unequal charges that just barely bond to each other (usually a small organic anion and a large cation). They exhibit high conductivity, great solvation ability, excellent electrochemical stability non-volatile and less toxic [88]. When an ionic liquid (1 butyl-3-metilimidazolium tetrafluoroborate ($BMIMBP_4$) was used to treat SWCNTs dispensed in chitosan solutions and deposited on an SPCE (SWCNT/SPCE), the anodic peaks of dopamine increased by 17% while that of uric acid increased by 70% with an extremely low LOD of 0.16 μM for dopamine [93]. It has been shown that the ionic liquids have a very high viscosity as electrolytes which

may affect mass transport in electrochemical studies; implying a desired need to use a co-solvent in the sensing system [94].

2.4.7. Polymeric modifiers

Generally, carbon polymers (CPs) have unique properties unlike other polymers i.e., low energy optical transition, low ionization energy, high electrical conductivity, and electron affinity. These are mainly attributed to the electrons' delocalization in the polymer backbone as a result of the carbon atoms' π-bond overlap of orbitals (pz-sp^2). Vying to their superior electrical conductivity, they can be termed as "synthetic metals" [95]. These CPs are most commonly deposited as monomer solutions onto the surface of the bare electrode through electrochemical means.

There are some notable inclusions of polymer modifiers i.e., the electro-polymerization of cinnamic acid to form a film on a bare carbon paste electrode to form a poly-cinnamic acid modified carbon paste electrode (PCA/CPE) [96]. This fabricated electrode showed excellent catalytic activity of dopamine, ascorbic acid, and uric acid with the ability to separate the obtained oxidation peaks. The disadvantage of this modifier is that the electrode obtains a high quantification limit (LOQ) 3.52×10^{-6}M [96]. Another reproducible application of electro-polymerization of poly 2-napthol orange film (P_2NO) on a paraffin wax-impregnated graphite electrode (PIGE) exhibited excellent dopamine oxidation with selective identification of dopamine in the presence of uric and ascorbic acid [97]. This was most likely due to the hydrogen bonds formed between the SO_3^- on the P_2NO and the OH^- on the dopamine thus oxidation due to the weakened O-H bond [88]. Electro-grafting process has also been used to coat 4-amino benzene sulfonic acid (4ABSA) on a graphite pencil lead electrode (GPLE) through covalent anchoring [98]. This polymer greatly improved selectivity, stability, and sensitivity of dopamine despite the presence of 1 $mmolL^{-1}$ of uric acid. However, the modified electrode exhibited a narrow calibration range during the study probably due to the small diameter size of the GPLE [98]. PEDOT, which is known for its low oxidation potential, biocompatibility, high conductivity and good thermal stability; has also been used to modify laser scribe graphene (LSG) for selective detection of dopamine when a mixture containing uric and ascorbic acid are utilized and it displayed a very low detection limit of 0.33 μM [99]. The PEDOT-LSG obtains a 3D porous morphology with an increased surface area and surface roughness which greatly elevates its sensitivity as compared to the unmodified LSG.

SPEEK on the other hand has been known to be an inert polymer when inside a physiological system due to its biocompatible structure. With current carbon electrodes leading to growth of glial cells in a short time upon implantation, exploitation of SPEEK to counter this problem was done. More so, SPEEK increases the mechanical strength, thermal stability and additionally exhibits a moderate conductivity of protons [100]. These added advantages enabled its utilization on the microelectrode surface. In the past, GO enhanced SPEEK solutions have mainly been used to improve proton conductivity in battery electrochemistry due to the ability of SPEEK to withstand corrosion during charge storage and functioning [65]. This is done by controlling the physiochemical properties of ion-exchange capacity, osmotic swelling, and proton conductivity during the sulfonation process. SPEEK composites when coated with amine functionalized GO also exhibited a higher coulombic and energy efficiency (CE, 96.9% and EE, 82.8% respectively) at 30 $mAcm^{-2}$ than nafion [101]. Even at such high efficiencies, the GO-SPEEK coatings showed a stable working performance with no significant decay. With its biocompatible nature and the above properties, utilization in designing the dopamine sensitive microelectrode for stable long-time performance without corrosion was suggested.

A comparative study using polypyrrole (ppy) polymer was done which similarly provides the same advantages as SPEEK above in addition to increasing durability as it resists corrosion after multiple FSCV analyses. However, ppy is less electrically conductive as compared to GO and this affected the microelectrode's sensitivity. In the design, the desired polymer must help create a biocompatible environment whilst maintaining a high sensitivity too in comparison to the existing electrodes. As previously discussed, GO-ppy coatings showed a rougher pore-like surface morphology with micrometer scale folding due to dopand intercalation within the polymer chain when a deposition potential is activated [102]. They further show that the total impedance of the electrode under study (platinum (Pt)) went down by over 90% of the bare electrode after coating at the relevant biological 1 kHz while obtaining a charge capacity density twice as much as the bare electrode. Even if ppy individually showed poor conductivity properties as compared to GO, it has the ability to resist surface corrosion and offer an advantage in long-term studies. A combination of GO-ppy gave superior results in the study. These advantageous properties of ppy influenced its use for designed gold-based sensing platform for future studies that require durable implantable microelectrodes.

CHAPTER 3

3. EXPERIMENTAL PART

After each step of coating, the electrode was gently rinsed with distilled water to remove any excess uncoated residue on the microelectrode surface, that may hinder surface sensitivity and then dried in a desiccator for 30 minutes.

3.1. Materials

Gold wires of diameter of 76.2 μm and 50.8 μm ($\geq$ 99.99%, A-M Systems) and copper wires of diameter 250 μm (> 99%, Metalal) were used as received. Platinum-Iridium wires of diameter 25 μm ($\geq$ 99%, A-M Systems) was used after scraping off the thin iridium surface coating. Potassium hydroxide (KOH) pellets ($\geq$ 85%, Sigma Aldrich), graphene oxide solution concentration of 4 mg/mL (GO, > 95%, Sigma Aldrich), dopamine hydrochloride powder (Sigma Aldrich), EPO-TEK OG116-31 (Epoxy Technology), anhydrous sodium chloride (NaCl) ($\geq$ 99%, Multicell), phosphate buffered saline (PBS) tablets and pyrrole ($\geq$ 97.0%, Merck) were used as received. Poly(ether ether ketone) (PEEK, Victrex) was used after sulfonation.

3.2. Software

The FSCV system was programmed with LabView, and the graphs were plotted using MATLAB (R2020a) with the code given in **Appendix A**. The ^{1}H-HMR analysis was done using MestrNova (14.2.0). Image designs and manipulation were done on Chemdraw Professional (16.0), Paint 3D and GIMP photoshop (2.10.24) environments. Other graphs were plotted using GraphPad prism (9.0.1) and Origin Pro (2020 (9.7)). Coating thickness was analyzed using ImageJ (1.51w).

3.3. Characterization

The pH of the GO was taken by the Hanna HI 2211 bench pH/mV/C meter. The electrode is first washed rinsing with distilled water and then dried. Calibration was done by using two solutions of pH 4.01 and pH 7.01. For studies on the surface morphology, the ultra-high-resolution Schottky scanning electron microscope (SEM) SU700 was used. The dried samples for the study are cut into short ≈0.5cm and firmly laid on the SEM grids at room temperature. This is followed by thin coating the sample with a gold/palladium vapor for 15 s before inserting it into the SEM chamber (to avoid any charging during imaging). Sample names (top left), image magnification scales (bottom right), and working conditions (in brackets) are indicated on the SEM images. Energy dispersive X-ray analysis (EDX) was done concurrently using the device mentioned above and it helped in identification of the elements within the coated surface material using X-rays. The results are given as atomic composition by percentages attached on the subsequent SEM image. For thermogravimetric analysis (TGA), the Perkin Elmer TGA 8000 was used. The samples were heated from 40 °C to a maximum temperature set at 800 °C with the heating rate of 10 °C/min and the percentage decompositions of the sample's constituents was analyzed. The Fourier-transform infra-red spectroscopy (FTIR) studies for structural analysis were done on Perkin Elmer's Spectrum 2IR spectrometer. The spectrum was recorded for a range of 4000 to 450 cm^{-1} using a 4 cm^{-1} resolution and the average after four consecutive measurements was taken into consideration. The proton nuclear magnetic resonance spectroscopy (^{1}H-NMR, 500 MHz) was recorded using an Agilent VNMRS 500 instrument in deuterated-DMSO with $Si(CH_3)_4$ as internal standard. The dynamic light scattering (DLS) to determine the effect of pH on the particle size, zeta potential and thus electrical conductivity using the Zetasizer Ultra (Malvern Instruments). 700 μL of the sample was put into the DLS glass cells and the variables to study are selected from the menu on the computer. The cell for zeta potential is different from the former as it contains two gold conducting plates.

3.4. Electrochemical Graphene Deposition on Copper Electrode (Cu-GO)

Due to the evidently high expenses of gold, all optimization experiments were first run on a copper wire of a diameter of 250 μm and length 5 cm to ensure the hypothesis can be replicated on a cheap, easy to find and relatively conductive material. With this insight as elaborated from literature, proceeding with gold microelectrodes was more supported.

The copper electrode was used as the anode and a platinum electrode was used as the cathode in the two-electrode electrochemical system with 2 cm separation in-between the aligned electrodes. A voltage of 10 V from a direct current (DC) supplier was applied using a pH 3.90 GO solution of 0.5 mg/mL solution concentration for 60 minutes. Both electrodes were vigorously washed with ethanol followed by distilled water prior and dried under a desiccator for 1 h. On the anode, the electrode loses electrons (oxidation) and the generated positive charge at the electrode leads to an immediate attraction of the electrically reduced and negatively charged graphene sheets groups within the solution vicinity, causing electrodeposition of a GO layer. Copper is known to easily erode during electrochemical processes in which it acts as a cathode since the atomic radius is big thus the loosely attached outer electrons are lost leading to erosion of copper ions (Cu^{2+}). In this initial experiment however, copper is an anode so any false results due to cathodic erosion are minimized. The inert platinum electrode was used at the cathode where reduction occurs as shown in **Figure 3.1** below; thus, enabling charge to flow without altering the solution's chemical composition.

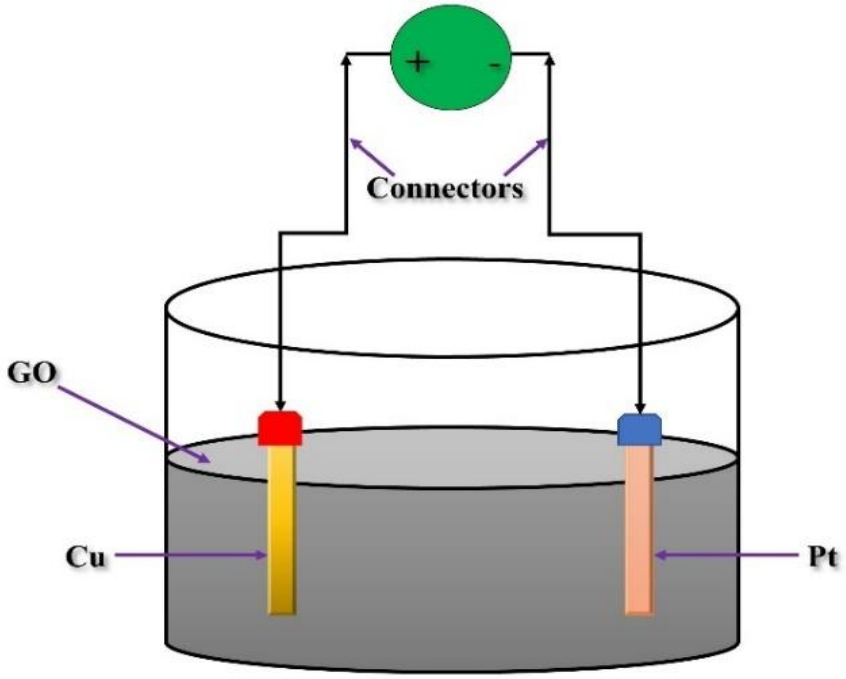


Figure 3.1: Illustration of electrochemical setup for GO deposition.

The copper electrode was slowly withdrawn and left to hang in an open atmosphere to dry. The electrode was then immersed in a solution of sodium borohydride for 30 minutes to induce further chemical reduction on the electrically deposited GO layer (rGO). The

eventual electrode is withdrawn and washed with distilled water and after dried in a desiccator for 30 minutes to ready it for characterization.

3.5. Electrochemical Graphene Deposition on Gold Electrode (Au-GO)

Gold electrode is inserted in a plastic capillary, and both ends sealed with biocompatible epoxy gel that hardens in 15 minutes upon disposure to UV radiation. After curing, one end of the electrode is cut under a microscope to expose only the blunt tip (circumferential disc) such that characterization occurs for only the exposed tip across its diameter. GO solution to be used is ultrasonicated for 30 minutes at 10 °C to exfoliate the graphene sheets and uniformly distribute in solution followed by nitrogen bubbling for 10 minutes to eliminate entrapped oxygen moieties in the graphene sheets. During coating, stirring is done at 200 rpm to prevent the sheets clumping together which may inhibit mass transfer during electrodeposition. The coated electrode is rigorously washed with distilled water to remove any excess loose deposition and then dried in a desiccator for 1 hour to eliminate any entrapped water molecules in the GO sheets. The effect of deposition potential (2, 5, 10 and 30 V), supporting electrolytes (distilled water, saline, phosphate buffered saline (PBS)), GO concentration (0.02, 0.1 and 0.3 mg/mL), and deposition time (7, 15, 30, and 60 min) were investigated on the performance of the deposited layer. All experiments were performed at room temperature.

3.6. Sulfonation of Poly(ether ether ketone) (PEEK) – SPEEK

Sulfonation was done to make PEEK water-soluble based on the previously published protocol [65]. Briefly, 5 g of PEEK in 100 mL concentrated sulfuric acid was stirred at 700 rpm and 55 ℃ for 5 hours. The obtained clear brown solution was added dropwise to ice-cold distilled water to form pellets and get rid of the excess sulfuric acid solution. The process should be done under a fume hood. Continued washing of the obtained pellets was done until white SPEEK pellets at neutral pH are obtained. The pellets were then dried for 24 hours in a desiccator to eliminate any entrapped water.

3.7. Electrochemical SPEEK Deposition on Graphene-Coated Gold Electrode (Au-GO-SPEEK)

With 20 mg/mL SPEEK (10 kDa or 100 kDa), the Au-GO electrode was used as the anode and the platinum electrode as the cathode. A constant voltage of 10 V was supplied

for 15 minutes, and the experiment was performed at room temperature without stirring. The procedure was also run as simultaneously onto the bare gold electrode i.e., GO and SPEEK mixture co-deposition for 30 minutes. The electrode was washed with distilled water to remove excess SPEEK outgrowth and left to dry for 1 hour in a desiccator.

3.8. Dip Coating of SPEEK on Graphene-Coated Gold Electrode (Au-GO-SPEEK)

The previously prepared Au-GO electrode was suspended freely and immersed in SPEEK solution while a stirring of 250 rpm was applied. Physical coating was performed through π-π interaction. The effect of the dipping duration was studied i.e., 15 and 130 mins. The electrode was then withdrawn slowly from the 20 mg/mL SPEEK (10 kDa or 100 kDa) solution and suspended freely at room temperature for 1 hour in order to dry prior to characterization.

3.9. Electrochemical Pyrrole Deposition on Graphene and SPEEK Coated Gold Electrode (Au-GO-SPEEK-ppy)

Utilization of 0.05 M pyrrole enabled comparison of effectiveness of the polymer with SPEEK. The electrochemical deposition process was applied on the previously coated gold electrode as the anode and the platinum used as the cathode. A constant voltage of 10 V at room temperature was used for the electrodeposition. A study of effect of the ppy layer was done by comparing the results after varying combinations of depositing or co-depositing the py alongside GO and SPEEK.

3.9.1. Measurements

The FSCV study analyzed the sensitivity of the developed electrodes. Since FSCV is the main analysis to observe the efficiency of designed surface modifications, the optimization of FSCV for dopamine detection using developed microelectrode is very crucial. Each new layer or conditions to optimize were analyzed on FSCV after visualizing its surface morphology. **Figure 3.2** explains the general steps for Au-GO fabrication as an example for the design and optimization process with the FSCV analysis.

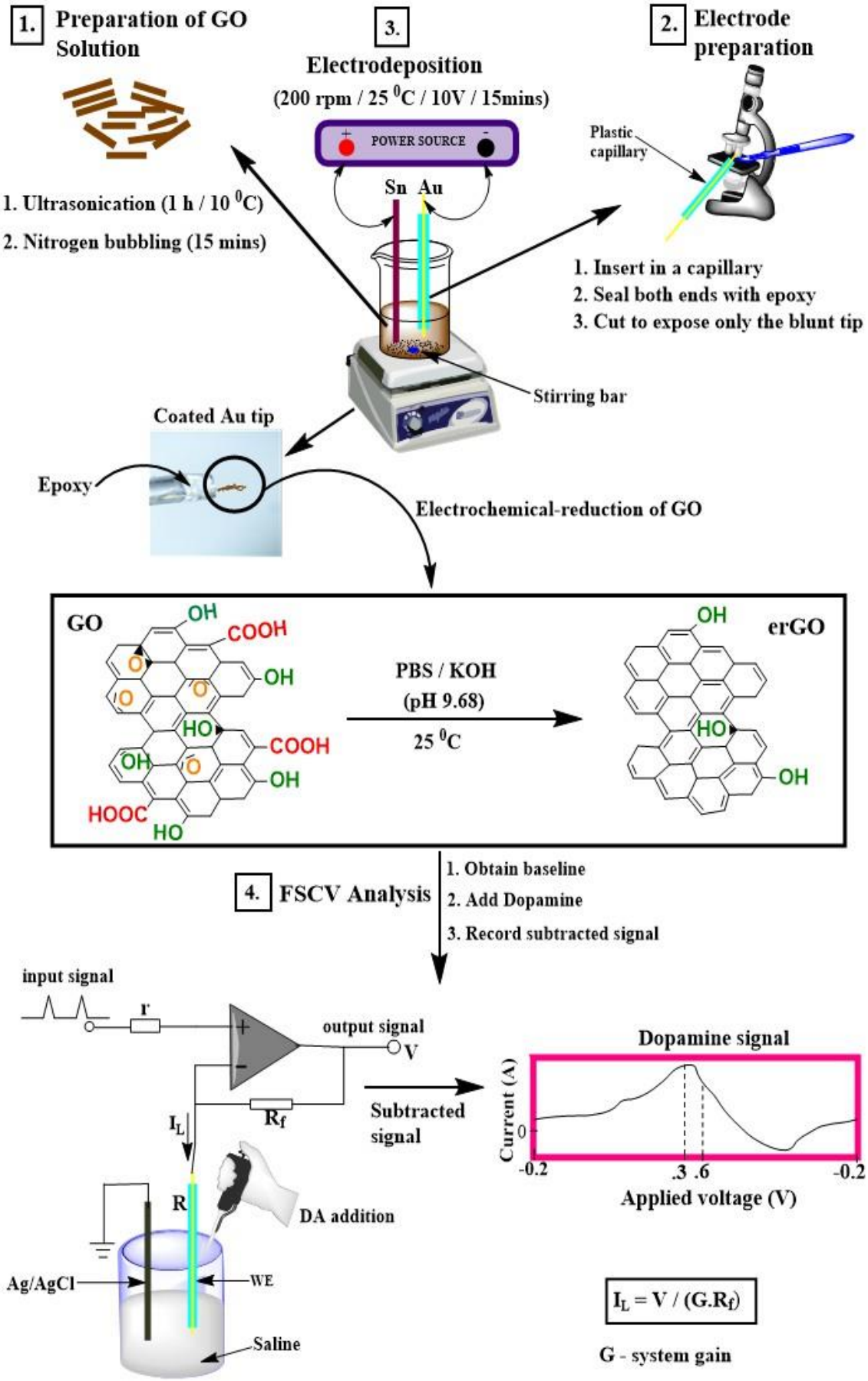


Figure 3.2: A summary of the fabrication and characterization of the electrode.

A waveform of bipolar nature is applied at 10 Hz having a scan rate of 100 V/s in the range of -0.2 V to +0.6 V. This is the optimized potential window for gold electrodes as studied by literature [79]. The fabricated electrode tip (disc) is the working electrode and a Ag/AgCl is the counter electrode. 100 mL of 0.154 mM saline solution was the supporting electrolyte for the FSCV study. 1 mM dopamine stock solution was made by dissolving dopamine hydrochloride powder in a saline solution of 0.154 mM concentration. Two charged Li-ion batteries (> 9V) were connected and a suitable feedback resistor (R_f), that does not lead to saturation. With stirring, the electrode is left to stabilize i.e., when the output voltage signal has no distinctive redox peaks. At stabilization, the electrode disc forms a double layer such that there are no more voltage variations, as observed from the LabView-based program. Obtain a baseline recording for the first 10 s due to the saline stock solution. Gently add 10 μM dopamine from the stock solution to the saline solution and let it dissolve for 20 seconds. Run the second reading for 10 s to obtain the new signal as a result of the baseline plus the dopamine signal. The subtracted signal from the baseline offers the required dopamine signal whose current-voltage relation is seen by using a MATLAB code given in **Appendix A**. The feedback resistors used for each microelectrode was varied to avoid saturation and the values tabled in **Appendix B**.

CHAPTER 4

4. RESULTS AND DISCUSSION

In recent years, various sensing platforms for detection of vital neurotransmitters like dopamine, serotonin or epinephrine have been developed [103]. To date, carbon electrodes are also utilized but they have disadvantages of poor sensitivity and a low flexibility. The factors of main focus during microelectrode fabrication are sensitivity and selectivity since the target analytes co-exist within the neural pathways. Gold microelectrode to detect dopamine has been gaining more attention not only because the high electrical conductivity and the ability to resist corrosion, but also its ductility which allows ease to reshape it into fine electrodes that do not resist the minor micro-movements of the brain tissue hence reducing the possible growth of glial cells as seen in the carbon fiber electrodes of the similar thickness [104]. This is mainly why gold has been selected as the main electrode material on to which other additional layers will be grown.

As mentioned before, this study mainly focuses on the development of a sensitive and durable gold microelectrode to detect dopamine using a handmade FSCV system. For this purpose, the gold surface was modified with different layers that contributes to the final structure of the microelectrodes. For instance, the gold electrode surface gains more sensitivity for very low dopamine concentrations ($< 10\ \mu$M) by using electrically reduced and deposited GO sheets on its surface. Since these microelectrodes are to be implanted in the brain, high biocompatibility is expected, and it was aimed to be achieved by the SPEEK coating on surface due to good chemical resistance, mechanical strength, and thermal stability of PEEK after implantation. Finally, an additional polypyrrole layer was deposited through electro-polymerization of its monomer solution; in order to present a microelectrode having high temporal and spatial resolution in addition to improved viability for chronical applications with insignificant corrosion.

To understand the possible coating potential, system setup, working conditions and the estimated required material quantities for the actual study; a preliminary experiment involving coating of copper electrodes was done. In the **Figure 4.1** below, the procedure and results of the electrodeposition of GO on the copper wire where a platinum and copper wires were used as cathode and anode, respectively. Upon application of a 10 V potential for 1 h in **Figure 4.1b**, the brown homogenous 0.5 mg/mL GO in distilled water (**Figure 4.1a**); is electrically reduced by losing the oxygen-based groups. This lowers its water solubility and forms a deposition cloud around the anode (Cu electrode).

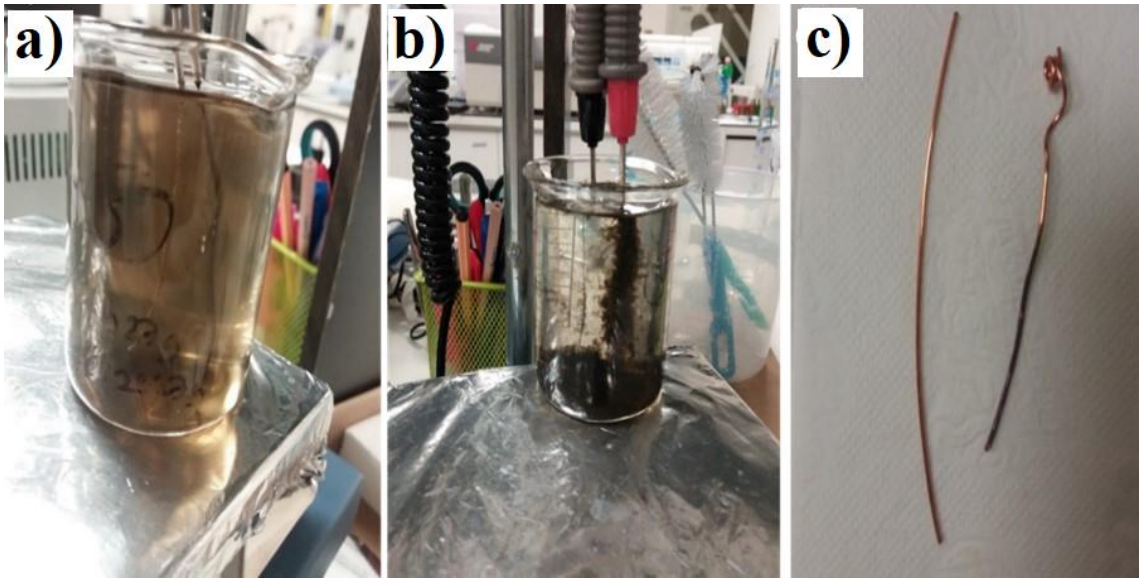


Figure.4.1: a) Appearance of GO solution and electrodes before application of a DC potential. **b)** Upon application of a constant voltage, the electrically reduced GO sheets collect at the copper anode. **c)** Appearance of rGO coated copper electrode.

For initial characterization, the electrodes' (**Figure 4.1c**) mass was put into consideration. While the platinum electrode at the cathode did not exhibit any mass change, the coated copper electrode mass at the anode did. This electrode, which was expected to increase, was observed to decrease in mass (from 15.3 mg to 13.4 mg). The situation is specific to copper materials which have been studied previously to display their susceptibility to corrosion [105].

GO upon oxidation gains more sp^3 carbons. It usually has a 2:1 ratio of C:O making it less conductive with a conductivity barely 1 S/m. Reduction increases the C:O by more than 6 folds which partially restores the sp^2 carbons in the graphene aromatic structure pulling the band gap closer and making it very conductive [106]. According to literature, the more the reduction of the GO layer, the more the surface roughness thus surface area and hence a very high conductivity [107]. With the initial study on copper electrodes:

At the cathode: $2H^{+}_{(aq)} + 2e^{-} \rightarrow H_{2(g)}$ gas bubbles are evolved and,

At the anode: $2O^{2-}_{(aq)} \rightarrow O_{2(g)} + 4e^{-}$, with GO deposition on the copper electrode.

Since the oxidation rate at the anode is higher than the rate at which the GO layers from the electrolyte are deposited, copper forms more ions into the electrolyte, thus causing more mass loss than the mass of layers deposited onto the surface. In this case, morphological changes that may occur on the electrode surface were observed by scanning electron microscopy (SEM) analysis as shown in **Figure 4.2** below.

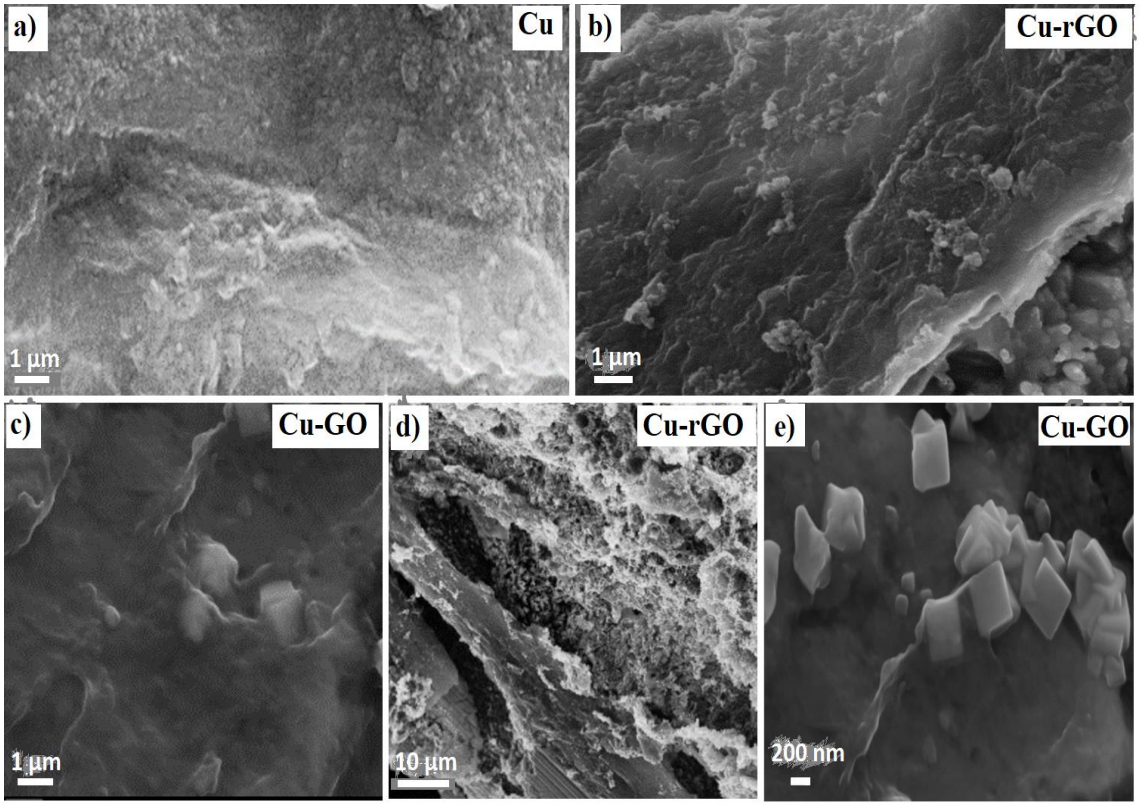


Figure 4.2: a) Bare Cu electrode surface **b)** Cu electrode surface appearance obtained as a result of coating with chemically reduced GO, **c)** Cu electrode surface with GO plates collected but not reduced chemically, **d)** Cu electrode surface view where GO sheets after electrocoating are then reduced with $NaBH_4$, **e)** Cu_2O cubic crystals formed by Cu^{2+} ions leaving the electrode surface accumulated on the electrode surface again.

Evidently, the graphene sheets seen in **Figure 4.2c** became stuck to the surface after they were reduced. However, in addition to electrochemical deposition, the reduction of the electrode at the anode, which can be seen in anodic coatings and copper-specific, caused corrosion on the copper surface (**Figure 4.2d**). In the obtained surface image **Figure 4.2e**, the Cu^{2+} ions that dissolved from the electrode surface are suggested to be redeposited in cubic structures onto the electrically reduced graphene sheets. With this shortcoming, irrespective of the fact that copper is cheap and easily accessible, it did not reflect a correct

optimization strategy for our target electrode of gold. However, it allowed us to understand how the electrochemical setup and process runs. This trial was repeated at lower voltage (5 V or 2 V) to reduce copper erosion and reveal the graphene coating clearly. On the other hand, although it is expensive, it was presumed that these optimizations would be more accurate using gold electrode, and in the light of the SEM data obtained with copper, the FSCV system was developed for studies on gold and brought a more applicable level of the microelectrode. From literature, it was found that however much $NaBH_4$ greatly reduced the impedance of the GO sheets and increases the surface roughness as seen in **Figure 4.2d** [108], the chemical is allergic and has potentially fatal side effects to the nervous system [109], [110] which would reduce the desired biocompatibility of the deposited GO layer. For that reason, chemical reduction was eliminated.

Besides resisting corrosion, gold has a notably high electro conductivity and ductile strength (Young' modulus of 79 Gpa) which allow both a high sensitivity and flexibility in case of implantation in the brain. As it is mentioned before, the proposed microelectrode will be produced on gold. Then, optimization of the gold electrode surface was initiated by coating with GO. Reduced graphene oxide (rGO) is known for its high conductivity [11] which further enhances sensitivity whilst altering the surface morphology with high dopamine adsorption-favoring roughness. Additional conductive polymers i.e., SPEEK and ppy are utilized in the fabrication process and then analyze their effect on both the sensitivity and surface morphology of the electrode. All coatings were optimized to ensure the right quantity is deposited for effective functioning by using the FSCV analysis technique.

In 1980's, John Miller developed an electrochemical method to study voltammetry called FSCV. With this technique, the temporal resolution of the classic cyclic voltammetry was increased further to typically 100 ms. During the detection of dopamine, a waveform of bipolar nature is applied at 10 Hz having a scan rate of 100 V/s in the range of -0.2 V to +0.6 V as the optimized potential window for gold electrodes from literature [79]. Adjustments of these parameters were applied on the developed FSCV system. To study the effect of the surface morphology modifications on the dopamine sensitivity using GO, SPEEK and ppy; the FSCV previously developed within our laboratory on the basis of the John Miller design principles, was used [58].

Various other supporting electrolytes for carrying the dopamine during the FSCV analysis were studied to optimize not only the one with the best detection properties but also lower stabilization time and closest relation to the brain environment. A physiological pH of 7.4 was maintained in all the samples. The findings are summarized in **Table 4.1** below.

Table 4.1: Different supporting electrolytes to apply in the FSCV as dopamine carrier.

Sample	Solution	Stability	Dopamine detection
1	15 mM tris, 1.2 mM $CaCl_2$, 3.25 mM KCl, 140 mM NaCl, 1.25 mM NaH_2PO_4, 1.2 mM $MgCl_2$, 2.0 mM Na_2SO_4	Closest ion composition to the cerebral environment. Stabilizes very quickly.	No detection of dopamine was observed since the solution precipitates.
2	100 mM tris, 0.1 M KCl, 0.1 M NaCl	Stabilizes faster than saline.	Prominent dopamine peaks but lower amplitude than for saline.
3	0.1 M PBS	Takes the longest duration to stabilize.	Gives oxidation peak amplitudes similar to saline but the reduction peak is less prominent.
4	0.154 M Saline	Stabilizes faster than PBS	Gives high dopamine peaks

On that accord, saline was used in the FSCV system. Nonetheless, there was need to reduce on the time required to stabilize the electrode, so, the potential triangle from the mains was initially supplied at 50 Hz and then eventually switched back to 10 Hz. Complementary, stirring at 300 rpm was applied to ensure that charges are equally distributed much faster through the saline solution in order to create a firm double layer reliable enough in a short period prior to injection of dopamine.

The **Figure 4.3** below illustrates the procedure of determining that the designed electrode is stable and how the plotted dopamine peaks are obtained from the MATLAB code in **Appendix A**.

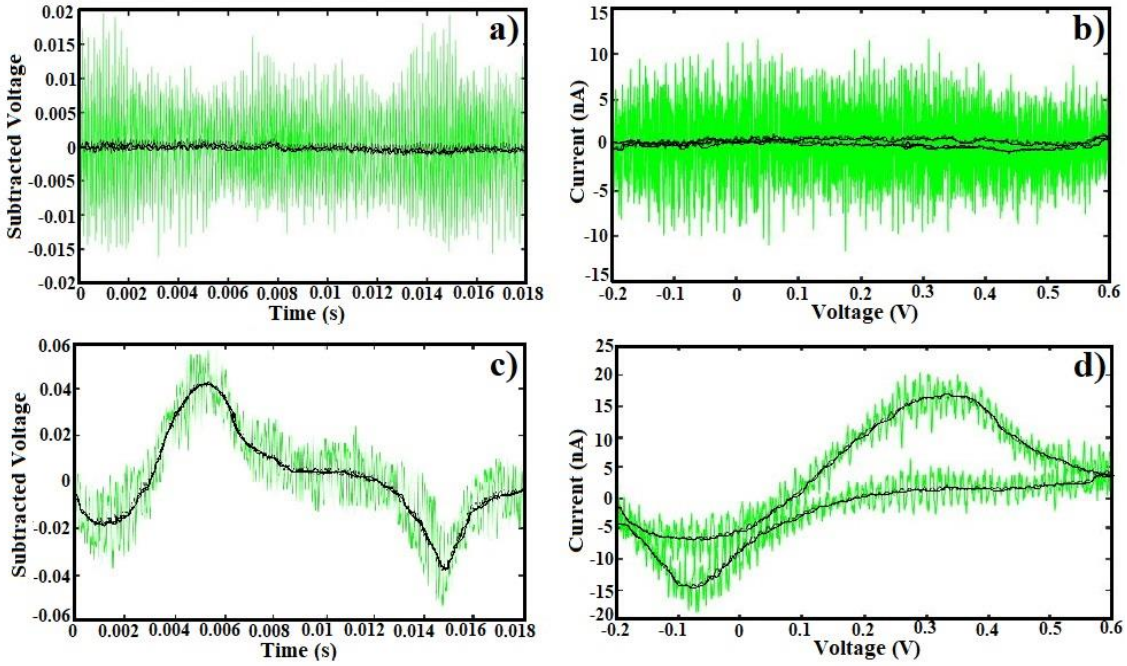


Figure 4.3: Graphical representation of obtained results after stabilization (**a)** and **b)**) and after addition of 10 μM dopamine (**c)** and **d)**).

At stabilization, a subtraction of the baseline (without dopamine) and the second signal obtained under the duration of 20 s gives a flat signal (**Figure 4.3a**) and the plotted cyclic voltammogram has no distinct peaks observed (**Figure 4.3b**). That showed that the system is now stable and ready. After taking another baseline, a recording of the signal having the baseline and the signal due to dopamine is taken within 20 s. Upon subtraction from the baseline using , an oxidation peak of the subtracted voltage due to dopamine is observed at about 0.005 s and a reduction peak at about 0.015 s. The graphs in **Figure 4.3a** and **Figure 4.3c** show the subtracted signals whereas **Figure 4.3b** and **Figure 4.3d** represent the cyclic voltammograms after converting the subtracted voltages and computing the value of current through the electrode using the formular below.

$$i = \frac{V}{G\,.R_feedback} \qquad \textbf{(4.1)}$$

,where; G is the system gain, V is the subtracted voltage and R_feedback is the feedback resistor value used at the head-stage.

The GO to be deposited was initially dissolved in distilled water to the desired concentration followed by ultrasonication for 1 h at 10 °C to allow uniform exfoliation of the stacked GO sheets. The system is very sensitive to minute variations in the resistance of the working electrode. With resistance being a factor of both electrode length and

surface area, the gold electrodes were inserted in a capillary and sealed with epoxy (which is electrically inert) such that and elongating tip is trimmed to expose only a cylindrical gold disc of the microelectrode's diameter. This allowed uniform characterization of the same area of exposure for all proceeding fabricated electrodes. Change in electrode length in the solution would alter the impedance and thus provide incomparable results according to the equation:

$$R = \frac{\rho L}{A} \quad \textbf{(4.2)}$$

where the resistance (R) is directly proportional to the length (L). ρ is the resistivity constant for gold and A is the surface area.

The other end of the gold wire is left hanging to allow connection to the power source terminal. Electrochemical reduction and deposition of the GO sheets occurs on the gold tip connected to the anode with the platinum used as the counter electrode. The electrode is then washed with distilled water at room temperature and left to stand for 1 h to eliminate any entrapped non-deposited residues from the surface of the modified electrode followed by 1 h drying in the desiccator. Drying was allowed to avoid any atomic compositional errors in the EDX study due to water molecules within the GO sheets.

Finally, an FSCV analysis was done where the fabricated gold-based microelectrode is the working and a Ag/AgCl as the counter electrode. The system's feedback resistance (R_f) is varied depending on the electrode's conductivity in such a way that saturation at the output does not occur. With the electrodes connected under the saline electrolyte, each modified electrode behaves uniquely, so sufficient time was allowed for the system to stabilize and in this time the electrical double layer is developed around the electrode. Stabilization is checked using the MATLAB code in **Appendix A** to ensure that the graph is straight with no prominent peaks in the saline solution before adding dopamine (plot the difference of the baseline from saline and the second recording without dopamine). With a 20 s delay after taking the baseline, dopamine solution was then injected into the saline supporting electrolyte to allow the dopamine to uniformly dissolve in the solution with stirring at 300 rpm. The reading was then taken comprising of the baseline and signal due to dopamine. The results obtained from the FSCV system, in form of a .csv file are then plotted into cyclic voltammograms using the MATLAB code attached in the **Appendix A** to obtain the subtracted dopamine signal.

4.1. Electrochemical Graphene Deposition on Gold Electrode (Au-GO)

GO offers many values in modern day fabrication processes i.e., known to be 100 times stronger than the equivalent thickness of steel with its sheets offering ballistic charge transfer over long distances. For this electrode, the already highly conductive gold was enhanced by the GO to boost dopamine sensitivity. With the pilot study done using the copper electrode previously, similar procedures were followed with gold replacing copper at the anode and platinum used as the cathode in a 0.5 mg/mL GO solution at room temperature.

Prior to studies involving sensitivity enhancement by use of biomaterials, an FSCV study on the effectiveness of the gold surface was performed as shown in **Figure 4.4** below. The rate of adsorption of dopamine to the electrode surface greatly affects the microelectrode's kinetic response. Pure gold electrodes form an oxide monolayer when cycled in an electrolyte [111]. In the setup, 100 mL of 0.154 M saline at room temperature is used as the supporting electrolyte for mass transfer of the dopamine molecules, the bare gold was the working electrode with the Ag/AgCl as a counter electrode. Varying dopamine concentrations were added after stabilization of the FSCV system and results plotted in MATLAB for analysis are given in **Figure 4.4** below. The oxidation peak of dopamine was observed in the region of 0.3 to 0.4 V whereas the reduction peak fell in the region of -0.1 to 0.1 V. As the concentration of dopamine was increased, the sensitivity of the system also increased since there are more dopamine molecules around the electrode double layer ready to oxidize.

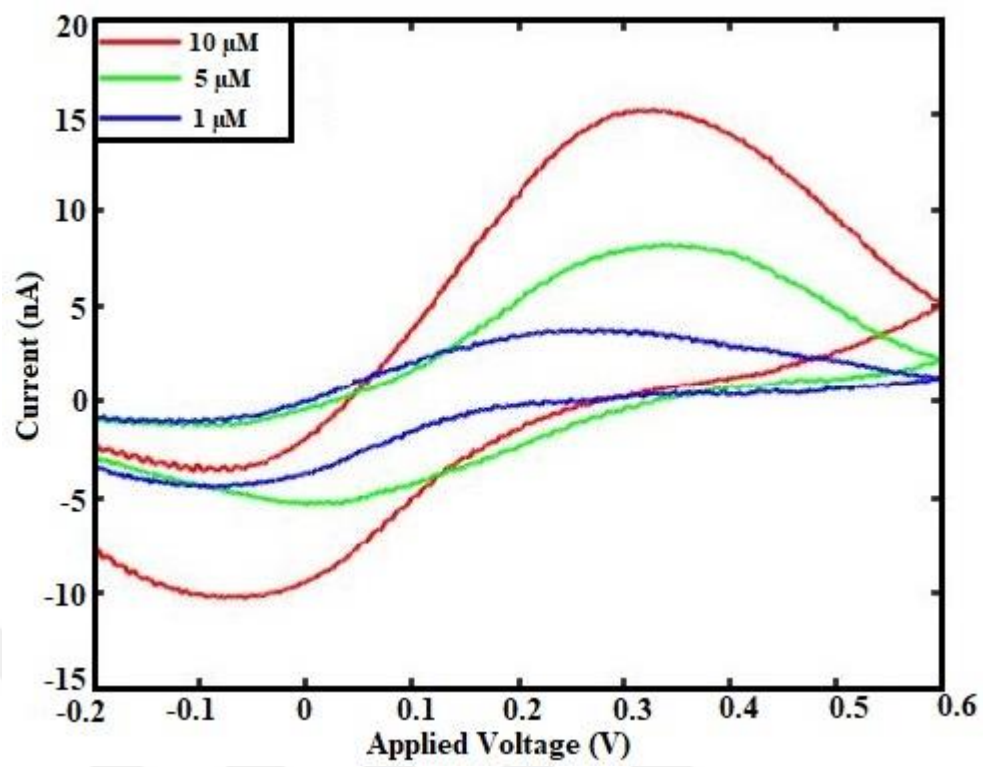


Figure 4.4: Detection of dopamine at different concentrations using bare gold electrode.

As the rate of oxidation increases, more electrons are lost from the increased dopamine molecules and a higher current is thus recorded. Under physiological conditions, the formed oxide monolayers around gold accelerate adsorption of cationic molecules i.e., dopamine through protonation [112]. Complementarily, the electrostatic forces between these protonated molecules and the negative holding potential on the microelectrode also increases adsorption [113]. With Flick's law, the observed peak currents from **Figure 4.4** above indeed confirm that peak currents for adsorptive electrolytes are linearly proportional to the number of electrons involved in the reaction (n) which is a direct relation to the concentration of the adsorbed electrolyte (Γ) as shown in equation (1) below [114]:

$$i_p = (2.69 \times 10^5)\, n^{3/2}\, A\, D_c^{1/2}\, v^{1/2}\, \Gamma \qquad \textbf{(4.3)}$$

where A is the electrode surface area, D_c is the diffusion coefficient and v is the scan rate.

Provided that the time is sufficiently short, and the dopamine concentration is kept constant in that given time of recording, the adsorption current become a time function [79]. The time taken between successive cyclic voltage waveforms recorded at which the system holds a constant potential greatly affects the amplitude of the dopamine species adsorbed on the electrode surface. Since the disease under study (Parkinson's disease)

leads to a decrease in dopamine concentration, it was important to work with a low dopamine concentration. However, to eliminate any systematic errors due to a possible poor baseline and to obtain more clear study results, basing on **Figure 4.4**, optimization of the next steps after deposition of the GO, SPEEK and ppy layers was performed with the 10 μM dopamine concentration.

By using Hamaker's law, the deposition yield is analyzed with consideration of different EPD parameters [115] in the equation below. An efficiency value (f) per experiment is included by linear regression of the coated mass [70], [116].

$$\frac{dW}{dt} = f\mu ECA \qquad \textbf{(4.4)}$$

where, w is coated mass (kg), t is coating duration (s), μ is electrophoretic mobility ($m^2(Vs^{-1})$), E is deposition potential (Vm^{-1}), A is the electrode's surface area (m^2), and C is the concentration of the solution (kgm^{-3}).

During electrochemical coating of the first surface, several conditions affect the overall sensitivity and morphology of the produced electrode. These include deposition potential, influence of a supporting electrolyte, concentration of the GO solution, and the deposition duration. Temperature is another vital condition to consider during electrochemical processes due to the fact that activation energy is lowered for molecules when the temperature rises. From literature however, it is explained that the rising temperature makes GO sheets unstable with sodium-based catalyst reactions and reduces its chemical properties by destroying the sp^2 structure [117]. However, GO is metastable at room temperature i.e., remains stable as long as minor disturbances in its structure are avoided [118]. For that case therefore, working under room temperature was the ideal working environment.

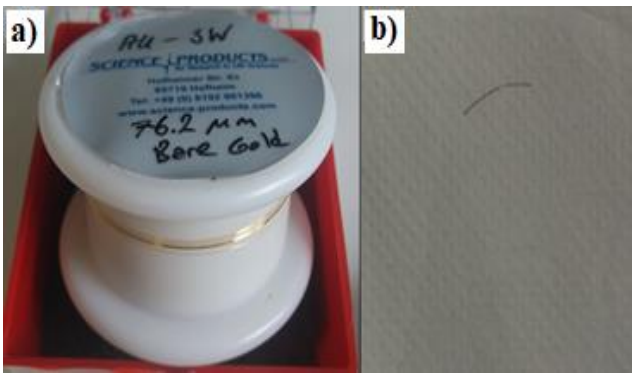
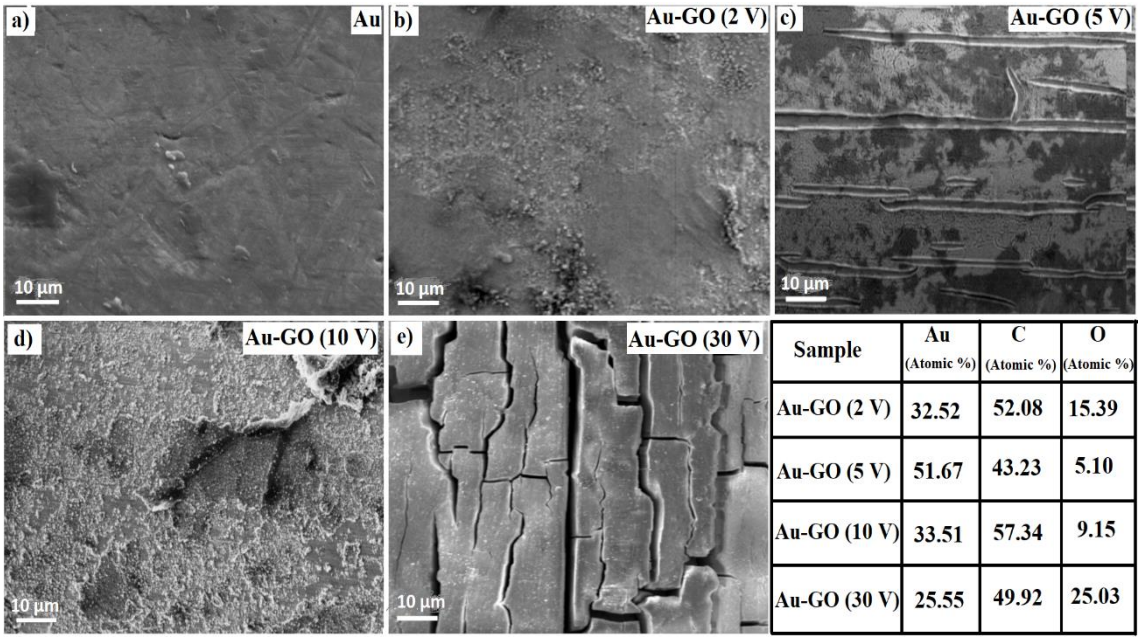


Figure 4.5: Uncoated gold wire and graphene coated electrode. **a)** 76.2 μL thick gold wire. **b)** Graphene coated gold wire.

Above we observe the effectiveness of GO deposition on the gold surface with a visible thin grey layer (**Figure 4.5b**) as compared to the smooth shiny uncoated surface (**Figure 4.5a**). With the success in deposition of GO, each parameter for the optimal sensing layer by this organic compound was then analyzed.

It would not be wrong to think that the higher the coating voltage value, the more GO will be deposited on the gold surface. However, with the increase in thickness on the surface, porosity, roughness, and surface cavities must be optimized to give the desired morphology. In addition, a high coating voltage can be used in a much shorter time, but it is necessary to examine whether these conditions will give the desired surface properties. Following up from the GO concentration of 0.5 mg/mL at room temperature, the gold electrode connected as the anode was coated for 1 h with the platinum as the counter electrode at various potentials of 2, 5, 10 and 30 V. After washing it in distilled water to get rid of excess residue on the surface and drying in the desiccator for 1 h, it was seen that a low potential allows a slow but maximized reduction of the oxygen-based groups in the GO structure while avoiding any structural damages (**Figure 4.6b-d**) caused by rapid evolution of oxygen gas at the anode. It was observed that when the voltage was raised, oxygen gas escape rapidly from the anode and this possibly caused the surface denaturation and deeper cavities with raise in deposition potential as seen in evidently in **Figure 4.6e** below.



Sample	Au (Atomic %)	C (Atomic %)	O (Atomic %)
Au-GO (2 V)	32.52	52.08	15.39
Au-GO (5 V)	51.67	43.23	5.10
Au-GO (10 V)	33.51	57.34	9.15
Au-GO (30 V)	25.55	49.92	25.03

Figure 4.6: SEM images (0.5 mg/mL, 1 hour, in distilled water) of GO coated Au electrode at different voltage values **a)** Bare Au, **b)** 2 V, **c)** 5 V, **d)** 10 V, and **e)** 30 V. EDX results of surface atomic composition (bottom right corner).

From the EDX results, the atomic percentages of the surface composition for each condition are given (in the attached table on **Figure 4.6** above), the C:O ratios at 2, 5, 10 and 30 V are 3.38, 8.48, 6.27 and 1.97, respectively. This indicates that the thickly coated layer at 30 V and the uniformly coated layer at 2 V seen to only have 25.55% and 32.52% of Au, respectively, at the surface have most of its GO sheets unreduced shown by the large oxygen content composition on the surface. A very low potential of 2V moderately reduces the GO sheets with C:O ratio of 3.38. It is well known that GO exists predominantly as a sp^3 compound making it very less conductive. Its conductivity is more realized in the reduced state where it partially regains the sp^2 structure by increasing the C:O ratio as seen by the 5 V (C:O of 8.48) and 10 V (C:O of 6.27). The high potential on the other side allows fast stacking of GO sheets during deposition whilst hindering reduction of the layers thus a C:O ratio of 1.97. This compositional variation at the surface was vital in optimizing both the required layer thickness and sensitivity using the FSCV technique.

With the high conductivity of GO, as its deposition thickness grows, the sensitivity is also expected to increase until the surface morphology is altered at 30 V where the reduction of GO sheets is hindered only giving a C:O ratio of 1.97. This makes most of the surface sheets of GO exist as sp^3 structures and lesser conductive as so does the effect observed at 2 V where not only the deposited layer is so thin but also having a low C:O ratio of 3.38. The electrical impedance of the deposited layer increases and simultaneously the electrophoretic deposition driving potential decreases, which makes the deposition yield tapered off reaching a maximum conductive deposition yield [70]. It was understood there after that as much as thickness of the deposited GO layer must be kept in check, the degree of reduction of that layer played a bigger role.

For the intended future implantation, a firmly coated electrode that may not peel off and introduce foreign bodies in the brain is favored, thus it was vital to select a coating potential as the primary condition upon which the conditions of concentration of GO and the deposition time would be decided. In the above study, the electrode failed to stabilize even after an overnight connection (oxidation and reduction peaks were seen to appear in the reverse order of the voltammogram phases which contradicts to voltammetry analysis). This may be attributed to a thick deposition of GO sheets over the prolonged time that probably makes them resistive. However, studies of various other supporting electrolytes were also required to understand the possible effect of the dissolved salts in

the GO and the pH of the solution used for coating. The 10 V deposition potential was chosen as the primary optimization parameter going forward. EDX results also show that we obtain more coating while maintaining a good carbon to oxygen ratio at 10 V with the C:O ratio of GO raised by over 6 folds.

4.1.1. Effect of supporting electrolytes

To this point, all studies were done in distilled water but it had been previously studied that different pH values of GO solution induce different zeta potentials which is a vital element in assessing the conductivity and particle sizes of materials in solution [119]. In this regard, three setups were arranged for 0.1 mg/mL of GO solutions. The initial solution in distilled water exists at an acidic pH of 3.90 (pH of the commercially available GO solution), the second was made by dissolving GO in 0.5 M NaCl solution and neutralized by 0.5 M KOH (pH 7.08), and the third was made by dissolving the GO in 0.067 M PBS and 0.5 M KOH was used to tune the pH to a basic 9.68. As the pH raised (more OH^- than H^+), the repulsion of the less acidic GO sheets by the electrons from the anode increases migrating and depositing the reduced GO sheets towards and onto the cathode [120]. The electrode connections were thus interchanged with gold used as the cathode and platinum connected to the anode at neutral and basic pH as summarized in **Table 4.2** below and a potential of 10 V is supplied for 15 minutes at room temperature.

Table 4.2: Arrangement of electrodes upon change of solution pH and varying supporting electrolytes mixed to make 50 mL solutions.

Sample	Chemicals	pH	Anode	Cathode
1	GO + distilled water	3.90	Gold	Platinum
2	GO + NaCl + (KOH to neutralize)	7.08	Platinum	Gold
3	GO + PBS + (KOH to make it basic)	9.68	Platinum	Gold

Zeta potential gives the magnitude of the negative charge around the particles in the solution due to ionization of the GO sheets' functional groups. The more the negative potential, the more the repulsion and vice versa. Ultrasonication for 30 minutes and bubbling nitrogen for 10 minutes at room temperature was performed after preparing of the solutions. The large size GO sheets in distilled water are in close proximity which results in an overlap interaction of adjacent GO sheets forming a uniform solution. Increasing the pH lowers the zeta potential thus the degree of attraction between particles increases leading to coagulation of the tiny GO particles. Using saline (NaCl) as a

supporting electrolyte introduces Na^+ that can attract the less remaining oxygen species (epoxy, hydroxyl) through physical charge attraction [119]. This is the interaction that occurs when metallic sodium is added to a GO solution with the OH^- ions acting in the ring-opening of the epoxy groups [121].

As more oxygen-containing species are attracted away from the GO sheets, the rate of reduction and formation of a sp^2 structure increases which would positively affect the surface conductivity. This results into highly activated GO sheets that stabilize themselves through reduction of the microscale particle size forming a mild brown less coagulated solution. The higher the zeta potential, the more the repulsive force between particles to resist any agglomeration and thus a more stable solution [122] having a more uniformly spaced profile within the beaker. The opposite is true when the zeta potential reduces forming a less stable solution with precipitates of GO but being more conductive and made up of very tiny, disintegrated GO sheets which would greatly impact the surface area after deposition. In that case therefore, stirring at 200 rpm was a necessity (mainly for coating solutions at neutral and basic pH**)**) to maintain the solution uniformity during the electrodeposition.

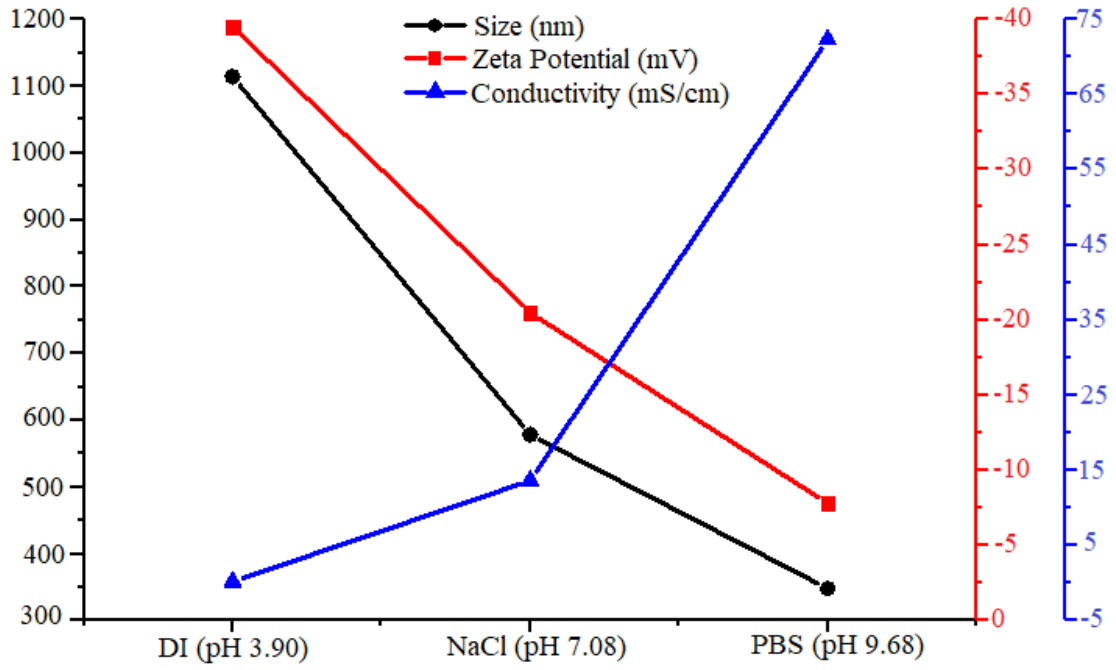
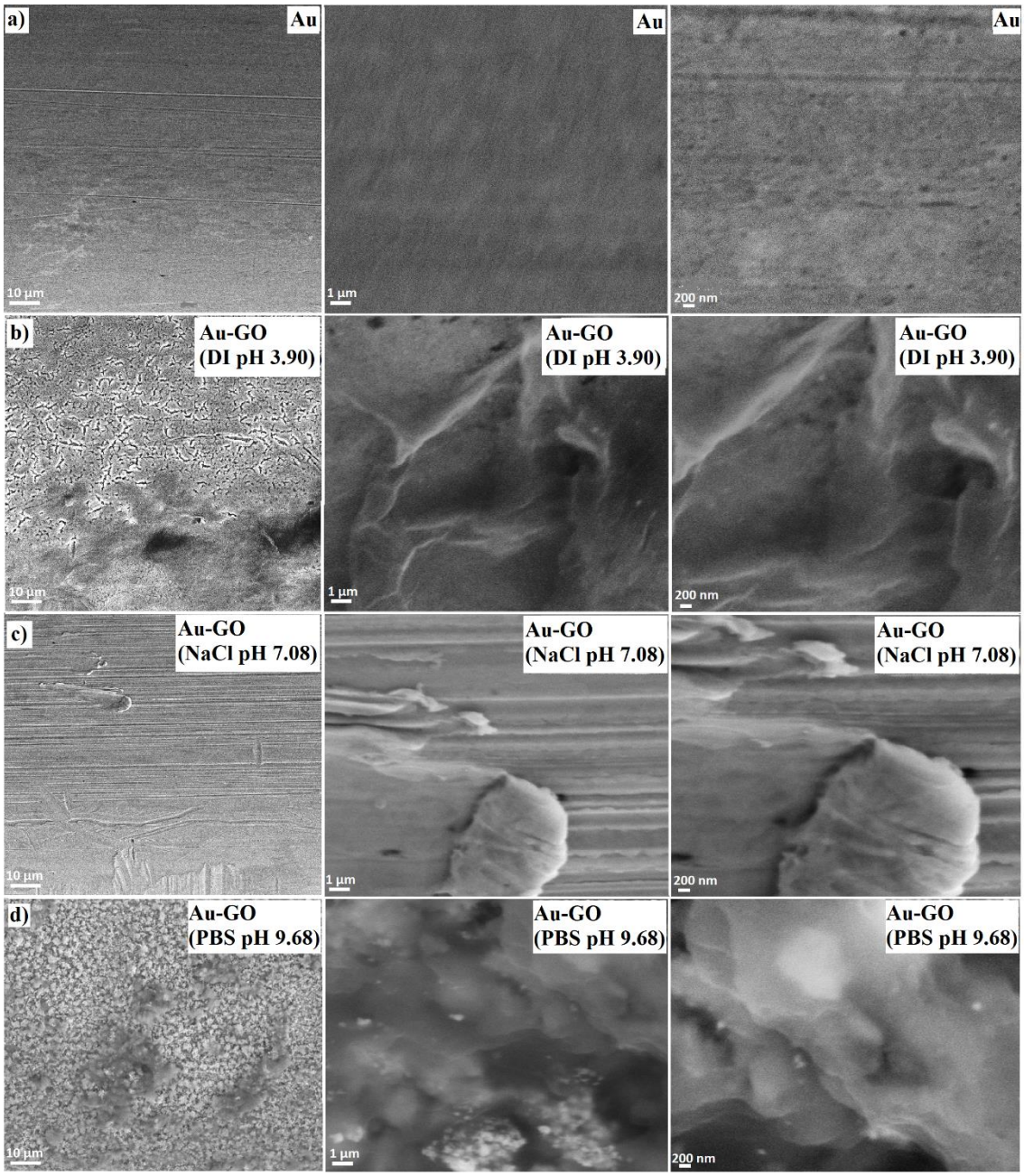


Figure 4.7: DLS results of GO in different supporting electrolytes of different pH.

Irrespective of the prolonged 1 h washing with distilled water after coating, minute quantities of conductive Na^+ may remain entrapped within the deposited GO sheets which may contribute to an elevation in the surface conductivity as compared to the GO

dissolved in distilled water. On the other hand, the highly disintegrated GO sheets at a pH of 9.68 in PBS offer an increased surface area upon deposition coupled with its greatly improved electrical conductivity by the pH rise as noted from the graph in **Figure 4.7** above. A high pH increases the concentration of OH^- ions whose strong negative charge may have repelled the negatively charged GO groups (-OH^-, -COO^-, and -O-), causing a phase separation in the solution and ultimately a precipitation of the highly conductive particulate GO sheets that are much readily reduced during electrodeposition. Given the poor conductivity of the large GO particles when dissolved in only distilled water (~2 mS/cm) noted in **Figure 4.7** above, this may have attributed to failure for the electrode to stabilize initially when a thick layer of it was deposited after 1 h. Even at 15 minutes of deposition, there was a notably longer stabilization duration in the FSCV study when the GO was at an acidic pH corresponding to this poor reduction potential.

The EDX data (attached to **Figure 4.8** below) also shows that the C:O ratio decreases with increase in pH with acidic pH having a ratio of 1.32, and neutral and basic pH having 9.91 and 1.56 ratios, respectively. The ultimate decrease in C:O ratio with PBS as a supporting electrolyte can be attributed to the inhomogeneity of the solution during deposition. The opened GO solution sheets can easily be electrically reduced and deposited forming a rough (at microscale) layer seen in **Figure 4.8** below. In the case of NaCl as a supporting electrolyte, the Na^+ ions act as catalysts through hydrogenation and more surface defects are formed due to the diffused epoxies from the negatively charged graphene sheets [123]. There is a notable firm and uniform high deposition roughness of the particulate GO sheets in the basic pH when using PBS which avails an increased surface area for anchoring of the dopamine molecules during the FSCV study and thus increase sensitivity.



Sample	Au (Atomic %)	C (Atomic %)	O (Atomic %)
Bare Au	100	-	-
Au-GO (DI pH 3.90)	27.52	41.31	31.17
Au-GO (NaCl pH 7.08)	46.97	48.17	4.86
Au-GO (PBS pH 9.68)	37.22	38.27	24.51

Figure 4.8: SEM images showing the effect of supporting electrolyte. **a)** Bare Au, **b)** Only distilled water, **c)** 0.5 M NaCl neutralized by 0.5M KOH, and **d)** 0.067 M PBS made basic with 0.5 M KOH.

The effect of the morphological variations and atomic composition on the sensitivity of dopamine (10 μM concentration) were performed using the FSCV and the results

presented below in **Figure 4.9**. The high C:O ratio at neutral pH while using NaCl as a supporting electrolyte showed a high reduction of the GO sheets which corresponds to the improved dopamine sensitivity of the surface as compared to the pH 3.90 solution in only distilled water. As the pH of the coating GO increased, not only did the sensitivity to dopamine increase but also the reduction peak shifts slightly towards the right (from the region of -0.05 V seen in bare gold detection to a region of 0.05 V), more evidently seen in the use of PBS in **Figure 4.9** below. This is in response to a decrease in the capacitive currents across the double layer as a result of the improved sensitivity.

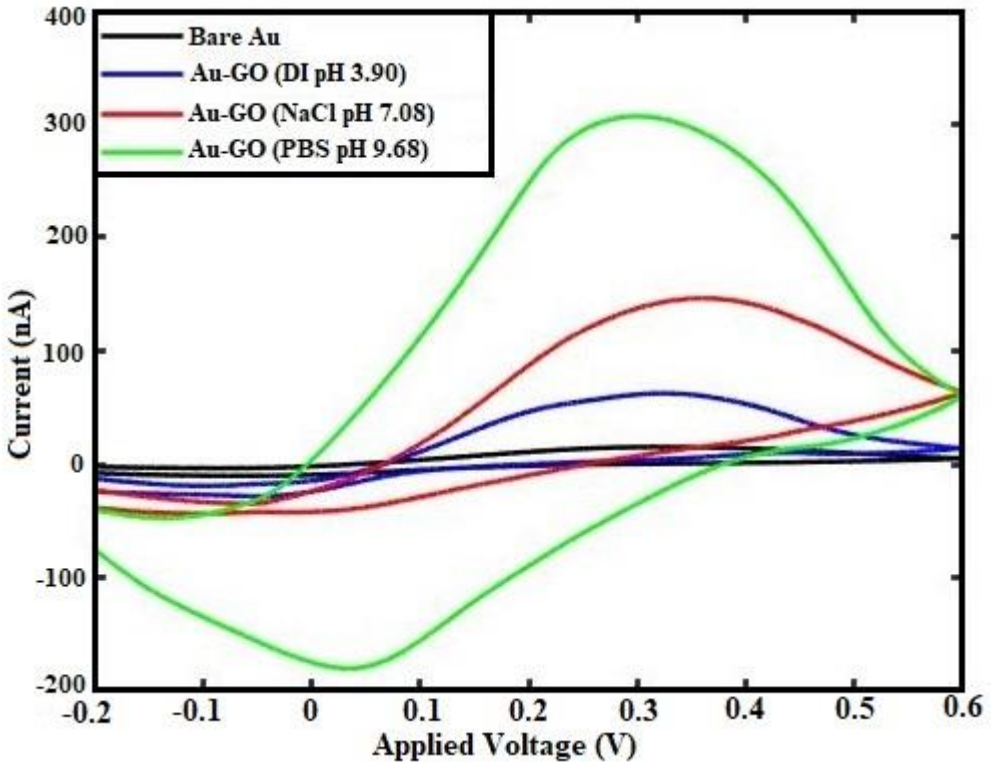


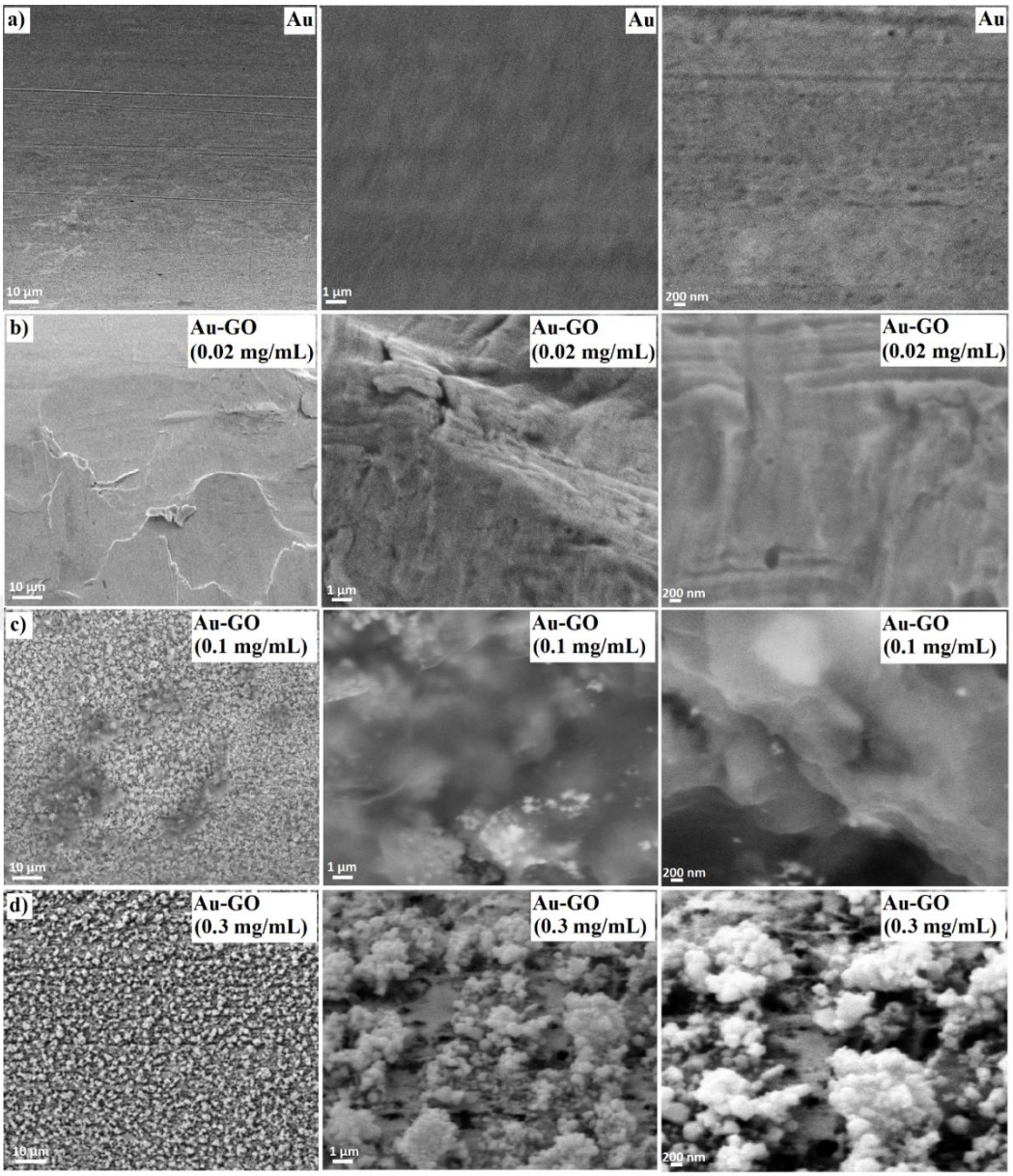
Figure 4.9: FSCV analysis using 10 μM dopamine solution showing the effect of supporting electrolyte. Only distilled water (green), 0.5 M NaCl neutralized by 0.5 M KOH (red), and 0.067 M PBS made basic with 0.5M KOH (blue) coated for 15 min.

The basic PBS noted a high conductivity in the DLS study (more than 15 folds higher than NaCl) with the high surface area particulate GO sheets. Both these factors contribute to the high sensitivity for dopamine seen in **Figure 4.9** above. It can also be noted that a basic PBS supporting electrolyte provided a GO surface that stabilized much faster than the counterparts. Regarding results in **Figure 4.9** and the clear layer-by-layer morphological outlay of the GO sheets while using basic PBS solution (**Figure 4.8d**), it was even more appropriate using it as the supporting electrolyte due to its additional sensitivity and fine morphology.

4.1.2. Effect of GO concentration

Theoretically, the high GO concentration reduces the electrolyte-electrode gap separation, thus allowing faster precipitation onto the electrode following the Hamaker's law [116]. In this case, negatively charged groups cause an unstable colloidal solution with GO sheets that repel each other to agglomerate and hence reduce the ability to deposit on the electrode surface [70]. Therefore, more agglomeration tendency is expected with the increase of GO concentration, and this situation affects the thickness and morphology of the layer formed on the electrode surface. By using the optimized voltage of 10V at room temperature for 15 minutes and platinum as the anode, the gold at the cathode is coated using various GO concentrations i.e., 0.02, 0.1 and 0.3 mg/mL while utilizing the neutralized PBS at a basic pH as a supporting electrolyte.

It can be seen in **Figure 4.10**, under the coating conditions that as the concentration increases, a thicker layer is formed on the surface, and it is seen that peeling from the surface begins with the increasing thickness as looser outgrowth of GO sheets developed. It has been observed that this situation decreases the stability and homogeneity of the coating and was expected to decrease the sensitivity during FSCV analysis. While the GO concentration was as low as 0.02 mg/mL, a thin and homogeneous layer was observed on the surface (**Figure 4.10b**). At 0.1 mg/mL, a smooth surface with fine pits was observed (**Figure 4.10c**). When the concentration continued to increase (**Figure 4.10d**), it was observed that the layers lost their homogeneity and formed thick clustered depositions at some regions of the electrode surface.



Sample	Au (Atomic %)	C (Atomic %)	O (Atomic %)
Bare Au	100	-	-
Au-GO (0.02 mg/mL)	44.79	49.72	5.48
Au- GO (0.1 mg/mL)	37.22	38.27	24.51
Au-GO (0.3 mg/mL)	46.76	38.24	15.00

Figure 4.10: Different GO concentrations. SEM images of Au-GO coated electrode at **a)** Bare Au, **b)** 0.02, **c)** 0.1, and **d)** 0.3 mg/mL GO concentration (10V, 15 mins).

From the SEM we indeed realize that the surface is more uniformly coated at the lowest concentration in **Figure 4.10b.** The deposition layer grows more with an increase in concentration to 0.1 mg/mL, with the surface less dominated by the Au atoms and more of the GO constituents. The 0.02 mg/mL concentration gave high C:O ratios of 9.07 since the rate of reduction is increased in the 15 minutes duration for the uniformly distributed

solution having less GO sheets. At this low 0.02 mg/mL GO concentration, the amount of deposited GO sheets is also few in the given time period to impact a huge surface modification as compared to 0.1 mg/mL in the same 15 minutes duration. However, the thick depositions at 0.3 mg/mL (**Figure 4.10d**) easily peel from the surface exposing back the gold surface (46.76%). The peeling provides loose contact between the charge conducting gold base and the surface in contact with the dopamine molecules (forming a rather resistive layer of exfoliated GO sheets). The slight raise in the C:O ratio of 2.55 at 0.3 mg/mL can be attributed to the increased reduction of the deposited layer once the outer layers start peeling off. More corrosion of this thick layer at a high GO concentration would be expected during the FSCV analysis and pose a toxicity threat in future implantation experiments. Even with a relatively low C:O ratio of 1.56 at 0.1 mg/mL, there seems to be a reasonably higher GO layer deposition (**Figure 4.10c**) with a more uniformly rough profile thus it was preliminary preferred in the morphology characteristics as the optimum to fabricate our desired electrode. Nevertheless, analysis with the FSCV shown in **Figure 4.11** below was required to ascertain the sensitivity variations imposed by these morphological changes.

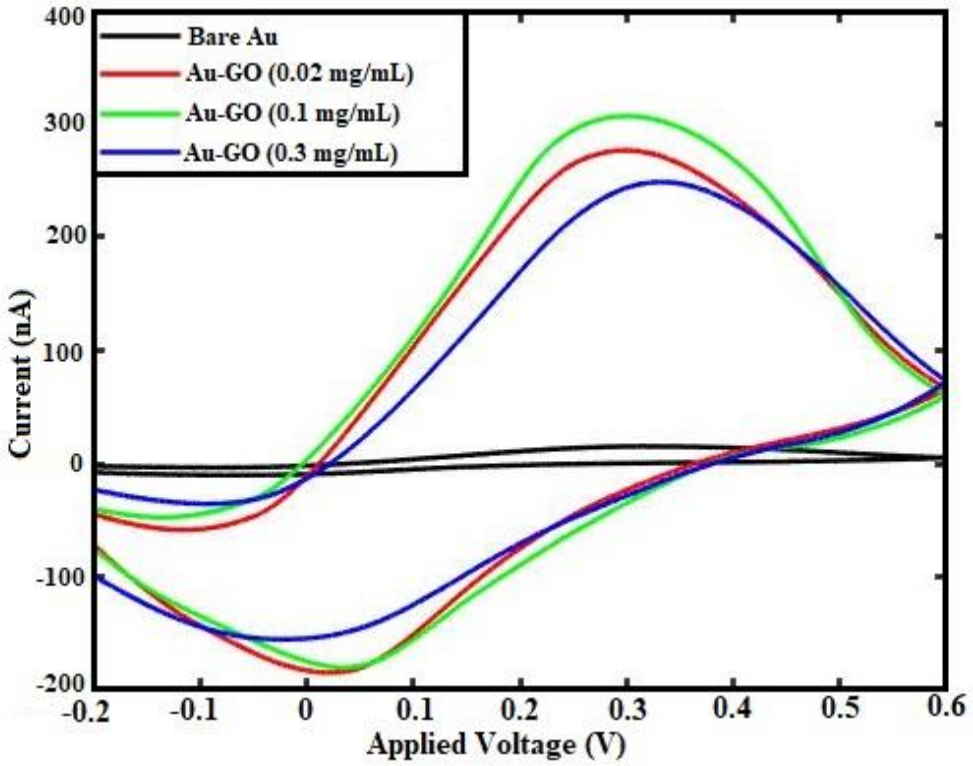
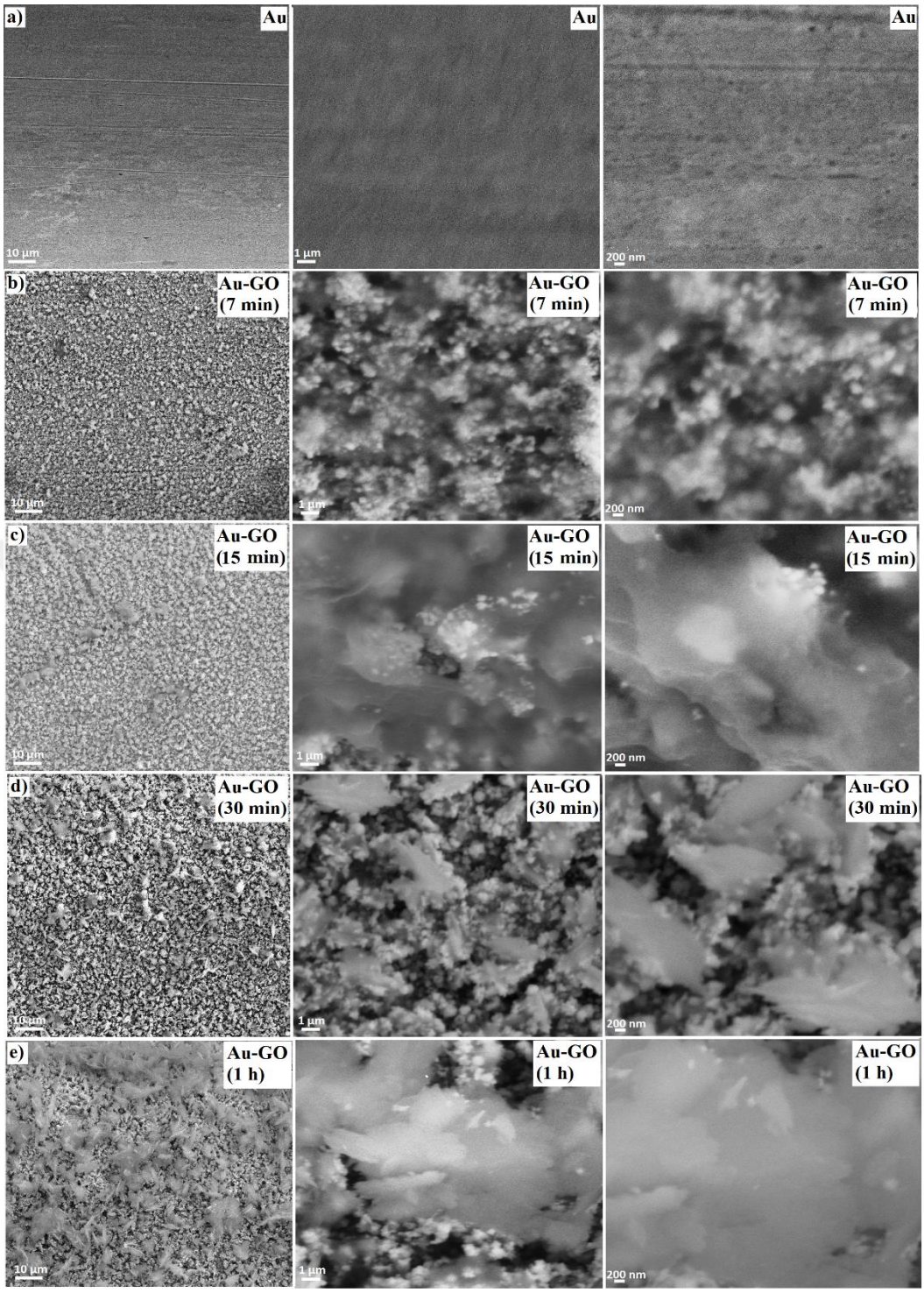


Figure 4.11: Voltammogram obtained with FSCV in 10 μM dopamine solution for Au electrodes coated for 15 mins at different GO concentration values. Deposition potential of 10 V.

When the performances of gold electrodes (Au-GO) coated in different GO concentrations were tested in dopamine solution with the aid of FSCV, it was observed that the highest sensitivity was obtained by electrodes coated with 0.1 mg/mL GO solutions at the (**Figure 4.11-green**). This stressed the previous results explained from the SEM results that 0.1 mg/mL offered the optimal GO concentration for the desired electro-reduction condition during fabrication.

4.1.3. Effect of deposition time

During electrochemical processes, the duration of exposure to the driving potential plays a significant role in determining how much of the electrolyte is deposited. By applying the previously optimized conditions i.e., potential of 10V, with a GO concentration of 0.1 mg/mL in PBS at pH 9.68 as a supporting electrolyte at room temperature, the gold at the cathode was coated for different time periods of 7, 15, 30 minutes, and 1 h while using the platinum as the working electrode in the 2-electrode system. The effect of the various deposition duration on surface morphology is given in **Figure 4.12** below. The performance of the deposited layer was greatly dependent on the thickness vs. degree of reduction relationship. After 7 minutes of coating time, a fine, rough but homogeneous surface was obtained (**Figure 4.12b**). When the coating time was increased (**Figure 4.12c-d**) the coating thickness increased gradually, and a relatively homogeneous surface was still seen with an increased outgrowth of loose GO sheets noted on the surface. The SEM images show that more GO deposition is realized with longer deposition time, and the surface loses the exposure of any gold.



Sample	Au (Atomic %)	C (Atomic %)	O (Atomic %)
Bare Au	100	-	-
Au-GO (7 min)	42.45	39.25	18.30
Au-GO (15 min)	37.22	38.27	24.51
Au-GO (30 min)	35.03	29.00	35.97
Au-GO (1 h)	26.23	23.92	49.85

Figure 4.12: SEM images of Au-GO coated microelectrodes at different coating times. **a)** Bare Au, **b)** 7, **c)** 15, **d)** 30, and **e)** 60 min.

The EDX elemental mapping showed that the 7 min duration allowed a very thin and uniform deposition which helped to increase the C:O ratio to 2.15 of the few sheets on the surface. The other durations gave C:O ratios of 1.56, 0.81 and 0.48 for 15, 30 and 60 minutes, respectively. The decreasing C:O ratios displayed a decrease in GO reduction which is vital in regaining the sp^2 structure that improves the layer's conductivity. The surface is however more coated with less gold exposed as duration of deposition increased in the order 42.45%, 37.22%, 35.03%, and 26.23% of surface gold exposed for 7, 15, 30, and 60 minutes, respectively. In general, it can be noticed that all the durations under study were sufficient enough to deposit a GO layer thickness for an improved dopamine detection in comparison to bare gold as seen in **Figure 4.13** below.

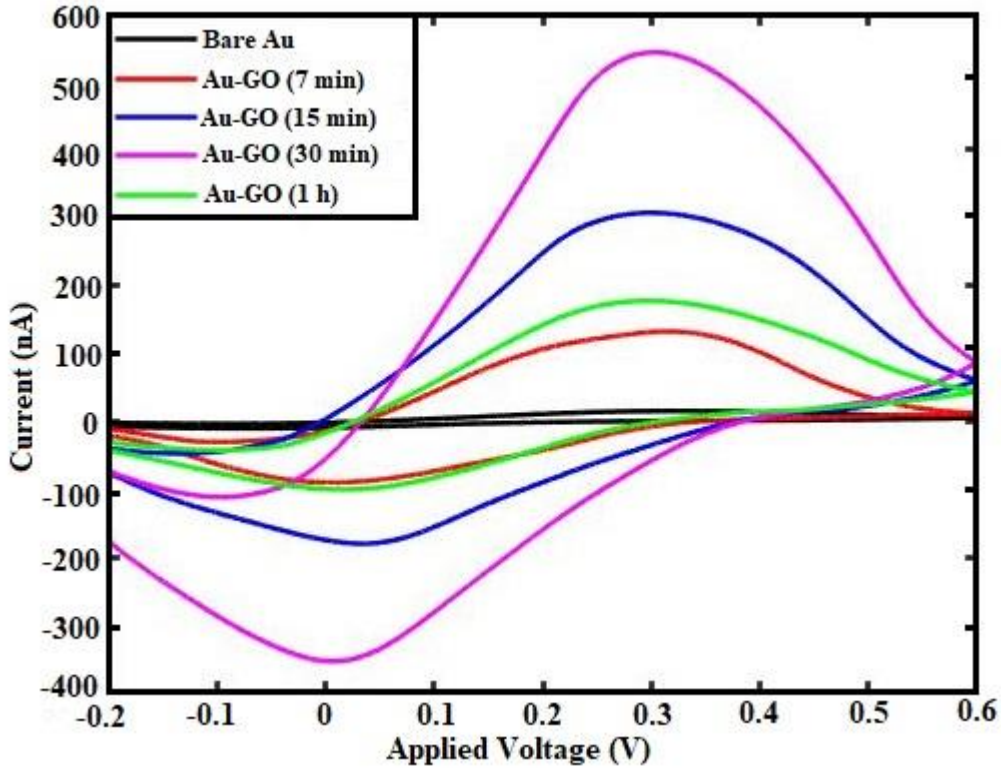


Figure 4.13: FSCV voltammogram obtained at different coating times with 10 μM dopamine solution of Coated Au electrodes at 0.1 mg/mL GO concentration (10V deposition potential).

It is evident that the deposition yield is directly proportional to the EPD time until an optimal plateau where the surface becomes resistive to further GO deposition. The high deposition of the conductive GO sheets initially outweighs the effect of their less reduction until a plateau where the latter provided an effect that overtook and lowered the sensitivity. This high yield observed in **Figure 4.12d** and the low C:O content on the surface in the EDX results, increases the electrical resistance of the GO sheets further

from the gold base and thus lower sensitivity [70], [115]. Following the SEM (**Figure 4.12**) and FSCV (**Figure 4.13**) results above, the 30 minutes deposition time was used for GO deposition to render optimal sensitivity and a firm surface morphological structure.

For that reason, therefore, the GO deposition step was optimized for conditions of 10V as deposition potential, 0.1 mg/mL GO concentration dissolved in 0.067 M PBS solution and made basic by 0.5 M KOH (i.e., pH 9.68) with nitrogen bubbled through this solution before electrodeposition for 30 minutes at room temperature. As the primary function of any sensing platform, the level of sensitivity was optimized first and then an important factor for any possible *in-vivo* system; toxicity effects of biomaterials, was tackled by a second layer of SPEEK discussed as follows in the **Chapter 4.2** below.

4.2. Sulfonation of Poly(ether ether ketone) (PEEK) -SPEEK

Firstly, it was planned to coat the surface of the graphene-coated electrodes (Au-GO) with a second layer of PEEK to make them more biocompatible. PEEK exists as water-insoluble brown pellets that cannot be utilized in chemical reactions in this raw state. To ensure the solubility of this polymer in water, the ionic sulphate groups ($-HSO_3^{2-}$) must be introduced in the structure as seen in **Figure 4.14** below.

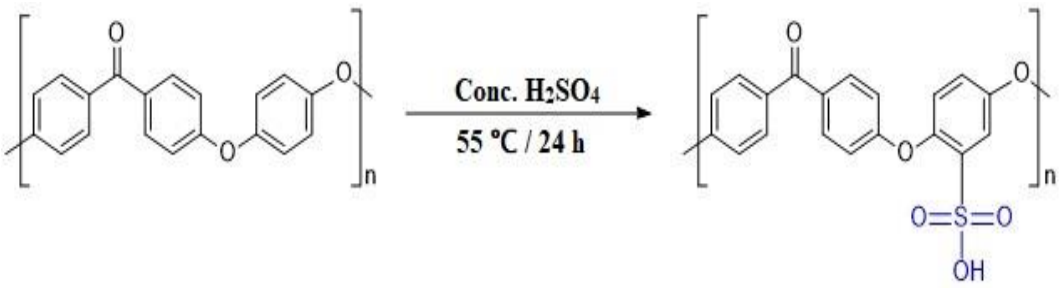


Figure 4.14: Schematic for the sulfonation of PEEK to form SPEEK.

For the microelectrode, the $-HSO_3^{2-}$ group is not only a group that provides solubility, wettability, high antifouling capacity, and more perm-selectivity to the PEEK, but also has a feature that minimizes the interaction of negatively charged components with the electrode surface, thanks to its negative charge [17]. Various studies in the past have elaborated nafion as a good alternative for selective detection of dopamine as it gives unique detection peaks for each of the neurotransmitters [92], [124], [125]. In the same regard, SPEEK for example, helps repel negatively charged ascorbic acid, whose spectrum is known to overlap with dopamine, from the electrode surface hence allowing

more selectivity to the target neurotransmitter of the study [80]. Increase in molecular weight, however, reduces the water uptake ability of the polymer forming more viscous solutions at 100 kDa as compared to the 10 kDa sample that forms a clear solution. The preparation was done with 5g of PEEK added in a beaker containing 100 mL of concentrated sulfuric (at 700 rpm, 55 ℃) for 5 hours. The obtained clear brown solution was added dropwise to ice-cold distilled water to form pellets and get rid of the excess sulfuric acid solution before drying them for 24 h in a desiccator. The higher the molecular weight, the less viscous the solution obtained for dip coating upon dissolving the produced white pellets of SPEEK in distilled water for 24 h (at 700 rpm, 37 ℃) as seen in **Figure 4.15** below.

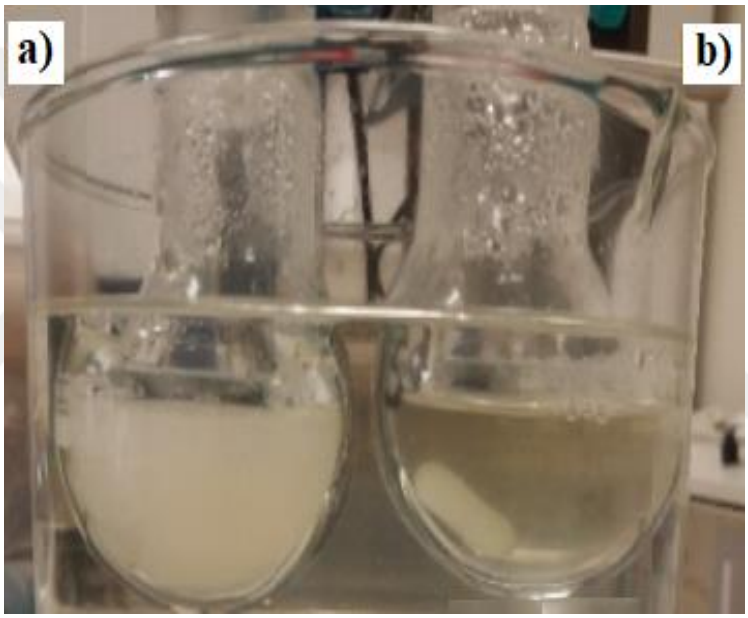


Figure 4.15: Solubility of SPEEK in water **a)** 100 kDa and **b)** 10 kDa at 700 rpm 24 h of stirring at 37 ℃.

After successful dissolution of the produced SPEEK samples, the characteristic peaks of the -HSO_3^{2-} groups were clearly observed for both molecular weights using the Fourier-Transform Infra-Red spectroscopy (FTIR) (**Figure 4.16** below). A new adsorption band of both symmetric and asymmetric -HSO_3^{2-} group is introduced upon sulfonation at a wavelength of 1255 cm^{-1} for the former while at 1020 cm^{-1} and 1080 cm^{-1} for the latter. The C=O bond at 1651 cm^{-1} is prominent due to the substitute group from sulfonation. The peaks between 450 cm^{-1} and 800 cm^{-1} stretch further after sulfonation as a result of the interaction between water and the substituted sulfonic group on the aromatic ring. The O-H vibration from the -HSO_3^{2-} group assigned at 3460 cm^{-1} further ascertains the successful sulfonation of PEEK. Similar results were reported by Xing *et al.* [126].

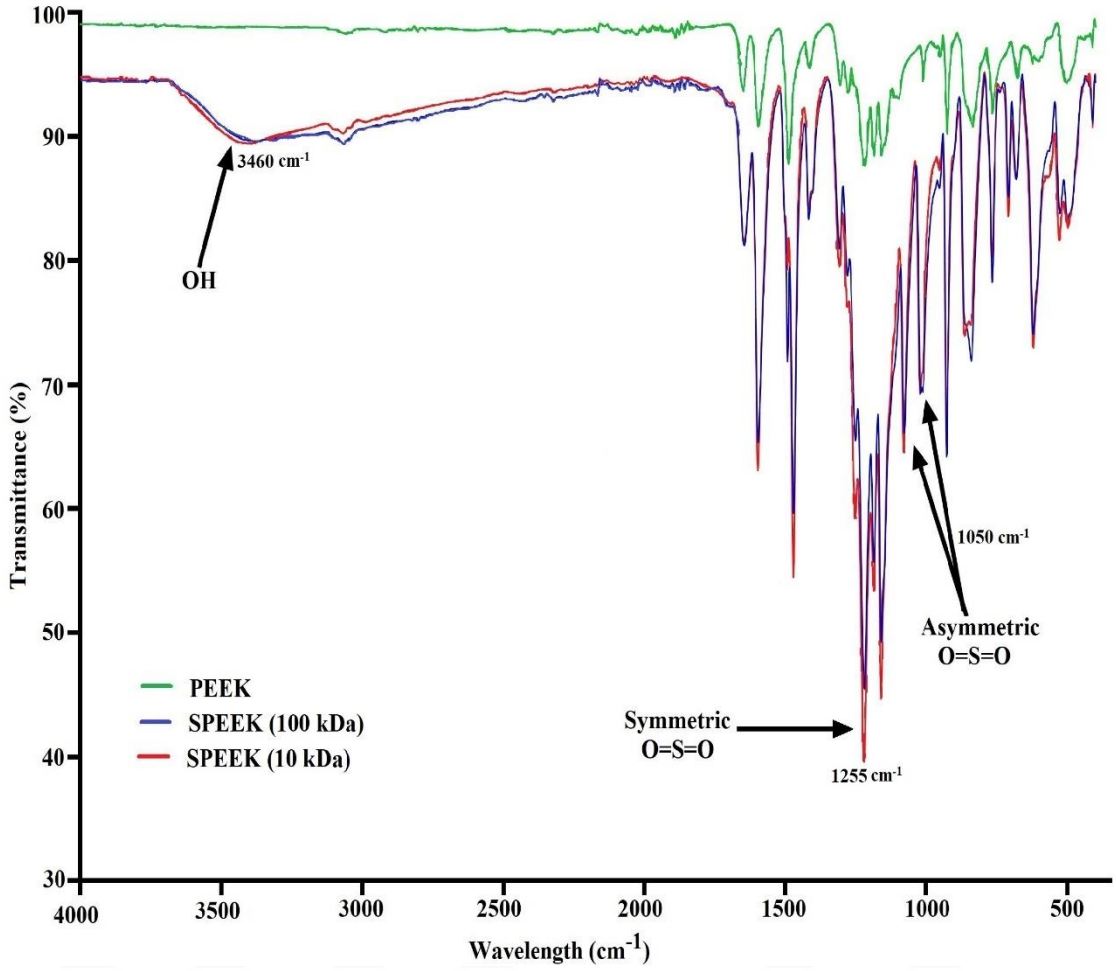


Figure 4.16: FTIR analysis for PEEK and SPEEK.

^{1}H-NMR was used not only to check the structural accuracy but also to calculate the degree of sulfonation of the PEEK. The labelled H_e, H_d and H_i in **Figure 4.17a** in the latter ^{1}H-NMR spectrum of 100 kDa are more prominent as compared to those of the former 10 kDa in **Figure 4.17b** due to the increased number of -HSO_3^{2-} groups. From the ^{1}H-NMR graph, the peak intensity of the distinct hydrogen (H_g) to the integrated intensities of the remaining hydrogen peaks ($\Delta(Hb, Ha, He, Hf, Hc, Hd)$) gives the value of degree of sulfonation (D^s) given below [127]:

$$\frac{D^S}{(11-2(D^S))} = \frac{\Delta Hg}{(\sum\Delta(Hb,Ha,He,Hf,Hc,Hd))} \text{ x } 100\ \% \qquad \Delta - \text{Spin intensity} \qquad \textbf{(4.5)}$$

In the formular above, 11 is the number of hydrogen atoms inside the pyrrole ring and 2 on the D^S value in the denominator is the result of the two SPEEK monomers that can attach on either side of the ring. D^S was calculated as 72.56% and 86.41% for the polymer with a molecular weight of 10 kDa and 100 kDa respectively, and both values were sufficient to impart water solubility to the SPEEK polymer.

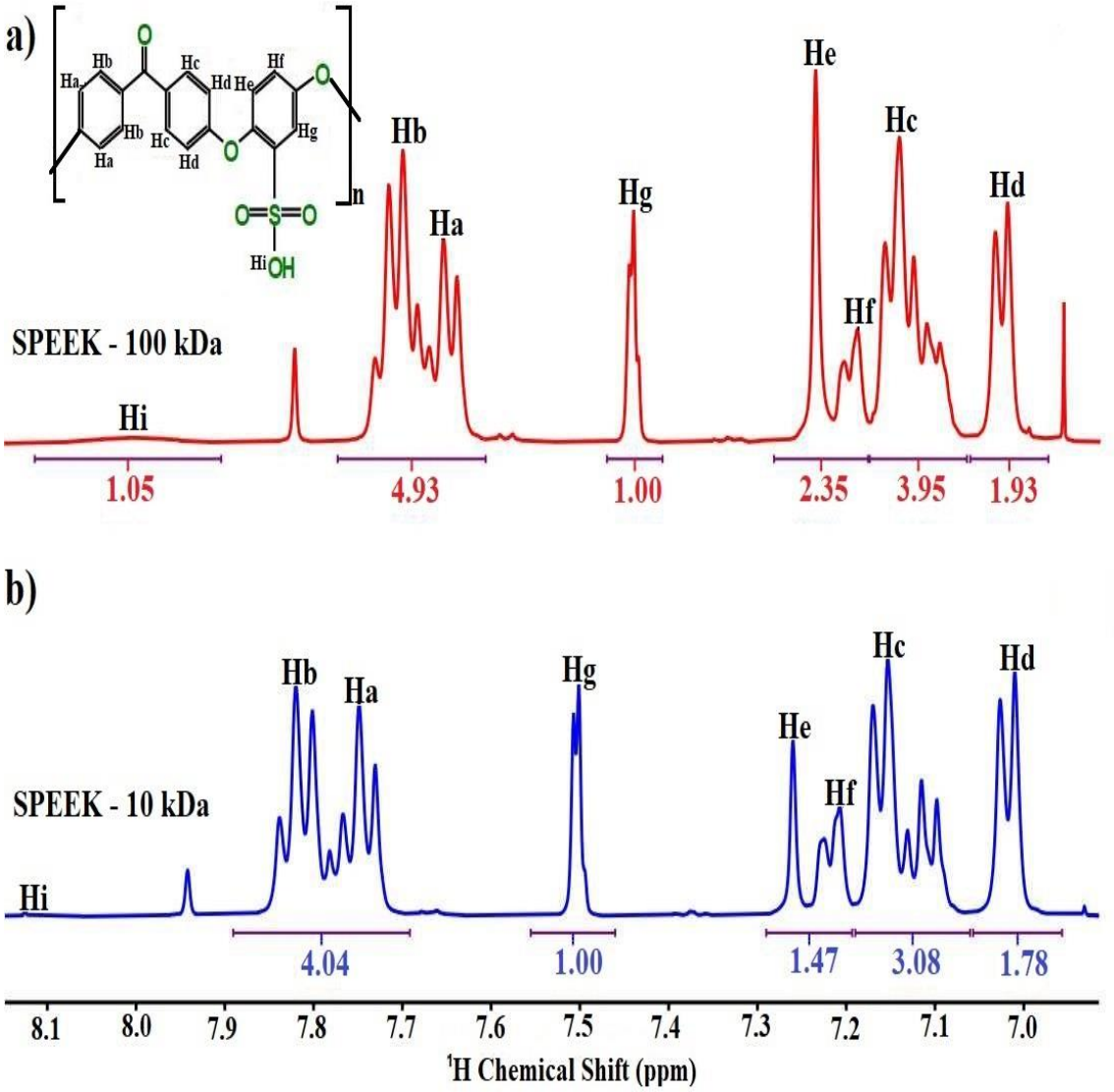


Figure 4.17: ^{1}H-NMR spectrum of **a)** 100 kDa and **b)** 10 kDa SPEEK sample.

The thermogravimetric analysis (TGA) in **Figure 4.18** below further confirms that more functional groups (due to -HSO_3^{2-}) are present within the 100 kDa chain because of increased sulfonation hence having more decomposition of the polymer mass at higher temperature in the analysis.

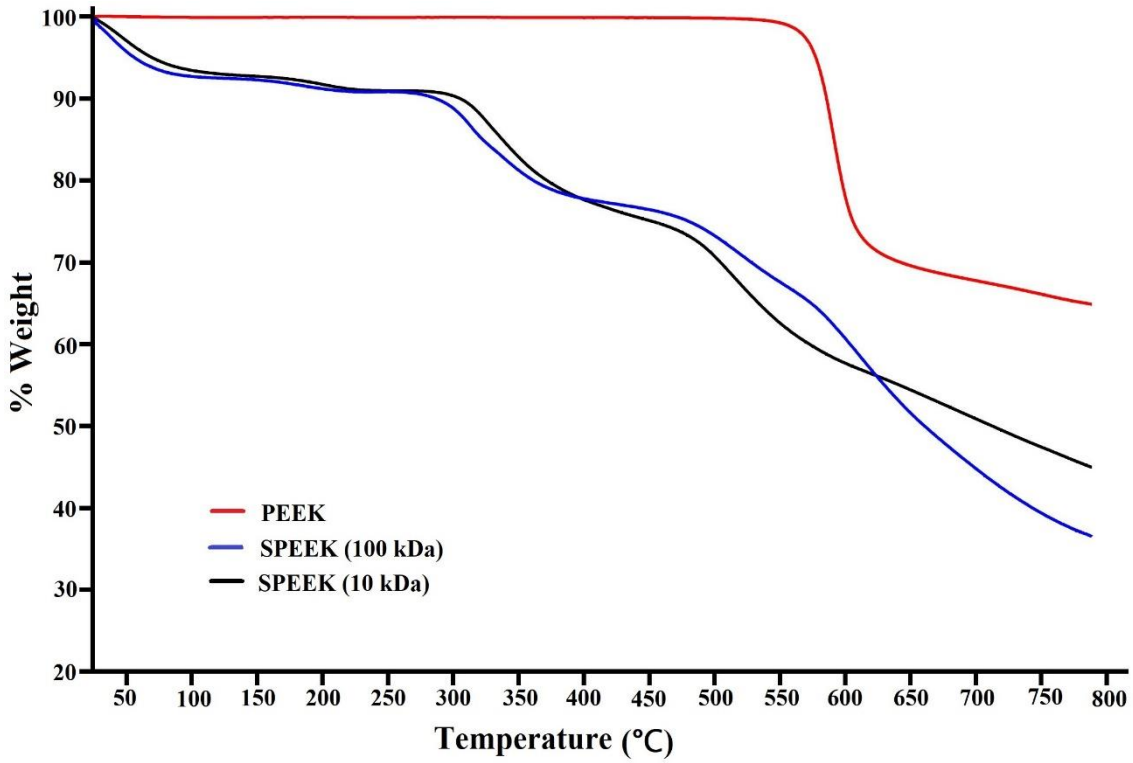


Figure 4.18: Thermogravimetric analysis of SPEEK.

SPEEK (100 kDa and 10 kDa molecular weights) were then deposited on the previously graphene coated gold electrode to mainly improve the electrode's biocompatibility after implantation. With sensitivity improved by the GO layer, among other values are that SPEEK improves thermal stability and mechanical properties of the sensitive surface. To deposit the SPEEK layer, two procedures were followed: electrochemical deposition i.e., using a potential to deposit the dissolved SPEEK; and dip coating where the electrodes are freely suspended into the SPEEK solution. In the following **Chapter 4.3 - 4.4**, the processes are further discussed and their overall effect on the performance efficiency of the Au-GO electrode.

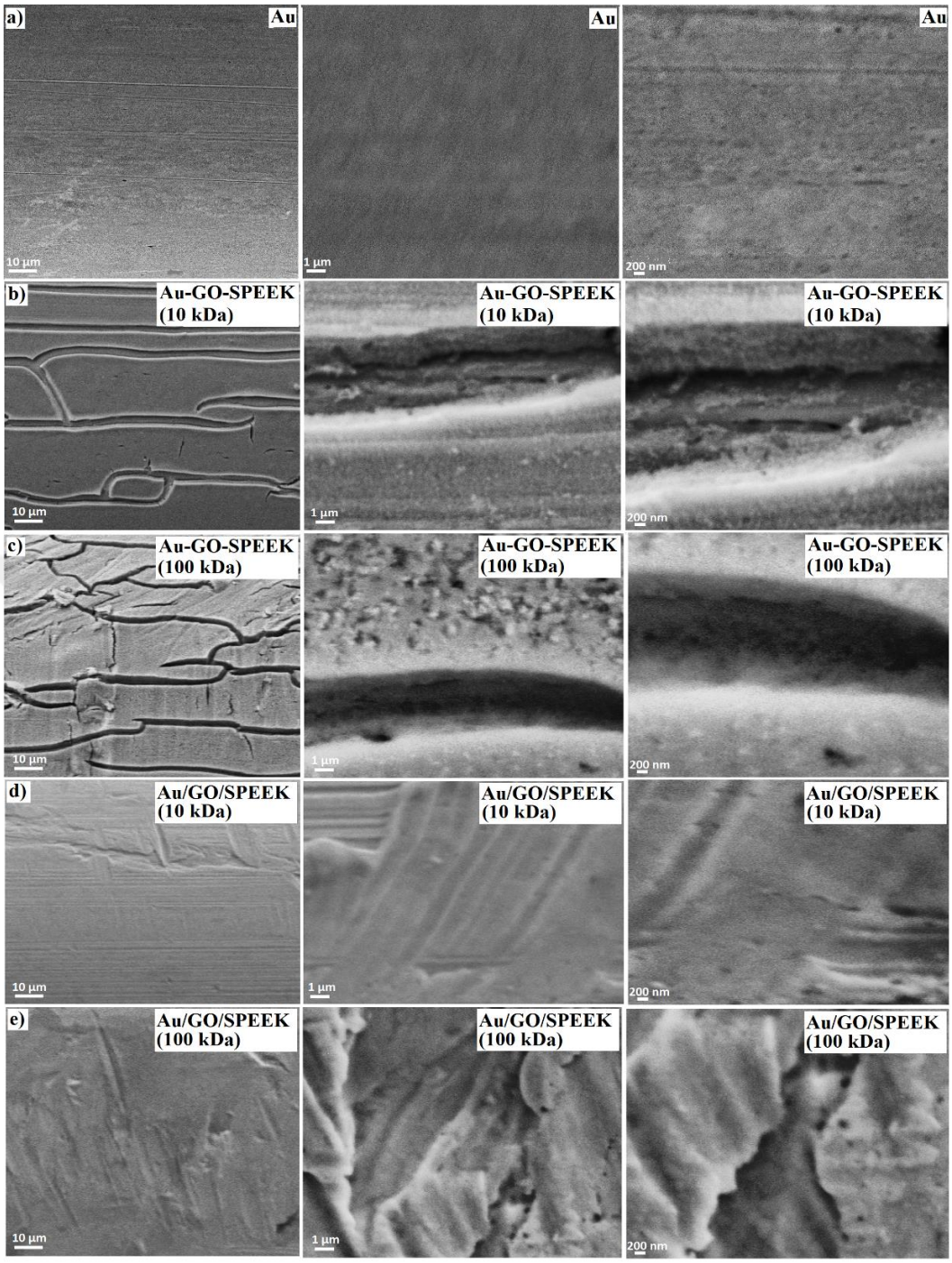
4.3. Electrochemical SPEEK Deposition on Graphene-Coated Gold Electrode (Au-GO-SPEEK)

By electrochemical means, a layer of the negatively charged SPEEK polymer due to the introduced HSO_3^{2-} group from sulfonation, is deposited at the positively charged anode where the graphene coated gold electrode (Au-GO) is connected and the platinum as the counter electrode. The layer thickness must be favorable enough to maintain optimal proton conductivity in the dopamine solution during FSCV studies. On that note therefore, 0.5 M SPEEK (10 kDa and 100 kDa) was coated for a duration of 15 minutes

at room temperature using 10V potential. There were two procedures followed during the process: - consecutive coating where the gold is initially coated with 0.1 mg/mL GO, washed and dried then 0.5 M SPEEK electrodeposited on top of that surface. - simultaneous coating where both 0.1 mg/mL GO and 0.5 M SPEEK solutions were mixed, and the solution used as the electrolyte in the prior explained setup at room temperature.[1] The latter helped in explaining the possible synergistic effect co-deposition of GO and SPEEK. It was assumed that in such a situation, the more conductive material would preferably be more deposited whereas allowing just enough of the other compound to maintain all the functionalities of sensitivity, biocompatibility, mechanical strength, and thermal stability on the gold surface as desired.

The process of SPEEK coating onto an electrode is very rapid and leads to a firm dark-brown film within 15 minutes. SPEEK is known to be electrically conductive and previously used in dopamine-sensitive electrodes [17], [18], [65]. Consecutive electrocoating (Au-GO-SPEEK) of high molecular weight SPEEK (100 kDa) onto the GO surface forms clearly very thick non-uniform layer-by-layer profiles in **Figure 4.19c** which eventually tend to peel off. In relation to the EDX results (attached table on **Figure 4.19** below), in consecutive deposition (Au-GO-SPEEK), the gold surface is more coated (only 27.26% exposed on the surface) while using 100 kDa of SPEEK and more sulfur derived from the SPEEK was almost constant for both molecular weights of SPEEK. This indicated more efficiency in terms of SPEEK electrodeposition. **Figure 4.19e** below shows that a more uniform and stable deposition is obtained with simultaneous deposition (Au/GO/SPEEK) of GO and SPEEK on the electrode surface. With a reduction in the electrophoretic mobility of the solution at a high molecular weight of SPEEK, the mass transfer of the GO and SPEEK for deposition is greatly hindered and the more conductive GO sheets got the preference forming thick GO predominant layers. However, increasing the molecular weight of SPEEK forms a very thick deposition that may hinder surface sensitivity as it might gradually peels off (**Figure 4.19e**). The deposition efficiency of either solution used would hugely be affected by the electrophoretic mobility when a coating potential is supplied.

[1] A-B-C representation indicates that A was coated consecutive with B and then followed by C. A/B/C representation indicates that A was simultaneously coated with a mixture of B and C.



Sample	Au (Atomic %)	C (Atomic %)	O (Atomic %)	S (Atomic %)
Bare Au	100	-	-	-
Au-GO-SPEEK (10 kDa)	30.39	38.22	30.71	0.08
Au-GO-SPEEK (100 kDa)	27.26	40.15	32.49	0.09
Au/GO/SPEEK (10 kDa)	46.81	48.98	4.14	0.09
Au/GO/SPEEK (100 kDa)	51.84	38.71	8.85	0.60

Figure 4.19: SEM images of microelectrodes coated with both GO and SPEEK using electrodeposition. **a)** Bare Au, **b)** Au-GO coated consecutively with 10 kDa SPEEK, **c)** Au-GO coated consecutively with 100 kDa SPEEK, **d)** Au coated simultaneously with GO and 10 kDa SPEEK, and **e)** Au coated simultaneously with GO and 100 kDa SPEEK.

These thick unstable depositions are known to reduce the general microelectrode sensitivity as seen in **Figure 4.20** below.

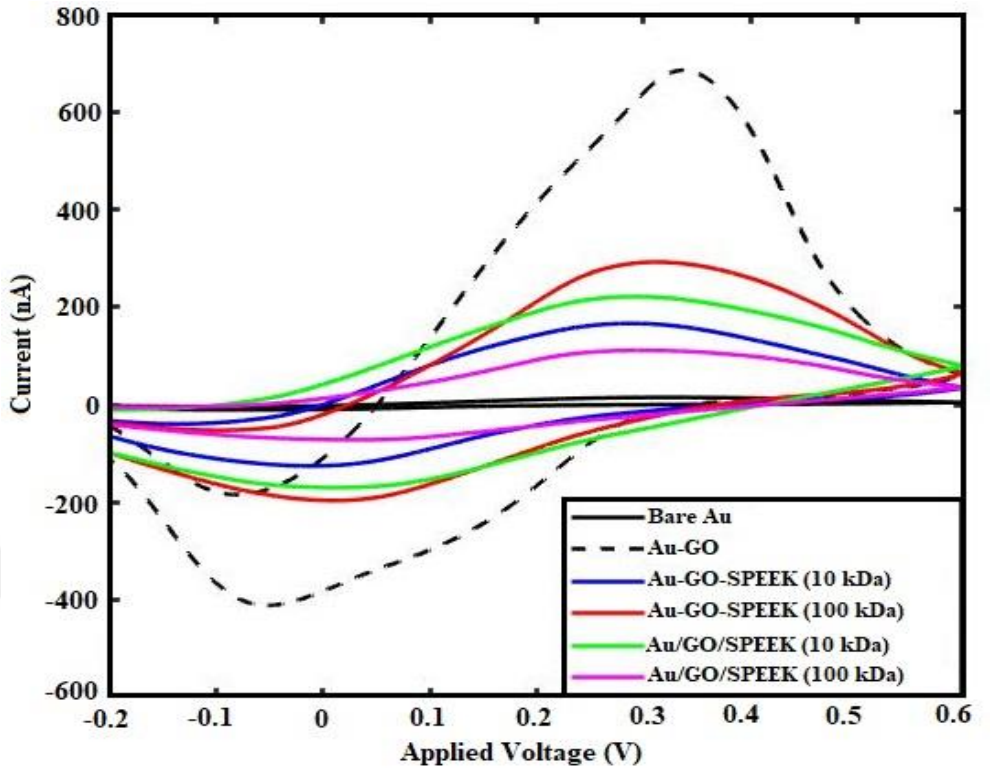


Figure 4.20: FSCV analysis of the Au microelectrode electrically coated with GO and SPEEK using 10 μM dopamine.

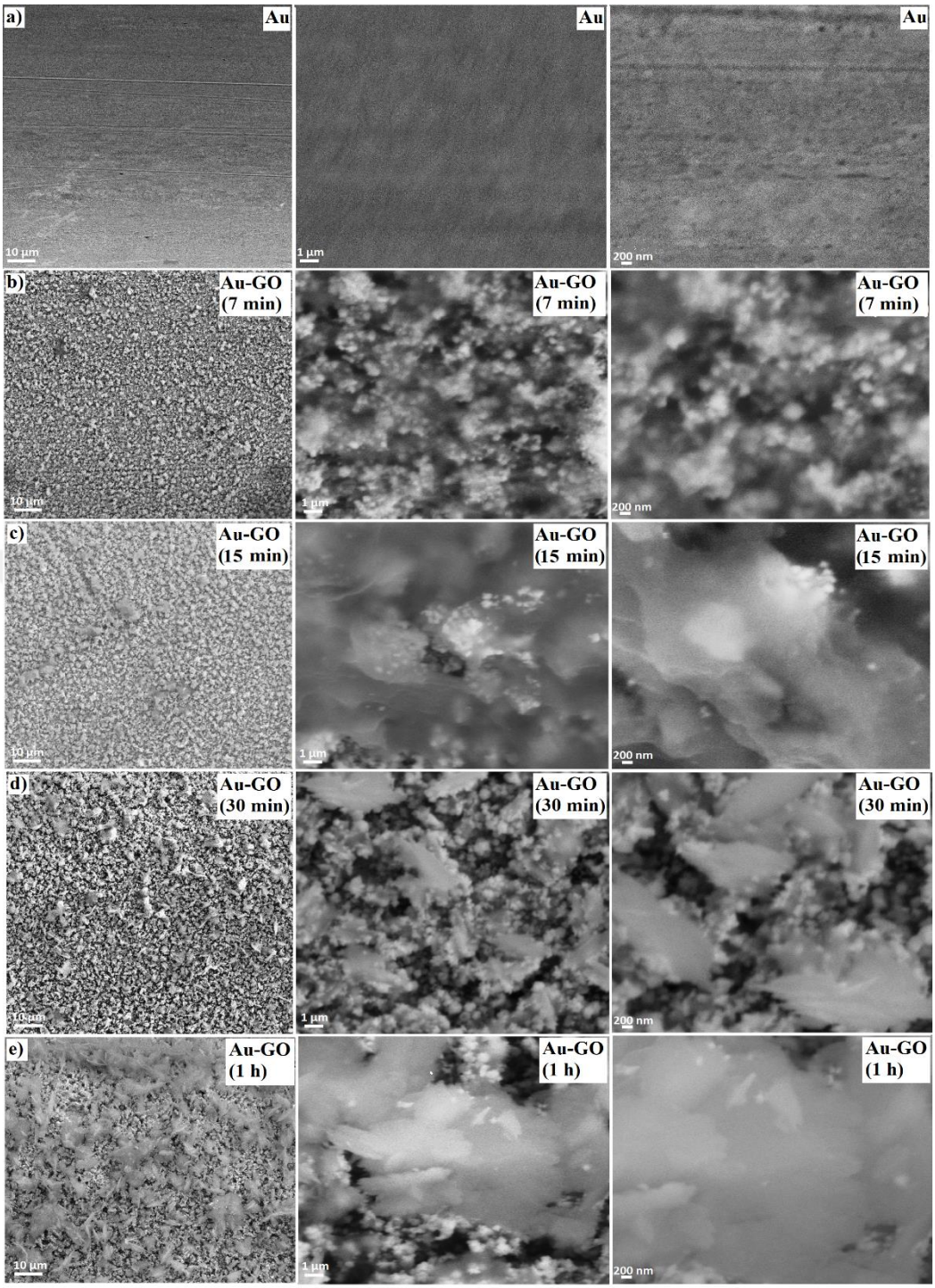
During consecutive coating (Au-GO-SPEEK), the dense 100 kDA molecular weight SPEEK is less deposited on the surface (0.09%) due to its poor mobility hence the previously coated highly conductive rough GO sheets dominate the surface to maintain a relatively higher sensitivity. Lowering the molecular weight to 10 kDa increases the mass transfer thus deposition of more SPEEK layers onto the Au-GO surface which further depreciates the dopamine sensitivity. On the other hand, the increased electrophoretic mobility of the solution (in relation to Hamaker's equation) during simultaneous coating (Au/GO/SPEEK) with 10 kDa SPEEK favors the GO such that the deposited layer is made up of less SPEEK (0.08%) and more highly conductive GO layers that increase the sensitivity towards dopamine. During simultaneous deposition of both GO and SPEEK, the effect is mainly seen in the changes of the degree of reduction of the surface deposition. PEEK has a large C:O ratio of 3 after complete sulfonation of its monomer which increases the oxygen content in the solution. The 100 kDa SPEEK may not be deposited in sufficient quantities because of its low mobility but it lowers the degree of reduction of the dissolved GO during electrodeposition thus a reduced conductivity (from

C:O ratio of 11.83 for 10 kDa to 9.13 for 100 kDa). For both molecular weights, simultaneous coating as compared to consecutive offers better sensitivity for dopamine. It can however be seen that consecutive electrodepositing 100 kDa SPEEK on Au-GO not only has a higher electro sensitivity for dopamine (**Figure 4.20 – red**), but also has a firmer and uniform distribution of the thick GO-predominantly composed layer (**Figure 4.19.c** above), and with moderate sulphate groups from the SPEEK (0.09 %).

4.4. Dip Coating of SPEEK on Graphene-Coated Gold Electrode (Au-GO-SPEEK)

Another method of introducing the mechanical strength and thermal stability-influencing biocompatible SPEEK layer was through $\pi - \pi$ stacking onto the GO sheets through direct dipping of the graphene coated gold electrode (Au-GO) in the SPEEK solutions at minimal 250 rpm stirring. Two durations were considered to understand the influence of the standing time during $\pi - \pi$ interaction of the GO and SPEEK layers (15 and 130 minutes at 25 °C) on the surface morphology and sensitivity efficiency. For surface-by-surface electrode design, the dip coating was favored as it avails a very uniform coating less of any excess uncoated surface residue which thus allows to analyze the effect of each additional layer deposited on the electrode. GO and SPEEK can form the $\pi - \pi$ interaction between their layers during the process.

A fine, less rough, and uniform distribution of the SPEEK is more rendered as seen in **Figure 4.21** below with prolonging sheets interlocking with the GO rough layers. The longer the GO-coated electrode is dipped in the solution, the more $\pi - \pi$ interaction and thus deposition of SPEEK onto the GO sheets (**Figure 4.21c** and **Figure 4.21e**). On the contrary, increasing the interaction time increases the amount of SPEEK embedded in the Au-GO layer noticed for both molecular weights in the EDX analysis. The deposition also became thicker (noticed by the reduction in the Au at the surface) with a long dipping duration allowing more sulfur groups which indicated more $\pi - \pi$ interaction between SPEEK and the existing reduced GO layers on the gold surface. This indicated that most of the surface layer is dominated by thick smoother 'chunks' of SPEEK in a given region that easily corroded over time as seen in **Figure 4.21c** and **Figure 4.21e**.



Sample	Au (Atomic %)	C (Atomic %)	O (Atomic %)
Bare Au	100	-	-
Au-GO (7 min)	42.45	39.25	18.30
Au-GO (15 min)	37.22	38.27	24.51
Au-GO (30 min)	35.03	29.00	35.97
Au-GO (1 h)	26.23	23.92	49.85

Figure 4.21: SEM images of SPEEK dip-coated Au-GO microelectrodes at 25 ℃. **a)** Bare Au, **b)** 10 kDa SPEEK (15 mins), **c)** 10 kDa SPEEK (130 min), **d)** 100 kDa SPEEK (15 min), and **e)** 100 kDa SPEEK (130 min).

An optimal SPEEK thickness is however required because as seen below in **Figure 4.22**, the higher the deposition due to SPEEK observed from the morphology studies above, the lower the electro sensitivity as the thick deposition tends to increase the overall electrode resistance and lower dopamine sensitivity.

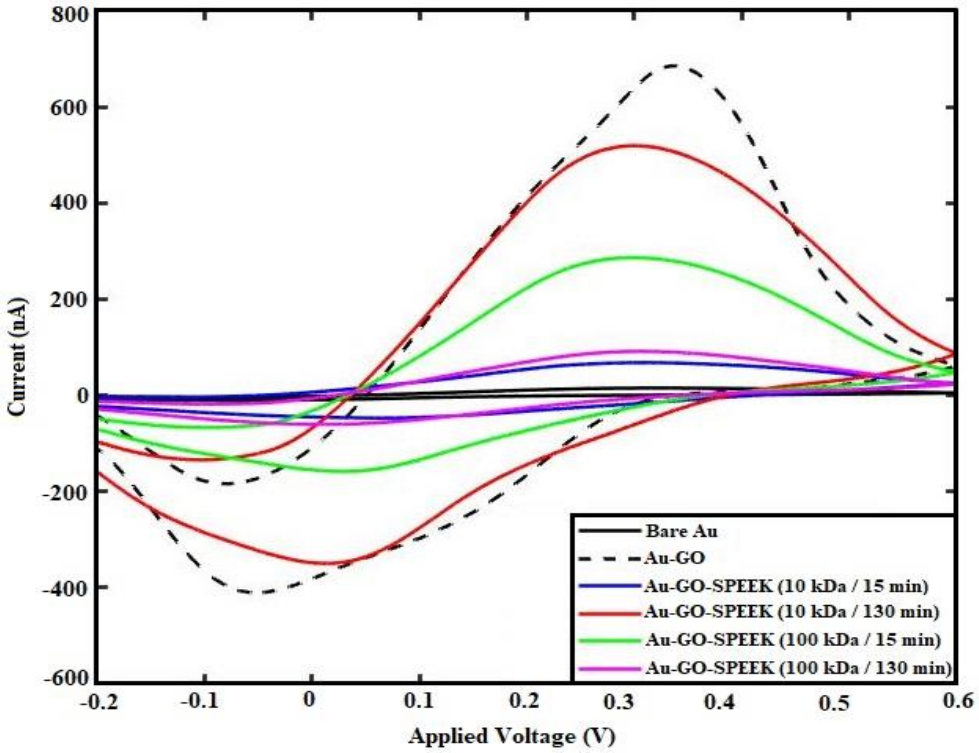


Figure 4.22: FSCV study using 10 μM dopamine for Au-GO microelectrodes dip-coated with SPEEK.

Besides the molecular weight, we see that deposition time greatly affects the sensitivity of the electrode. This is due to the notable increase in deposition thickness of the SPEEK together with the used molecular weight. A very high deposition of sulfur groups (1.14%) realized with 100 kDa forms a less conductive surface due to the relatively lower conductivity of SPEEK as compared to GO as seen in **Figure 4.22 – magenta**. It was seen that use of the less viscous 10 kDa SPEEK for 130 minutes in dip coating (**Figure 4.22 – red**) offers not only a reliable surface morphology but also a higher dopamine sensitivity. The reduction in viscosity increased the ability of the SPEEK molecules to fully incorporate in the GO layer pits (0.80%) and form a firm surface that resists early corrosion as opposed to the counterpart at 15 minutes (0.63%). With both types of SPEEK analyzed, a comparative study was performed to obtain the most favorable for both electrical sensitivity and surface morphology. **Figure 4.21c** (optimal for dip coating) displayed a more stable and uniform morphology compared the **Figure 4.19e** (optimal

for electrodeposition). At that point, FSCV for both microelectrodes were done to compare sensitivity as shown in **Figure 4.23** below.

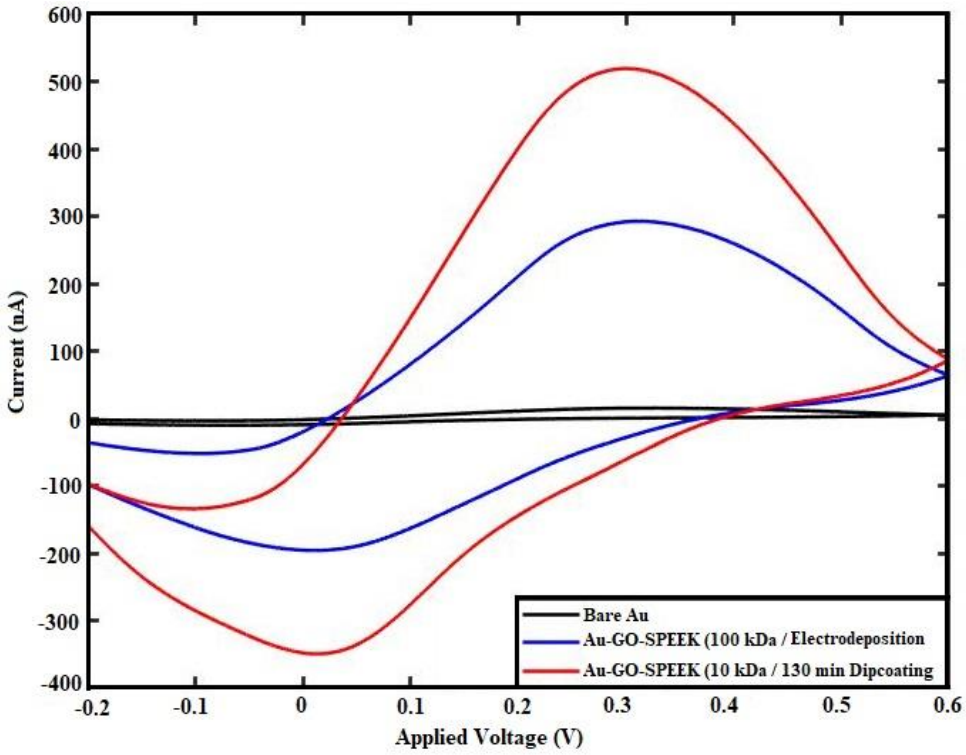


Figure 4.23: FSCV study using 10 μM dopamine to compare the optimal SPEEK coating.

It is then seen from the FSCV results (**Figure 4.23 – red**), that the optimal condition for our microelectrode design in order to include the characteristics of biocompatibility, improved mechanical strength and thermal stability for future implantation applications; is the use of dip coating for 10 kDa SPEEK solution over 130 minutes. Finally, optimization was done for a layer that would impact the durability of the microelectrode follows up with employing a ppy polymer as discussed in the following section.

4.5. Electrochemical Pyrrole Deposition on Graphene and SPEEK Coated Gold Electrode (Au-GO-SPEEK-ppy)

Not only is ppy an inert polymer that would potentially prevent formation of glial cells around implanted microelectrodes, but also known to be an intrinsic conductive polymer in both electronic and ionic surfaces [128]–[130], and biocompatible with brain tissue [131], [132]. From the previously designed electrode having both GO and SPEEK, we added a third and final layer through electrophoretic deposition, to understand its impact on the electrode effectiveness in terms of surface morphology, sensitivity, thickness, and the effectiveness in future chronic implantation. In the FSCV analysis shown in **Figure**

4.24 below, an initial study compared the effect of ppy on bare gold after electrodeposition of the polymer (0.05 M py) for 30 s using the gold electrode as the anode and platinum as the counter electrode at room temperature. It can be seen that the less conductive pyrrole surface only oxidizes minute dopamine (≈10 nA, 0.25 V) which is slowly reduced back by the system indicated by the rapid return to the resting potential and wide reduction peak with a shift of reduction peak slightly to the left (≈-0.1 V). From this study, it is understood that pyrrole was indeed conductive but its inevitably low electro conductivity would potentially reduce the overall microelectrode's sensitivity to dopamine.

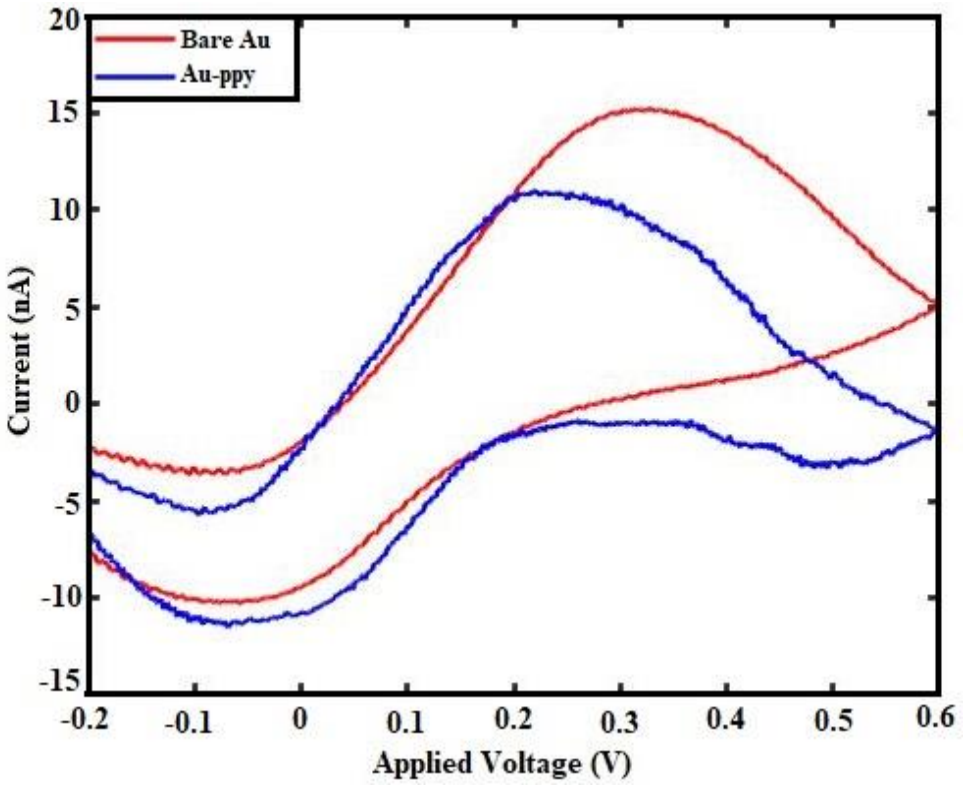


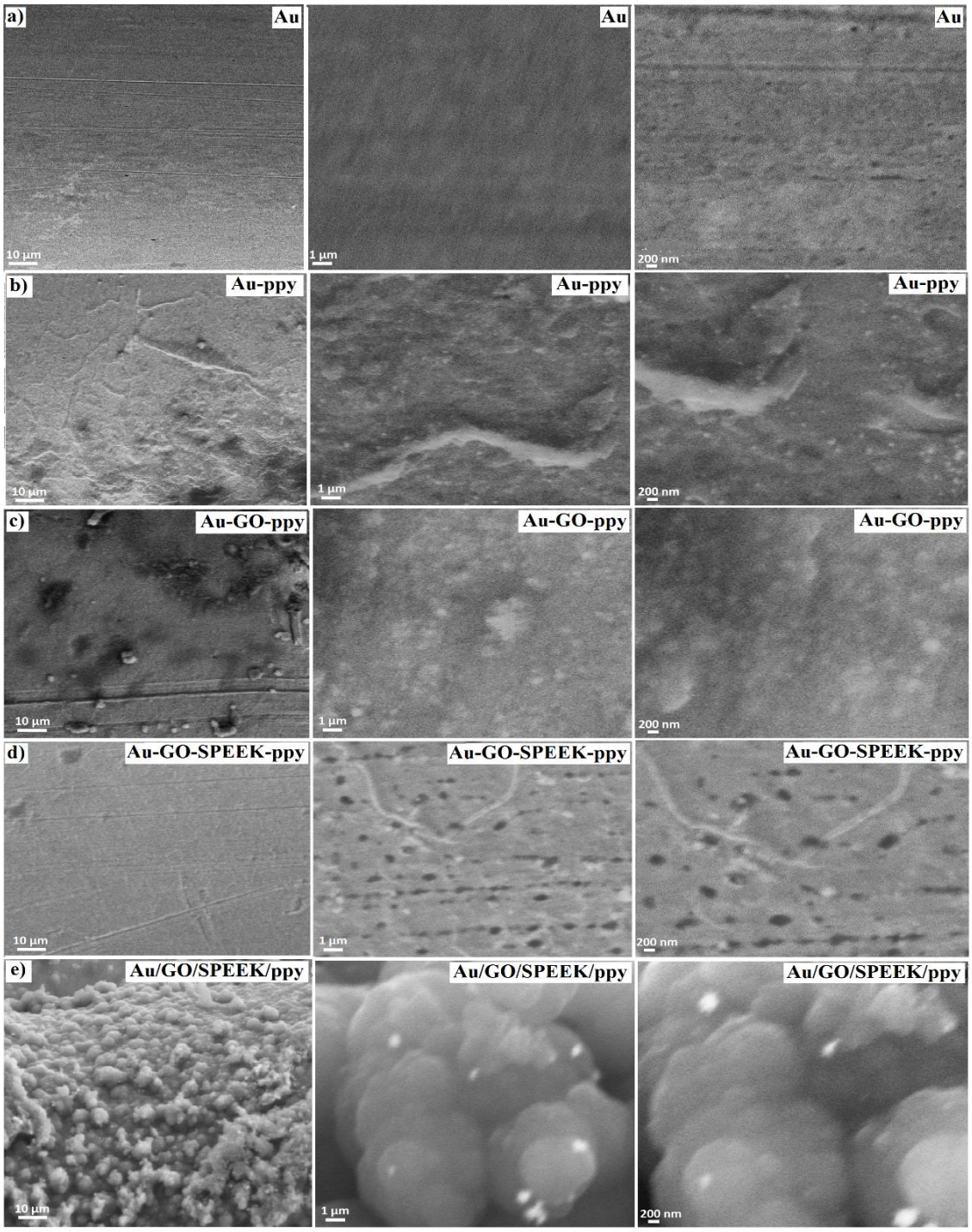
Figure 4.24: FSCV graph of Au microelectrode coated with py for 30s. 10 μM dopamine.

The material conductivities of the solutions i.e., GO, SPEEK and py were compared using DLS to further ascertain the effect of this factor on the general surface properties and the results presented in **Table 4.3** below shows that py indeed offers the poorest conductivity and the probable less conductivity seen in **Figure 4.24** above.

Table 4.3: Electrical properties of the materials.

Material	**Electric conductivity (mS/cm)**
Au	442
GO	13.63
SPEEK	2.15
py	0.0184

The deposition was performed in the following order: with only 0.05 M py electrodeposition, with 0.1 mg/mL GO consecutively followed by 0.05 M py electrodeposition, dip coating 0.5M SPEEK (10 kDa) on the Au-GO electrode coated with 0.1 mg/mL GO and electrodepositing the mixture (0.1 mg/mL GO with 0.05 M py and 0.5 M SPEEK (100 kDa)) on the gold surface. A morphological comparison of the ppy deposited layer was done in the SEM study shown in **Figure 4.25** below.



Sample	Au (Atomic %)	C (Atomic %)	O (Atomic %)	S (Atomic %)	N (Atomic %)
Bare Au	100	-	-	-	-
Au-ppy	20.72	68.50	-	-	10.79
Au-GO-ppy	25.09	58.47	9.48	-	6.95
Au-GO-SPEEK-ppy	37.49	50.93	6.39	0.00	5.19
Au/GO/SPEEK/ppy	0.00	69.64	17.45	1.67	11.25

Figure 4.25: SEM images of the Au microelectrode coated with GO, SPEEK and py to show the effect of ppy on the surface morphology. **a)** Bare Au, **b)** Au-ppy, **c)** Au-GO-ppy, **d)** Au-GO-SPEEK-ppy, and **e)** Au/GO/SPEEK/ppy.

The high conductivity of the Au-GO surface leads to a high electroreduction of py (C:O ratio of 6.17) and a thick coating is formed with only 25.09% noticed of Au on the surface and a very high 6.95% of N from the py ring **Figure 4.25c.** On the other hand, consecutive electrodeposition of GO followed by dip coating 10 kDa SPEEK for 130 minutes provided the preferential deposition of the compositional materials with the more conductive GO sheets deposited instead of the less conductive SPEEK when a 10 V potential is applied. The GO sheets are seen protruding on the surface in **Figure 4.25d** as layers of ppy are interlocking in them however, all the surface is covered by the ppy as a result of non-existent sulfur that exists in the layer of SPEEK. A combination of all materials simultaneously electrodeposited (Au/GO/SPEEK/ppy) leads to a very thick non-uniform deposition (seen non-existent Au atomic composition on the surface, Au = 0.00%) that undesirably forms multilayered profiles without clear orientation of layer alignment, that evidently easily could peel off as seen in **Figure 4.25e**. The less viscous SPEEK material is less deposited (S = 1.67%) of the three probably due to low mass transfer capability by the applied 10 V driving potential in favor of the uniformly less viscous GO and py solutions that are more electro active.

After 3 s, the deposited ppy film is so thin that the electrode displays a smooth morphology profile on a Au-GO-SPEEK coated surface (**Figure 4.25d**) while a high deposition at 30 minutes leads to a thick deposition bulges on the surface (**Figure 4.25e**) that probably grows resistive to dopamine oxidation. The fine uniform surface in **Figure 4.25c** also shows fine graphene sheets on the surface with more efficient coating of the ppy noticed from the moderate atomic percentage of nitrogen (5.19%). In simultaneous deposition (Au/GO/SPEEK/ppy) in **Figure 4.25e** the high nitrogen content (11.25%) may contribute to repulsion of dopamine molecules in addition to the increased capacitive currents before the oxidation phase which lowers the sensitivity. Consecutive coating of GO and SPEEK followed by electrical deposition of py for 3 s, however, forms a uniformly rough surface with deep GO grooves and less ppy on the surface (**Figure 4.25d**, EDX N=5.19%) that fairly maintains the sensitivity as that of bare gold in **Figure 4.26** below.

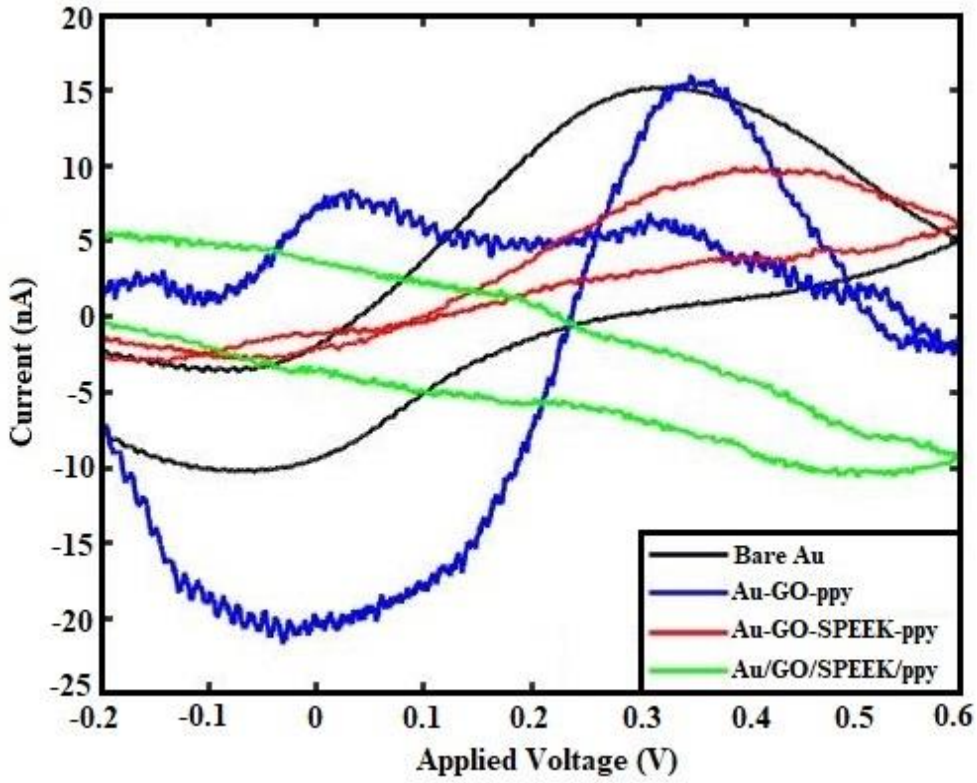


Figure 4.26: FSCV study of Au-GO-SPEEK-ppy consecutively coated microelectrode to analyze the optimal deposition time for the py layer. 10 μM dopamine.

Since an increase in deposition time increases the deposition yield as seen in Hamaker's law [116], an analysis of the optimal time needed to offer a surface coated with 0.1 mg/mL GO (electrodeposition), 0.5 M SPEEK (dip coating) and 0.05 M py (electrodeposition) was done at the optimized 30 minutes for GO deposition and the FSCV results to show the modifications in morphology are shown in **Figure 4.26** above. The thickness of the deposited layer can be seen to increase with increase in deposition time with the EDX results further suggesting that the gold surface is not exposed after 30 minutes of simultaneous ppy coating with GO and SPEEK. The nitrogen atomic composition is ultimately from the ppy ring, and it gives an indication of how much of ppy exists on the electrode's surface. The highly reactive nitrogen on ppy ensures that a very thick layer of the monomer is deposited in a short time.

In the above **Figure 4.26**, it does not only show that the thicker the ppy coating as a result of increased deposition time, the less sensitivity it becomes; but it also shows that ppy may be disables the electrodes' ability to oxidize the dopamine effectively (flattening of oxidation peaks) whereas increasing the capacitive currents prior to oxidation and lowering the reduction of the less dopamine-o-quinone in the saline solution (raised small

reduction peaks) back to dopamine [133]. For that reason, a thin py deposition is desired and thus two combinations for depositing ppy were considered. The optimized consecutive deposition of GO and SPEEK (Au-GO-SPEEK) followed by ppy and the simultaneous deposition of the three materials (Au/GO/SPEEK/ppy). Due to the high electrical reactivity of the nitrogen, the deposited layer in the simultaneous case is mainly composed of the ppy material which negatively impacts the surface sensitivity. A short electrodeposition time of 3 s is sufficient to deposit just enough of the highly electroactive ppy layer for optimal sensitivity in the designed microelectrode whilst ensuring enough of the ppy layer for durability post-implantations in future studies

As earlier discussed, the combined mixture forms a thick layer that may be predominantly made of ppy which attributes to the non-sensitive nature to dopamine seen in **Figure 4.26**. The surface behaves as an entirely ppy coated layer since GO that is very conductive is embedded in the ppy polymer and rendered less functional in the surface properties. Such a combination forms a very thick disoriented profile that can easily peel off and it also may limit other factors such as the targeted biocompatibility and thermal stability attributed to SPEEK (only 1.67% S content observed) as well as the ability to detect lower dopamine levels. Consecutive coating with GO-SPEEK-ppy ensures that the surface is almost completely covered by the less conductive ppy polymer which greatly lowers the sensitivity of the electrode. Moreover, the effect of surface morphology on conductivity of the surface results in the poor ppy sensitivity where it becomes less rough and minimal grooves. The desired rough surface increases both surface area and the capacitance which is inversely proportional to the electrode's impedance [102].

Prior to a combined analysis of all the optimal conditions for each surface, bare gold was compared to the currently marketable carbon electrodes used for dopamine detection and results of the FSCV study given in **Figure 4.27** below. The results gave a basis of how the fabricated electrode would match against the already existing electrodes of carbon fiber.

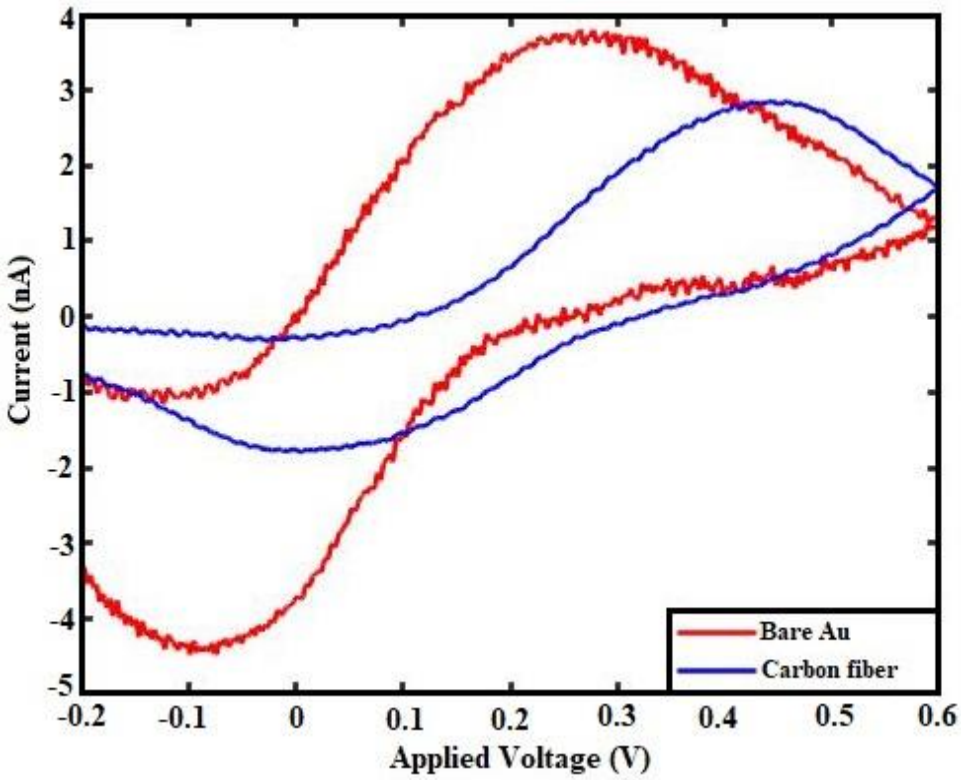
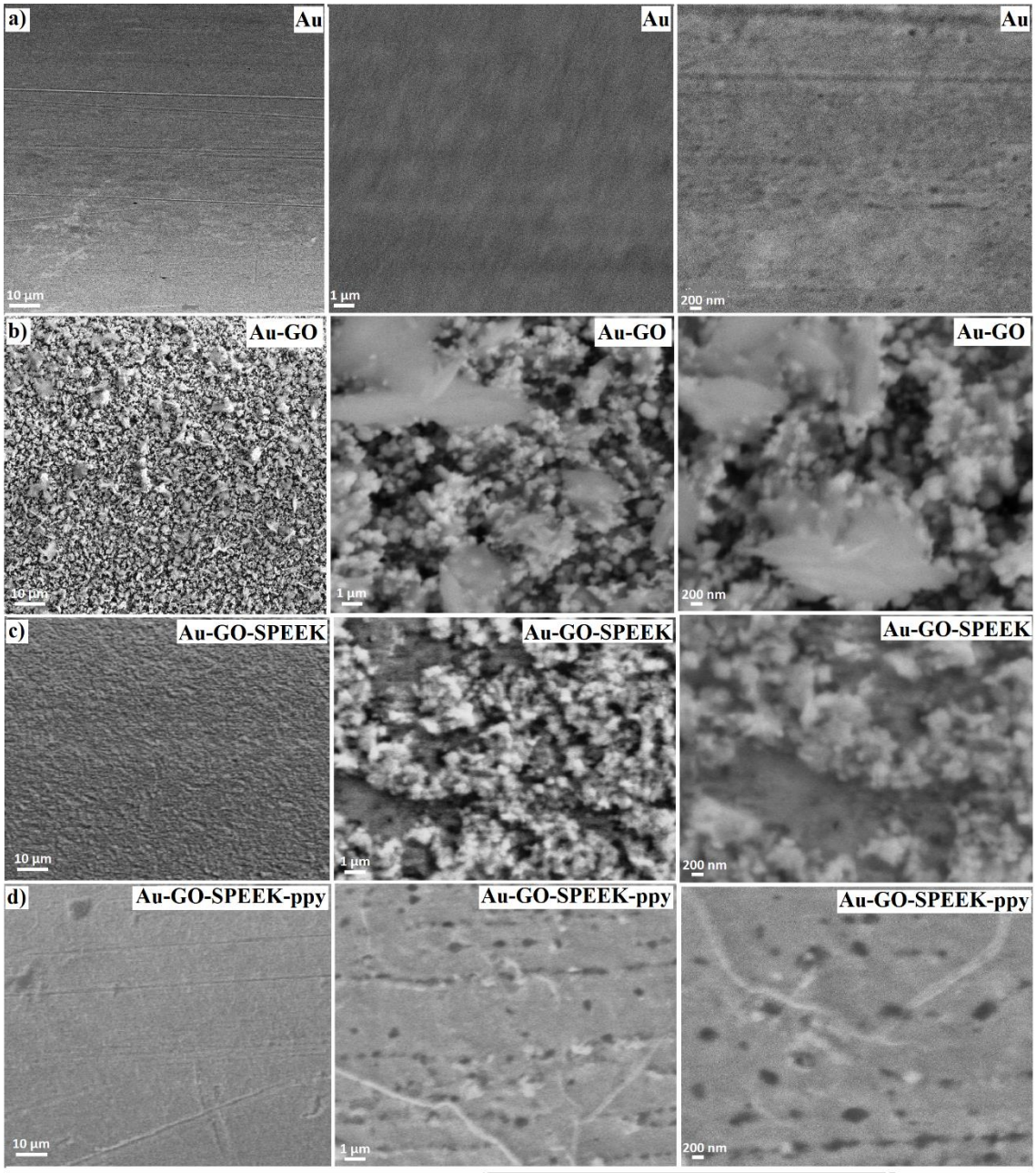


Figure 4.27: FSCV analysis using 1 μM of dopamine to compare the sensitivity of the carbon fiber (C) electrode with bare gold (Au). 50 μm gold disc and a 7 μm diameter by 150 μm length carbon fiber microelectrode.

To date, the main problems of carbon fiber electrodes have been poor sensitivity and poor ductility which limits micromovements in the implanted area and may result in glial cells depending on the electrode thickness [104]. This ascertains a necessity for new electrode designs. From **Figure 4.27**, a 50 μm gold disc and a 7 μm diameter by 150 μm length carbon fiber microelectrode is compared with a 1 μM dopamine solution for a potential window of -0.2 V to +0.6 V. It can be seen that while using a very low concentration 1 μM of dopamine in the FSCV and analyzing the raw data in MATLAB, bare gold still exhibits better detection capability as compared to the carbon fiber. Supplementation of this sensitivity with other materials would not only ensure a superior sensitivity and provide extra surface properties like bio-inertness and resistance to corrosion upon future studies after implantation.

After the optimization for inclusion of each coating biomaterial, we compare the effect of each material at optimized condition on the gold surface. Results of GO, SPEEK and py deposition to improve surface sensitivity are studied in reference to the bare gold surface and the morphological modifications given by the SEM analysis results given in **Figure 4.28** below. This elaborated the change in surface morphology and atomic

mapping by percentages from the EDX study; obtained while using the optimal design conditions for each step. The amount of gold exposed on the surface reduces with addition of each coat layer as seen by the EDX results in the attached table below.



Sample	Au (Atomic %)	C (Atomic %)	O (Atomic %)	S (Atomic %)	N (Atomic %)
Bare Au	100	-	-	-	-
Au-GO	35.03	29.00	35.97	-	-
Au-GO-SPEEK	37.41	50.70	11.09	0.80	-
Au-GO-SPEEK-ppy	37.49	50.93	6.39	0.00	5.19

Figure 4.28: SEM image of a gold electrode coated with the optimal conditions of the GO, SPEEK and py biomaterial coatings. **a)** Bare Au, **b)** Au-GO, **c)** Au-GO-SPEEK, and **d)** Au-GO-SPEEK-ppy.

Gold is known for its high conductivity, but the highly conductive rGO sheets largely increased its sensitivity by over five folds. Addition of an SPEEK layer onto the GO-coated gold electrode by the optimized dip coating method however slightly reduced this sensitivity since the SPEEK is less conductive compared to GO. **Table 4.4** below shows the thickness of the coating on the optimized electrodes for each step. A relationship between thickness to sensitivity shows that the thicker the coating, the more resistive it becomes. The thick layer creates a barrier between the charge carrying gold microelectrode base and the coat surface in contact with dopamine solution. This reduces the ability of the double layer to fully stabilize and initiate the redox reaction of the dopamine.

Table 4.4: Coat thickness after deposition of the biomaterials.

Sample	**Layer Thickness (μm)**
Au-GO	0.666 +/- 0.088
Au-GO-SPEEK	0.970 +/- 0.034
Au-GO-SPEEK-ppy	1.111 +/- 0.015

A py deposition is very less conductive and reduces the sensitivity even below that of gold even if coated together with the former conductive biomaterials in simultaneous or consecutive form. It can be seen that irrespective of the high conductivity of GO (Au-GO-ppy), a massive deduction in surface sensitivity was recorded when ppy layer was deposited, up to nearly the same charge transfer as bare gold. Nonetheless, a synergistic effect of GO co-deposited with SPEEK decreased the poor electrical conductivity by the later deposited ppy layer such that the Au-GO-SPEEK-ppy electrode can effectively detect the 10 μM dopamine solution in 100 mL of saline.

Even with poor sensitivity, the ppy layer is added to improve durability upon implantation and the study was simulated *in-vitro* by running the Au-GO-SPEEK and Au-GO-SPEEK-ppy electrodes continuously in the FSCV at 10 Hz for up to 5 hours to check if there were any presented changes in both morphology (SEM). The results are presented in **Figure 4.29** below. With more runs of the FSCV for 2 h, the outer SPEEK surface continuously degenerates creating a peeled off profile in **Figure 4.29b.** Since these electrodes were coated layer-by-layer, running the FSCV for 5 h **in Figure 4.29c**, showed that the outer SPEEK layer is almost all but corroded and entirely smooth underlying GO sheets embedded with less SPEEK can be noticed. The FSCV process in presence of the ppy layer further makes the surface depositions firmer and the surface grooves become less.

The surface morphology is embedded with closely interconnected curving as the duration of FSCV increases in the presence of py (**Figure 4.29e-f**) unlike in its absence where corrosion and surface distortion start being evident after 2 h (**Figure 4.29b**). This morphological profile was relatively unchanged which displayed the possible positive effect of py in maintaining the surface characteristics after long studies.

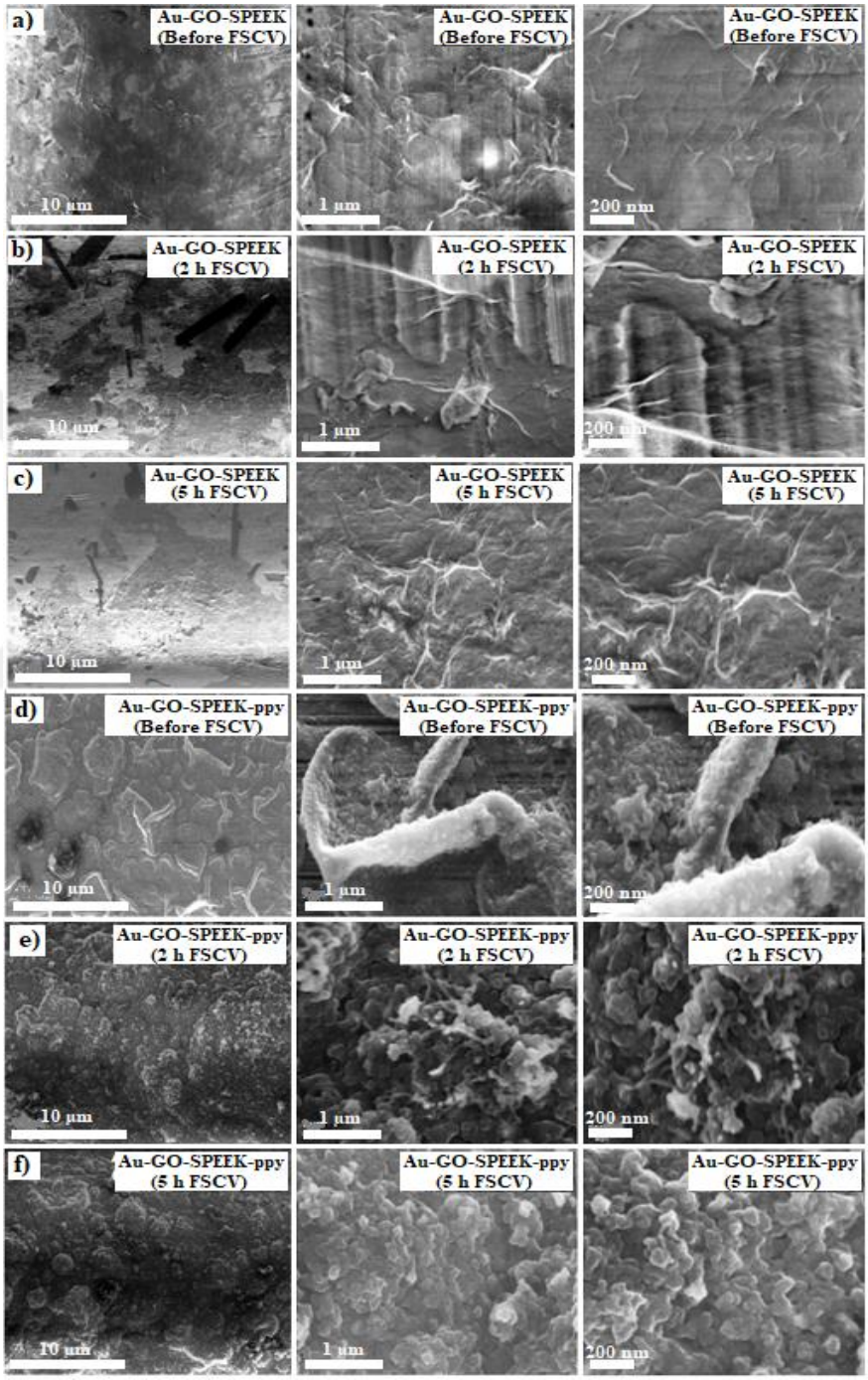


Figure 4.29: SEM image showing the durability of the surface coating before and after running the electrode in the FSCV for 2 and 5 h at 10 Hz. Consecutive electrodeposition of GO (30 min) and 100 kDa SPEEK (15 min) (Au-GO-SPEEK) followed by 10 s ppy coating.

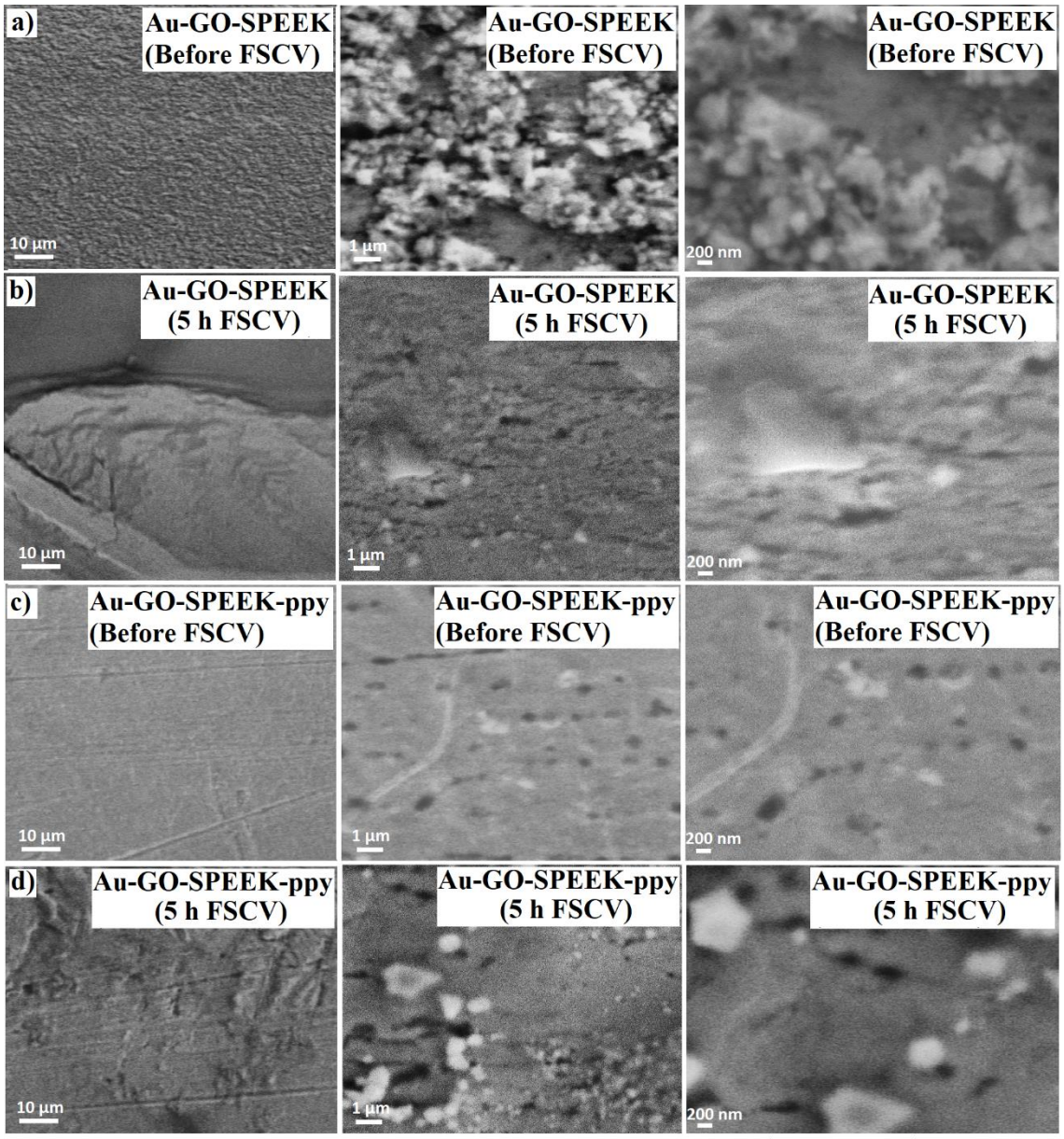
Table 4.5: EDX results of microelectrodes before the FSCV study, after running the electrode in the FSCV for 2 h, and for 5 h at 10 Hz.

Sample (Atomic %)	**Au**	**C**	**O**	**S**	**N**
Au-GO-SPEEK(Before FSCV)	40.68	48.24	10.53	0.55	-
Au-GO-SPEEK(2h FSCV)	55.47	38.62	5.43	0.47	-
Au-GO-SPEEK(5h FSCV)	54.28	39.66	5.67	0.39	-
Au-GO-SPEEK-ppy (Before FSCV)	16.53	64.45	7.27	0.08	11.67
Au-GO-SPEEK-ppy (2h FSCV)	13.06	66.45	9.70	0.15	10.64
Au-GO-SPEEK-ppy (5h FSCV)	12.86	64.91	9.72	0.18	12.32

With an increase in duration during the FSCV process for the Au-GO-SPEEK microelectrodes, more electrical reduction of the outer coating occurred which is noticed between the variations in the EDX results of the oxygen atomic percentages in **Table 4.5** above, before (10.53%) as compared to after 2 h (5.43%) and 5h (5.67%). The sulfur content (primarily in SPEEK) gradually reduced with further FSCV durations; an indication of surface corrosion of the outer SPEEK layer.

Corrosion in the absence of the ppy polymer coating can also be related to the progressive increase in the Au base layer on the surface composition from 40.68% before the study to 54.28% after the 5 h. However, the EDX results in **Table 4.5** showed that Au-GO-SPEEK-ppy microelectrodes, generally maintained the surface atomic compositions which validated the increase of durability for the microelectrodes. The sulfur content increases likely as the loosely attached layers of SPEEK embedded in the GO sheets are exposed to the surface after minimum loss of the ppy layer. The composition of Au on the surface remains almost similar during the FSCV study and the outer ppy layer indicated by the nitrogen content from the polymer ring remains relatively unchanged.

Another FSCV for 5 h while supplying the potential triangle at a high 50 Hz frequency from the system provided more corrosion of the surface in the absence of ppy whereas minimal loss on the nitrogen content was realized when coated with 0.05 M ppy for only 3 s as seen in the **Figure 4.30** below.



Sample	Au (Atomic %)	C (Atomic %)	O (Atomic %)	S (Atomic %)	N (Atomic %)
Au-GO-SPEEK (Before FSCV)	37.41	50.70	11.09	0.80	-
Au-GO-SPEEK (5 h FSCV)	35.03	51.06	12.60	1.31	-
Au-GO-SPEEK-ppy (Before FSCV)	37.49	50.93	6.39	0.00	5.19
Au-GO-SPEEK-ppy (5h FSCV)	37.85	50.18	7.87	0.02	4.08

Figure 4.30: SEM image showing the durability of the surface coating before and after running the electrode in the FSCV for 5 h at 50 Hz. Consecutive dip coating of 10 kDa SPEEK for 130 minutes on Au-GO (30 min) (Au-GO-SPEEK) followed by 3 s ppy coating.

In the above FSCV run, we can also deduct that the SPEEK layers actually do not remain on the outer layer but get embedded into the GO rough grooves as dipping time is increased. In that sense, there is an improved layer-to-layer connecting among the GO

sheets which ultimately favored the 10 kDa SPEEK as optimal due to its small molecular sizes. From the EDX table above on **Figure 4.30**, upon corrosion at 50 Hz for 5 hours, the embedded sulfur content increases as the outer rough GO sheets are eroded away by the high frequency.

The above results indicate that the surface composition and morphology is not only maintained but made firmer by the presence of py even after long FSCV studies due to further reduction of the coating such that polymer layers interlock on the surface. The given findings simulate the improved durability for the microelectrode by the ppy layer in case it is used in future chronical implantations to maintain the surface properties during and after the long study period.

From the findings above, the designed and optimized gold microelectrode improved sensitivity of dopamine by more than 50 folds for Au-GO-SPEEK and 2 folds for Au-GO-SPEEK-ppy as compared to the carbon electrodes whilst allowing the clear analysis of both the oxidation (region of 0.3 to 0.4 V) and reduction (region -0.1 to 0.1 V) phases of the dopamine neurotransmitter. Therefore, the designed and optimized electrode is effective in detecting the dopamine than the existing carbon electrodes. These electrodes also enable reproducibility by utilizing the desired optimized conditions for the desired characteristics while using biomaterials that enable possible chronical implantation while preventing growth of glial cells in future studies.

CHAPTER 5

5. CONCLUSIONS AND FUTURE WORK

Dopamine is a very important neurotransmitter mainly in human behavior but also for memory, adaptive learning, motor control, cognition, and reward-based conditioning (Pavlovian conditioning). Altering the normal dopamine concentrations results in a number of complications including addiction, depression, schizophrenia, and PD. This work focused on the design and optimization of the surface properties of a gold sensing platform to detect dopamine. The deposition conditions of GO considered include deposition potential, concentration, coating duration, and supporting electrolytes. For the case of SPEEK, optimal molecular weight for deposition methods (electrochemical deposition or dip coating) was studied. Lastly, the time and sequence of deposition for the ppy layer was analyzed to offer a thick enough coating without depreciation of the properties influenced by GO and SPEEK.

The gold disc-shaped electrodes are highly conductive and exhibit unique voltammograms for dopamine that are ultimately different from those of other neurotransmitters. The surface area for anchoring dopamine molecules and the electrical conductivity were improved primarily by the deposited GO sheets. SPEEK on the other hand improves the microelectrode's mechanical strength, thermal stability, biocompatibility and exhibits moderate proton conductivity . The ppy layer was vital in improving the electrode durability by resisting surface corrosion after prolonged FSCV runs. SEM and EDX analysis were used to study the effect of each layer on the morphological structure of the gold microelectrode while the FSCV technique helped to study the sensitivity. Fabrication of the optimized electrodes was done by both electrochemical deposition and dip coating techniques.

The electric conductivities of the materials from the DLS analysis of the solutions, prior to electrodeposition revealed that the order GO > SPEEK > py. However, it should be

recalled that GO further increases conductivity upon electrical reduction when it partly retains the graphene aromatic ring, which is after application of the electro deposition potential. The already highly conductive gold microelectrode (442 mS/cm) adapts the sensitivity depending on the conductivity of the material on the outermost surface which explains the superior sensitivity when initially only coated with GO (13.62 mS/cm). The relatively less conductive SPEEK (2.148 mS/cm) narrowly lowers the surface sensitivity when dip coated on it. The less conductive py (0.0184 mS/cm) may be attributed for the great lowering of the surface conductivity far below that of the bare gold making the surface more resistive and less sensitive to dopamine. However, a recent study showed that indeed polypyrrole is among the most conductive polymers with over 100 mS/cm [134]. This helps to explain the high deposition obtained in a very short period during the electro-polymerization of its monomer in coating and thus the negative effect of the large, deposited layer thickness of the polymer on this sensing platform as it tends to become resistive as displayed by the thick deposition of GO layers. It has been seen that irrespective of the thickness obtained at 3 or 10 s of ppy deposition, surface corrosion was inhibited after FSCV analysis. In that case henceforth, future studies involving further lower py monomer concentration can be investigated in combination with a small deposition duration to ensure a smooth and fine less resistive thickness of the ppy layer is formed during the electro-polymerization.

The sensitivity of the gold electrode can be seen to greatly depend on both the surface morphology and the type of biomaterial on the outer surface. The electrode's sensitivity will behave in correspondence to the outermost deposited biomaterial layer. The biomaterial does not only depend on its electrical conductivity to influence sensitivity but also the surface roughness and thickness of the deposited coating. The altered surface morphology together with the electrical conductivity enable the outermost material to anchor the dopamine in the saline solution into the electrode's double layer to initiate oxidation and reduction during the FSCV study. With each material's difference in these factors, the higher the electrical conductivity, the faster and longer the dopamine is held in the double layer of the electrode and thus the more sensitive the coated gold electrode will behave in detecting the dopamine.

The fabricated and optimized gold-based electrode having GO and SPEEK was compared with the existing and commonly marketed carbon electrodes to analyze the effect on the sensitivity and the FSCV results. In the results, it was seen that the superior electrical

conductivity of the flexible gold microelectrodes offered an advantage over the carbon electrodes. Further optimization with biomaterials does not only improve the dopamine sensitivity using the GO high conductivity, but also the SPEEK improves the mechanical strength of the electrode and the biomaterials inert nature enable the electrodes to prevent the possible growth of glial cells.

The firm and thick ppy layer displays resistive properties and reduces sensitivity by a large magnitude but from the EDX atomic composition quantization results after long FSCV runs, it was shown that this polymer improves durability noticed by the maintained surface composition. SEM analysis further stressed the durability property by showing that the surface morphology was maintained before and after the FSCV study. How fast the electrode stabilizes in the FSCV analysis greatly depends on how quickly the surface layer forms the electric double layer. This duration however did not give a direct indication of how sensitive that surface layer was.

The results are satisfactory for the intended purpose however there are more biocompatible polymers which need to be studied to understand their functioning in combination with GO. These include PEDOT and nafion. To optimize sensitivity and durability with the highest temporal and spatial resolution, these polymers can be studied in varying combinations, deposition techniques and concentrations.

Concurrent with the fabrication process of the microelectrode, an electronic system will be developed to enable multichannel voltametric recordings; the single channel recording system previously developed by the project team will be converted into an 8-channel system. The fabricated microelectrode will be assembled into an array of 8 recording sites. The current FSCV system developed is still undergoing further optimization steps with a prospect of getting a patent. The results obtained using the system gave an insight of the system stability and efficiency with comparison to results obtained using the carbon fiber electrodes. However, more studies basically on the system software still need deeper understanding using the gold-coated electrodes produced.

From literature, the potential window for pure gold electrodes was selected but more studies need to be done for each step to optimize the effect of the coating material on the electrode functioning potential window. The potential window is characteristic to each material and having deposited SPEEK and pyrrole, studies need to be done to ascertain the effect caused on the potential window and its level of significance.

As part of a future study, the microelectrode produced will be chronically implanted into the rat ventral striatum (NAc) for short (1 month and 10 days), medium (2 months) and long (7 months) terms, and the variations in the dopamine concentration will be recorded through the 8 channels during behavioral experiments. The dopamine concentration recordings observed in these experiments with high temporal and spatial resolution will reveal novel neuroscientific knowledge related to the dopamine-dependent learning mechanisms (e.g., Pavlovian conditioning) in the brain. By the end of each chronic implantation term, the microelectrodes will be removed from the tissue and the structural changes on the surface of the microelectrode arrays will be investigated using a scanning electron microscope. For biotic characterization of the microelectrode arrays, the modification in the brain tissue around the implantation area will be investigated using immunohistochemical techniques.

BIBLIOGRAPHY

[1] S. Herculano-Houzel, "The human brain in numbers: A linearly scaled-up primate brain," *Frontiers in Human Neuroscience*, vol. 3, no. NOV. Frontiers Media SA, Nov. 09, 2009, doi: 10.3389/neuro.09.031.2009.

[2] Z. M. Sheffler and L. S. Pillarisetty, *Physiology, Neurotransmitters*. StatPearls Publishing, 2019.

[3] M. O. Klein, D. S. Battagello, A. R. Cardoso, D. N. Hauser, J. C. Bittencourt, and R. G. Correa, "Dopamine: Functions, Signaling, and Association with Neurological Diseases," *Cellular and Molecular Neurobiology*, vol. 39, no. 1. Cell Mol Neurobiol, pp. 31–59, Jan. 31, 2019, doi: 10.1007/s10571-018-0632-3.

[4] Q. Cao, P. Puthongkham, and B. J. Venton, "Review: New insights into optimizing chemical and 3D surface structures of carbon electrodes for neurotransmitter detection," *Analytical Methods*, vol. 11, no. 3. Royal Society of Chemistry, pp. 247–261, Jan. 21, 2019, doi: 10.1039/c8ay02472c.

[5] R. L. McCreery, "Advanced carbon electrode materials for molecular electrochemistry," *Chemical Reviews*, vol. 108, no. 7. American Chemical Society , pp. 2646–2687, Jul. 2008, doi: 10.1021/cr068076m.

[6] F. He, R. Lycke, M. Ganji, C. Xie, and L. Luan, "Ultraflexible Neural Electrodes for Long-Lasting Intracortical Recording," *iScience*, vol. 23, no. 8. Elsevier Inc., p. 101387, Aug. 21, 2020, doi: 10.1016/j.isci.2020.101387.

[7] L. Luan *et al.*, "Ultraflexible nanoelectronic probes form reliable, glial scar–free neural integration," *Sci. Adv.*, vol. 3, no. 2, Feb. 2017, doi: 10.1126/sciadv.1601966.

[8] B. Wu, A. Heidelberg, and J. J. Boland, "Mechanical properties of ultrahigh-strength gold nanowires," *Nat. Mater.*, vol. 4, no. 7, pp. 525–529, Jun. 2005, doi: 10.1038/nmat1403.

[9] J. J. Clark *et al.*, "Chronic microsensors for longitudinal, subsecond dopamine detection in behaving animals," *Nat. Methods*, vol. 7, no. 2, pp. 126–129, Feb. 2010, doi: 10.1038/nmeth.1412.

[10] J. Tiberghien, S. Pérès, and G. Tiberghien, "Metal properties comparison: electric conductivity, thermal conductivity, density, melting temperature," *tibtech.com*, 2018. https://www.tibtech.com/conductivite.php?lang=en_US (accessed Apr. 17, 2021).

[11] V. B. Mohan, R. Brown, K. Jayaraman, and D. Bhattacharyya, "Characterisation of reduced graphene oxide: Effects of reduction variables on electrical conductivity," *Mater. Sci. Eng. B*, vol. 193, no. C, pp. 49–60, Mar. 2015, doi: 10.1016/j.mseb.2014.11.002.

[12] I. Jung, D. A. Dikin, R. D. Piner, and R. S. Ruoff, "Tunable electrical conductivity of individual graphene oxide sheets reduced at 'Low' temperatures," *Nano Lett.*, vol. 8, no. 12, pp. 4283–4287, Dec. 2008, doi: 10.1021/nl8019938.

[13] A. N. J. Rodgers, M. Velický, and R. A. W. Dryfe, “Electrostatic Stabilization of Graphene in Organic Dispersions,” *Langmuir*, vol. 31, no. 48, pp. 13068–13076, Nov. 2015, doi: 10.1021/acs.langmuir.5b04219.

[14] G. Cui, Z. Bi, R. Zhang, J. Liu, X. Yu, and Z. Li, “A comprehensive review on graphene-based anti-corrosive coatings,” *Chem. Eng. J.*, vol. 373, pp. 104–121, Oct. 2019, doi: 10.1016/j.cej.2019.05.034.

[15] A. R. Meier, M. Matteucci, R. F. Vreeland, R. Taboryski, and M. L. Heien, “Rapid Voltammetric Measurements at Conducting Polymer Microelectrodes Using Ultralow-Capacitance Poly(3,4-ethylenedioxythiophene):Tosylate,” *Langmuir*, vol. 32, no. 32, pp. 8009–8017, Aug. 2016, doi: 10.1021/acs.langmuir.6b01423.

[16] I. M. Taylor, E. M. Robbins, K. A. Catt, P. A. Cody, C. L. Happe, and X. T. Cui, “Enhanced dopamine detection sensitivity by PEDOT/graphene oxide coating on in vivo carbon fiber electrodes,” *Biosens. Bioelectron.*, vol. 89, pp. 400–410, Mar. 2017, doi: 10.1016/j.bios.2016.05.084.

[17] R. Malik, S. Lata, and R. S. Malik, “Electrochemical behavior of composite electrode based on sulphonated polymeric surfactant (SPEEK/PSS) incorporated polypyrrole for supercapacitor,” *J. Electroanal. Chem.*, vol. 835, pp. 48–59, Feb. 2019, doi: 10.1016/j.jelechem.2019.01.022.

[18] S. Zhai, W. Dai, J. Lin, S. He, B. Zhang, and L. Chen, “Enhanced proton conductivity in sulfonated poly(ether ether ketone) membranes by incorporating sodium dodecyl benzene sulfonate,” *Polymers (Basel).*, vol. 11, no. 2, Jan. 2019, doi: 10.3390/polym11020203.

[19] C. Sherman, “Impacts of Drugs on Neurotransmission | National Institute on Drug Abuse (NIDA),” *Natl. Inst. Drug Abus.*, pp. 1–11, 2017, Accessed: Apr. 17, 2021. [Online]. Available: https://archives.drugabuse.gov/news-events/nida-notes/2017/03/impacts-drugs-neurotransmission.

[20] G. Ayano, “Dopamine: Receptors, Functions, Synthesis, Pathways, Locations and Mental Disorders: Review of Literatures,” *J. Ment. Disord. Treat.*, vol. 2, no. 2, 2016, doi: 10.4172/2471-271X.1000120.

[21] N. Ben-Jonathan and R. Hnasko, “Dopamine as a prolactin (PRL) inhibitor,” *Endocrine Reviews*, vol. 22, no. 6. Endocrine Society, pp. 724–763, Dec. 01, 2001, doi: 10.1210/edrv.22.6.0451.

[22] Susan Perry, “Dopamine and Movement,” *Brain facts.org*, 2015. https://www.brainfacts.org/thinking-sensing-and-behaving/movement/2015/dopamine-and-movement (accessed Apr. 17, 2021).

[23] V. S. Chakravarthy, D. Joseph, and R. S. Bapi, “What do the basal ganglia do? A modeling perspective,” *Biological Cybernetics*, vol. 103, no. 3. Springer, pp. 237–253, Sep. 20, 2010, doi: 10.1007/s00422-010-0401-y.

[24] K. C. Berridge, “The debate over dopamine’s role in reward: The case for incentive salience,” *Psychopharmacology*, vol. 191, no. 3. Springer, pp. 391–431, Apr. 27, 2007, doi: 10.1007/s00213-006-0578-x.

[25] D. J. Nutt, A. Lingford-Hughes, D. Erritzoe, and P. R. A. Stokes, “The dopamine theory of addiction: 40 years of highs and lows,” *Nat. Rev. Neurosci.*, vol. 16, no. 5, pp. 305–312, May 2015, doi: 10.1038/nrn3939.

[26] R. A. Wise and M. A. Robble, “Dopamine and addiction,” *Annual Review of Psychology*, vol. 71. Annual Reviews Inc., pp. 79–106, Jan. 04, 2020, doi: 10.1146/annurev-psych-010418-103337.

[27] D. K. Grandy, G. M. Miller, and J. X. Li, “‘TAARgeting Addiction’-The Alamo Bears Witness to Another Revolution. An Overview of the Plenary Symposium of the 2015 Behavior, Biology and Chemistry Conference,” *Drug and Alcohol Dependence*, vol. 159. Elsevier Ireland Ltd, pp. 9–16, Feb. 01, 2016, doi: 10.1016/j.drugalcdep.2015.11.014.

[28] M. Jaber, S. W. Robinson, C. Missale, and M. G. Caron, “Dopamine receptors and brain function,” *Neuropharmacology*, vol. 35, no. 11. Neuropharmacology, pp. 1503–1519, 1996, doi: 10.1016/S0028-3908(96)00100-1.

[29] C. MISSALE, S. R. NASH, S. W. ROBINSON, M. JABER, and M. G. CARON, “Dopamine Receptors: From Structure to Function,” *Physiol. Rev.*, vol. 78, no. 1, pp. 189–225, Jan. 1998, doi: 10.1152/physrev.1998.78.1.189.

[30] L. Belkacemi and N. A. Darmani, “Dopamine receptors in emesis: Molecular mechanisms and potential therapeutic function,” *Pharmacol. Res.*, vol. 161, p. 105124, Nov. 2020, doi: 10.1016/j.phrs.2020.105124.

[31] F. Guzman, “The Four Major Dopamine Pathways Relevant to Antipsychotics Pharmacology,” *Psychopharmacology Institute*, 2019. https://psychopharmacologyinstitute.com/publication/the-four-dopamine-pathways-relevant-to-antipsychotics-pharmacology-2096?canonical=/publication/the-four-dopamine-pathways-relevant-to-antipsychotics-pharmacology-2096 (accessed Apr. 18, 2021).

[32] A. Mishra, S. Singh, and S. Shukla, “Physiological and Functional Basis of Dopamine Receptors and Their Role in Neurogenesis: Possible Implication for Parkinson’s disease,” *Journal of Experimental Neuroscience*, vol. 12. SAGE Publications Ltd, May 31, 2018, doi: 10.1177/1179069518779829.

[33] S. Yang, M. Boudier-Revéret, Y. J. Choo, and M. C. Chang, “Association between chronic pain and alterations in the mesolimbic dopaminergic system,” *Brain Sciences*, vol. 10, no. 10. MDPI AG, pp. 1–14, Oct. 01, 2020, doi: 10.3390/brainsci10100701.

[34] B. Adinoff, “Neurobiologic processes in drug reward and addiction,” *Harvard Review of Psychiatry*, vol. 12, no. 6. pp. 305–320, Nov. 2004, doi: 10.1080/10673220490910844.

[35] T. M. Powledge, “Addiction and the brain: The dopamine pathway is helping researchers find their way through the addiction maze,” *Bioscience*, vol. 49, no. 7, pp. 513–519, 1999.

[36] M. V. Puig, J. Rose, R. Schmidt, and N. Freund, “Dopamine modulation of learning and memory in the prefrontal cortex: Insights from studies in primates, rodents, and birds,” *Frontiers in Neural Circuits*, vol. 8, no. AUG. Frontiers Research Foundation, p. 93, Aug. 04, 2014, doi: 10.3389/fncir.2014.00093.

[37] D. Blum *et al.*, “Molecular pathways involved in the neurotoxicity of 6-OHDA, dopamine and MPTP: Contribution to the apoptotic theory in Parkinson’s disease,” *Progress in Neurobiology*, vol. 65, no. 2. Prog Neurobiol, pp. 135–172, 2001, doi: 10.1016/S0301-0082(01)00003-X.

[38] M. Habibi, “Dopamine Receptors,” in *Encyclopedia of Movement Disorders*, Elsevier, 2010, pp. 326–329.

[39] N. S. Hudepohl and H. A. Nasrallah, “Antipsychotic drugs,” in *Handbook of Clinical Neurology*, vol. 106, Elsevier B.V., 2012, pp. 657–667.

[40] S. E. Zauber, P. A. Smith, and L. V. Metman, “Fundamentals of deep brain stimulation programming,” in *Deep Brain Stimulation Management*, Cambridge University Press, 2015, pp. 64–76.

[41] A. J. Fenoy, L. Goetz, S. Chabardès, and Y. Xia, “Deep brain stimulation: Are astrocytes a key driver behind the scene?,” *CNS Neurosci. Ther.*, vol. 20, no. 3, pp. 191–201, Mar. 2014, doi: 10.1111/cns.12223.

[42] A. E. L. Jose A. Obeso, C.W. Olanow, M.C. Rodriguez-Oroz, P. Krack, R. Kumar, “Deep-Brain Stimulation of the Subthalamic Nucleus or the Pars Interna of the Globus Pallidus in Parkinson’s Disease,” *N. Engl. J. Med.*, vol. 345, no. 13, pp. 956–963, Sep. 2001, doi: 10.1056/NEJMoa000827.

[43] P. S. Larson, “Deep Brain Stimulation for Movement Disorders,” *Neurotherapeutics*, vol. 11, no. 3. Neurotherapeutics, pp. 465–474, 2014, doi: 10.1007/s13311-014-0274-1.

[44] L. Penicaud, A. Benani, F. Datiche, X. Fioramonti, C. Leloup, and F. Lienard, “Animal Models and Methods to Study the Relationships Between Brain and Tissues in Metabolic Regulation,” in *Animal Models for the Study of Human Disease*, Elsevier, 2013, pp. 569–593.

[45] M. E. Morgan, D. Singhal, and B. D. Anderson, “Quantitative assessment of blood-brain barrier damage during microdialysis,” *J. Pharmacol. Exp. Ther.*, vol. 277, no. 2, pp. 1167–1176, 1996.

[46] A. S. Khan and A. C. Michael, “Invasive consequences of using micro-electrodes and microdialysis probes in the brain,” in *TrAC - Trends in Analytical Chemistry*, 2003, vol. 22, no. 8, pp. 503–508, doi: 10.1016/S0165-9936(03)00908-7.

[47] J. A. Bourne, “Intracerebral microdialysis: 30 Years as a tool for the neuroscientist,” *Clinical and Experimental Pharmacology and Physiology*, vol. 30, no. 1–2. Clin Exp Pharmacol Physiol, pp. 16–24, Jan. 2003, doi: 10.1046/j.1440-1681.2003.03789.x.

[48] T. Ros *et al.*, “PET Imaging of Dopamine Neurotransmission During EEG Neurofeedback,” *Front. Physiol.*, vol. 11, p. 1749, Jan. 2021, doi: 10.3389/fphys.2020.590503.

[49] H. Marzbani, H. R. Marateb, and M. Mansourian, “Methodological note: Neurofeedback: A comprehensive review on system design, methodology and clinical applications,” *Basic Clin. Neurosci.*, vol. 7, no. 2, pp. 143–158, Mar. 2016, doi: 10.15412/j.bcn.03070208.

[50] P. Redgrave *et al.*, “Goal-directed and habitual control in the basal ganglia: Implications for Parkinson’s disease,” *Nature Reviews Neuroscience*, vol. 11, no. 11. Nature Publishing Group, pp. 760–772, Oct. 14, 2010, doi: 10.1038/nrn2915.

[51] W. Mier and D. Mier, “Advantages in functional imaging of the brain,” *Frontiers in Human Neuroscience*, vol. 9, no. MAY. Frontiers Media S. A., May 19, 2015, doi: 10.3389/fnhum.2015.00249.

[52] M. D. Guimaraes, A. Schuch, B. Hochhegger, J. L. Gross, R. Chojniak, and E. Marchiori, “Functional Magnetic Resonance Imagine in Oncology: State of the art,” *Radiologia Brasileira*, vol. 47, no. 2. Publicação do Colégio Brasileiro de Radiologia e Diagnóstico por Imagem, pp. 101–111, 2014, doi: 10.1590/S0100-39842014000200013.

[53] N. K. Logothetis, J. Pauls, M. Augath, T. Trinath, and A. Oeltermann, “Neurophysiological investigation of the basis of the fMRI signal,” *Nature*, vol. 412, no. 6843, pp. 150–157, Jul. 2001, doi: 10.1038/35084005.

[54] T. Lee, L. X. Cai, V. S. Lelyveld, A. Hai, and A. Jasanoff, “Molecular-level functional magnetic resonance imaging of dopaminergic signaling,” *Science (80-.).*, vol. 344, no. 6183, pp. 533–535, 2014, doi: 10.1126/science.1249380.

[55] P. J. Britto, K. S. V. Santhanam, and P. M. Ajayan, “Carbon nanotube electrode for oxidation of dopamine,” in *Bioelectrochemistry and Bioenergetics*, Oct. 1996, vol. 41, no. 1, pp. 121–125, doi: 10.1016/0302-4598(96)05078-7.

[56] E. Ghodsevali *et al.*, “Miniaturized FDDA and CMOS based potentiostat for bio-applications,” *Sensors (Switzerland)*, vol. 17, no. 4, p. 810, Apr. 2017, doi: 10.3390/s17040810.

[57] B. P. Jackson, S. M. Dietz, and R. M. Wightman, “Fast-Scan Cyclic Voltammetry of 5-Hydroxytryptamine,” *Anal. Chem.*, vol. 67, no. 6, pp. 1115–1120, 1995, doi: 10.1021/ac00102a015.

[58] M. Haziq, R. Riaz, S. Kocatürk, A. Ayyaz, and M. Kocatürk, “An Analog FSCV Device Combined with a Phase-Locked Loop for in Vivo Detection of Dopamine,” TechRxiv, May 2021. doi: 10.36227/techrxiv.14428133.v4.

[59] M. Ouellette, J. Mathault, S. D. Niyonambaza, A. Miled, and E. Boisselier, “Electrochemical detection of dopamine based on functionalized electrodes,” *Coatings*, vol. 9, no. 8, pp. 1–15, 2019, doi: 10.3390/coatings9080496.

[60] B. E. K. Swamy and B. J. Venton, “Carbon nanotube-modified microelectrodes for simultaneous detection of dopamine and serotonin in vivo,” *Analyst*, vol. 132, no. 9, pp. 876–884, Aug. 2007, doi: 10.1039/b705552h.

[61] Y. Fu, Q. Sheng, and J. Zheng, “Au nanoparticles anchored on Ni(OH)2 nanowires with multiple cavities for selective electrochemical detection of dopamine,” *Anal. Methods*, vol. 9, no. 19, pp. 2812–2820, May 2017, doi: 10.1039/c7ay00090a.

[62] S. Palanisamy *et al.*, “Facile synthesis of cellulose microfibers supported palladium nanospindles on graphene oxide for selective detection of dopamine in pharmaceutical and biological samples,” *Mater. Sci. Eng. C*, vol. 98, pp. 256–265, May 2019, doi: 10.1016/j.msec.2018.12.112.

[63] L. P. Mei *et al.*, “A glassy carbon electrode modified with porous Cu2O nanospheres on reduced graphene oxide support for simultaneous sensing of uric acid and dopamine with high selectivity over ascorbic acid,” *Microchim. Acta*, vol. 183, no. 6, pp. 2039–2046, Jun. 2016, doi: 10.1007/s00604-016-1845-0.

[64] T. Kokulnathan, A. Joseph Anthuvan, S. M. Chen, V. Chinnuswamy, and K. Kadirvelu, “Trace level electrochemical determination of the neurotransmitter dopamine in biological samples based on iron oxide nanoparticle decorated graphene sheets,” *Inorg. Chem. Front.*, vol. 5, no. 3, pp. 705–718, Mar. 2018, doi: 10.1039/c7qi00716g.

[65] T. Kuila, A. K. Mishra, P. Khanra, N. H. Kim, M. E. Uddin, and J. H. Lee, “Facile Method for the Preparation of Water Dispersible Graphene using Sulfonated Poly(ether–ether–ketone) and Its Application as Energy Storage Materials,” *Langmuir*, vol. 28, no. 25, pp. 9825–9833, Jun. 2012, doi: 10.1021/la301469u.

[66] M. Hilder, B. Winther-Jensen, D. Li, M. Forsyth, and D. R. MacFarlane, “Direct electro-deposition of graphene from aqueous suspensions,” *Phys. Chem. Chem. Phys.*, vol. 13, no. 20, p. 9187, 2011, doi: 10.1039/c1cp20173e.

[67] C. He *et al.*, “A gold electrode modified with a gold-graphene oxide nanocomposite for non-enzymatic sensing of glucose at near-neutral pH values,” *Microchim. Acta*, vol. 186, no. 11, 2019, doi: 10.1007/s00604-019-3796-8.

[68] L. Chen, Y. Tang, K. Wang, C. Liu, and S. Luo, “Direct electrodeposition of reduced graphene oxide on glassy carbon electrode and its electrochemical application,” *Electrochem. commun.*, vol. 13, no. 2, pp. 133–137, 2011, doi: 10.1016/j.elecom.2010.11.033.

[69] R. M. Alonso, M. I. San-Martín, A. Sotres, and A. Escapa, “Graphene oxide electrodeposited electrode enhances start-up and selective enrichment of exoelectrogens in bioelectrochemical systems.,” *Sci. Rep.*, vol. 7, no. 1, p. 13726, 2017, doi: 10.1038/s41598-017-14200-7.

[70] M. J. Hwang *et al.*, “Cathodic electrophoretic deposition (EPD) of phenylenediamine-modified graphene oxide (GO) for anti-corrosion protection of metal surfaces,” *Carbon N. Y.*, vol. 142, pp. 68–77, 2019, doi: 10.1016/j.carbon.2018.10.017.

[71] P. Moozarm Nia, H. Salarzadeh Jenatabadi, P. M. Woi, E. Abouzari-Lotf, and Y. Alias, “The optimization of effective parameters for electrodeposition of reduced graphene oxide through Taguchi method to evaluate the charge transfer,” *Meas. J. Int. Meas. Confed.*, vol. 137, pp. 683–690, 2019, doi: 10.1016/j.measurement.2019.02.015.

[72] H. Zhang, N. Zhang, and F. Fang, “Fabrication of high-performance nickel/graphene oxide composite coatings using ultrasonic-assisted electrodeposition,” *Ultrason. Sonochem.*, vol. 62, no. October 2019, p. 104858, 2020, doi: 10.1016/j.ultsonch.2019.104858.

[73] X. Zhang, Y. C. Zhang, and L. X. Ma, “One-pot facile fabrication of graphene-zinc oxide composite and its enhanced sensitivity for simultaneous electrochemical detection of ascorbic acid, dopamine and uric acid,” *Sensors Actuators, B Chem.*, vol. 227, pp. 488–496, May 2016, doi: 10.1016/j.snb.2015.12.073.

[74] Y. Veera Manohara Reddy *et al.*, “Ultrafine Pt-Ni bimetallic nanoparticles anchored on reduced graphene oxide nanocomposites for boosting electrochemical detection of dopamine in biological samples,” *New J. Chem.*, vol. 42, no. 20, pp. 16891–16901, Oct. 2018, doi: 10.1039/c8nj03894e.

[75] L. Yang *et al.*, “A quadruplet electrochemical platform for ultrasensitive and simultaneous detection of ascorbic acid, dopamine, uric acid and acetaminophen based on a ferrocene derivative functional Au NPs/carbon dots nanocomposite and graphene,” *Anal. Chim. Acta*, vol. 903, pp. 69–80, Jan. 2016, doi: 10.1016/j.aca.2015.11.021.

[76] X. Wang *et al.*, “Highly dispersible and stable copper terephthalate metal-organic framework-graphene oxide nanocomposite for an electrochemical sensing application,” *ACS Appl. Mater. Interfaces*, vol. 6, no. 14, pp. 11573–11580, Jul. 2014, doi: 10.1021/am5019918.

[77] J. J. Fang, N. N. Yang, and E. Q. Gao, “Making metal–organic frameworks electron-deficient for ultrasensitive electrochemical detection of dopamine,” *Electrochem. commun.*, vol. 89, pp. 32–37, Apr. 2018, doi: 10.1016/j.elecom.2018.02.014.

[78] Y. Y. Zheng *et al.*, “Detection of dopamine at graphene-ZIF-8 nanocomposite modified electrode,” *Chinese Chem. Lett.*, vol. 28, no. 7, pp. 1473–1478, Jul. 2017, doi: 10.1016/j.cclet.2017.03.014.

[79] M. K. Zachek, A. Hermans, R. M. Wightman, and G. S. McCarty, “Electrochemical dopamine detection: Comparing gold and carbon fiber microelectrodes using background subtracted fast scan cyclic voltammetry,” *J. Electroanal. Chem.*, vol. 614, no. 1–2, pp. 113–120, 2008, doi: 10.1016/j.jelechem.2007.11.007.

[80] J. Singh *et al.*, “Preparation of sulfonated poly(ether–ether–ketone) functionalized ternary graphene/AuNPs/chitosan nanocomposite for efficient glucose biosensor,” *Process Biochem.*, vol. 48, no. 11, pp. 1724–1735, Nov. 2013, doi: 10.1016/j.procbio.2013.07.025.

[81] Š. Komorsky-Lovrić, “Working Electrodes,” in *Electroanalytical Methods*, 2005, pp. 245–260.

[82] H. Xu, J. Xiao, L. Yan, L. Zhu, and B. Liu, “An electrochemical sensor for selective detection of dopamine based on nickel tetrasulfonated phthalocyanine functionalized nitrogen-doped graphene nanocomposites,” *J. Electroanal. Chem.*, vol. 779, pp. 92–98, Oct. 2016, doi: 10.1016/j.jelechem.2016.04.032.

[83] H. Dai, D. Chen, Y. Li, P. Cao, N. Wang, and M. Lin, “Voltammetric sensing of dopamine based on a nanoneedle array consisting of NiCo2S4 hollow core-shells on a nickel foam,” *Microchim. Acta*, vol. 185, no. 3, pp. 1–7, Mar. 2018, doi: 10.1007/s00604-018-2718-5.

[84] A. F. Khan, D. A. C. Brownson, E. P. Randviir, G. C. Smith, and C. E. Banks, “2D Hexagonal Boron Nitride (2D-hBN) Explored for the Electrochemical Sensing of Dopamine,” *Anal. Chem.*, vol. 88, no. 19, pp. 9729–9737, Oct. 2016, doi: 10.1021/acs.analchem.6b02638.

[85] X. Yan *et al.*, “Morphology-controlled synthesis of Bi2S3 nanorods-reduced graphene oxide composites with high-performance for electrochemical detection of dopamine,” *Sensors Actuators, B Chem.*, vol. 257, pp. 936–943, Mar. 2018, doi: 10.1016/j.snb.2017.11.037.

[86] S. Priyatharshni, A. Tamilselvan, C. Viswanathan, and N. Ponpandian, “LaCoO 3 Nanostructures Modified Glassy Carbon Electrode for Simultaneous Electrochemical Detection of Dopamine, Ascorbic Acid and Uric Acid,” *J. Electrochem. Soc.*, vol. 164, no. 4, pp. B152–B158, Feb. 2017, doi: 10.1149/2.1391704jes.

[87] S. Priyatharshni, M. Divagar, C. Viswanathan, D. Mangalaraj, and N. Ponpandian, “Electrochemical Simultaneous Detection of Dopamine, Ascorbic Acid and Uric Acid Using LaMnO 3 Nanostructures,” *J. Electrochem. Soc.*, vol. 163, no. 8, pp. B460–B465, Jun. 2016, doi: 10.1149/2.1181608jes.

[88] M. Sajid, N. Baig, and K. Alhooshani, “Chemically modified electrodes for electrochemical detection of dopamine: Challenges and opportunities,” *TrAC - Trends in Analytical Chemistry*, vol. 118. Elsevier B.V., pp. 368–385, Sep. 01, 2019, doi: 10.1016/j.trac.2019.05.042.

[89] A. P. Sandoval-Rojas, L. Ibarra, M. T. Cortés, M. A. Macías, L. Suescun, and J. Hurtado, “Synthesis and characterization of copper(II) complexes containing acetate and N,N-donor ligands, and their electrochemical behavior in dopamine detection,” *J. Electroanal. Chem.*, vol. 805, pp. 60–67, Nov. 2017, doi: 10.1016/j.jelechem.2017.10.018.

[90] A. Gorczyński *et al.*, “Electrochemical deposition of the new manganese(II) Schiff-base complex on a gold template and its application for dopamine sensing in the presence of interfering biogenic compounds,” *Talanta*, vol. 149, pp. 347–355, Mar. 2016, doi: 10.1016/j.talanta.2015.11.050.

[91] E. Nagles, L. Ibarra, J. P. Llanos, J. Hurtado, and O. Garcia-Beltrán, “Development of a novel electrochemical sensor based on cobalt(II) complex useful in the detection of dopamine in presence of ascorbic acid and uric acid,” *J. Electroanal. Chem.*, vol. 788, pp. 38–43, Mar. 2017, doi: 10.1016/j.jelechem.2017.01.057.

[92] M. M. Rahman, N. S. Lopa, M. J. Ju, and J. J. Lee, “Highly sensitive and simultaneous detection of dopamine and uric acid at graphene nanoplatelet-modified fluorine-doped tin oxide electrode in the presence of ascorbic acid,” *J. Electroanal. Chem.*, vol. 792, pp. 54–60, May 2017, doi: 10.1016/j.jelechem.2017.03.038.

[93] E. Nagles, O. García-Beltrán, and J. A. Calderón, “Evaluation of the usefulness of a novel electrochemical sensor in detecting uric acid and dopamine in the presence of ascorbic acid using a screen-printed carbon electrode modified with single walled carbon nanotubes and ionic liquids,” *Electrochim. Acta*, vol. 258, pp. 512–523, Dec. 2017, doi: 10.1016/j.electacta.2017.11.093.

[94] M. J. A. Shiddiky and A. A. J. Torriero, “Application of ionic liquids in electrochemical sensing systems,” *Biosensors and Bioelectronics*, vol. 26, no. 5. Elsevier, pp. 1775–1787, Jan. 15, 2011, doi: 10.1016/j.bios.2010.08.064.

[95] M. Gerard, A. Chaubey, and B. D. Malhotra, “Application of conducting polymers to biosensors,” *Biosensors and Bioelectronics*, vol. 17, no. 5. Elsevier, pp. 345–359, May 01, 2002, doi: 10.1016/S0956-5663(01)00312-8.

[96] V. P. Rao, Y. V. Manohara Reddy, K. Gangadhar Reddy, C. Madhuri, D. Saritha, and G. Madhavi, “Simultaneous determination of dopamine, ascorbic acid and uric acid at poly (Cinnamic acid) modified carbon paste electrode: A voltammetric investigation,” *Anal. Bioanal. Electrochem.*, vol. 9, no. 7, pp. 874–887, Nov. 2017.

[97] R. Manikandan, P. N. Deepa, and S. S. Narayanan, “Fabrication and characterization of poly 2-napthol orange film modified electrode and its application to selective detection of dopamine,” *J. Solid State Electrochem.*, vol. 21, no. 12, pp. 3567–3578, Nov. 2017, doi: 10.1007/s10008-017-3604-5.

[98] S. Devaramani, M. Sreeramareddygari, M. R. Reddy, and R. Thippeswamy, “Covalently Anchored p-Aminobenzene Sulfonate Multilayer on a Graphite Pencil Lead Electrode: A Highly Selective Electrochemical Sensor for Dopamine,” *Electroanalysis*, vol. 29, no. 5, pp. 1410–1417, May 2017, doi: 10.1002/elan.201600627.

[99] G. Xu, Z. A. Jarjes, V. Desprez, P. A. Kilmartin, and J. Travas-Sejdic, “Sensitive, selective, disposable electrochemical dopamine sensor based on PEDOT-modified laser scribed graphene,” *Biosens. Bioelectron.*, vol. 107, pp. 184–191, Jun. 2018, doi: 10.1016/j.bios.2018.02.031.

[100] S. Sonpingkam and D. Pattavarakorn, “Mechanical Properties of Sulfonated Poly (Ether Ether Ketone) Nanocomposite Membranes,” *Int. J. Chem. Eng. Appl.*, vol. 5, no. 2, pp. 181–185, Apr. 2014, doi: 10.7763/ijcea.2014.v5.374.

[101] L. Kong, L. Zheng, R. Niu, H. Wang, and H. Shi, “A sulfonated poly(ether ether ketone)/amine-functionalized graphene oxide hybrid membrane for vanadium redox flow batteries,” *RSC Adv.*, vol. 6, no. 102, pp. 100262–100270, 2016, doi: 10.1039/C6RA22665E.

[102] M. Deng *et al.*, “Electrochemical deposition of polypyrrole/graphene oxide composite on microelectrodes towards tuning the electrochemical properties of neural probes,” *Sensors Actuators B Chem.*, vol. 158, no. 1, pp. 176–184, Nov. 2011, doi: 10.1016/j.snb.2011.05.062.

[103] N. Xiao and B. J. Venton, “Rapid, sensitive detection of neurotransmitters at microelectrodes modified with self-assembled SWCNT forests,” *Anal. Chem.*, vol. 84, no. 18, pp. 7816–7822, Sep. 2012, doi: 10.1021/ac301445w.

[104] M. Hejazi, W. Tong, M. R. Ibbotson, S. Prawer, and D. J. Garrett, “Advances in Carbon-Based Microfiber Electrodes for Neural Interfacing,” *Frontiers in Neuroscience*, vol. 15. Frontiers, p. 403, Apr. 12, 2021, doi: 10.3389/fnins.2021.658703.

[105] A. K. Satpati and A. V. R. Reddy, “Electrochemical Study on Corrosion Inhibition of Copper in Hydrochloric Acid Medium and the Rotating Ring-Disc Voltammetry for Studying the Dissolution,” *Int. J. Electrochem.*, vol. 2011, pp. 1–8, 2011, doi: 10.4061/2011/173462.

[106] T. S. Sreeprasad and V. Berry, “How do the electrical properties of graphene change with its functionalization?,” *Small*, vol. 9, no. 3, pp. 341–350, 2013, doi: 10.1002/smll.201202196.

[107] H. Liu *et al.*, “Reduction of graphene oxide to highly conductive graphene by Lawesson’s reagent and its electrical applications,” *J. Mater. Chem. C*, vol. 1, no. 18, pp. 3104–3109, May 2013, doi: 10.1039/c3tc00067b.

[108] M. R. Muda *et al.*, “Fundamental study of reduction graphene oxide by sodium borohydride for gas sensor application,” in *AIP Conference Proceedings*, Mar. 2017, vol. 1808, no. 1, p. 020034, doi: 10.1063/1.4975267.

[109] TGSC, “Scientific Opinion on the safety evaluation of the active substances, sodium borohydride and palladium acetate for use in active food contact materials,” *EFSA J.*, vol. 10, no. 3, Mar. 2012, doi: 10.2903/j.efsa.2012.2642.

[110] NJ Health, “Hazardous substance fact sheet : Sodium Borohydride,” *New Jersey Dep. Heal. Sr. Serv.*, 2002, [Online]. Available: https://nj.gov/health/eoh/rtkweb/documents/fs/2063.pdf.

[111] J. O. Zerbino and M. G. Sustersic, “Ellipsometric and electrochemical study of dopamine adsorbed on gold electrodes,” *Langmuir*, vol. 16, no. 19, pp. 7477–7481, Sep. 2000, doi: 10.1021/la991704t.

[112] B. D. Bath, D. J. Michael, B. J. Trafton, J. D. Joseph, P. L. Runnels, and R. M. Wightman, “Subsecond adsorption and desorption of dopamine at carbon-fiber microelectrodes,” *Anal. Chem.*, vol. 72, no. 24, pp. 5994–6002, Dec. 2000, doi: 10.1021/ac000849y.

[113] M. L. A. V. Heien, P. E. M. Phillips, G. D. Stuber, A. T. Seipel, and R. M. Wightman, “Overoxidation of carbon-fiber microelectrodes enhances dopamine adsorption and increases sensitivity,” *Analyst*, vol. 128, no. 12, pp. 1413–1419, Dec. 2003, doi: 10.1039/b307024g.

[114] A. Quiroga, “Cyclic Voltammetry - Chemistry LibreTexts,” *University of California - Davis*, no. CV. pp. 2–3, 2014, Accessed: Aug. 14, 2021. [Online]. Available: https://chem.libretexts.org/Bookshelves/Analytical_Chemistry/Supplemental_Modules_(Analytical_Chemistry)/Instrumental_Analysis/Cyclic_Voltammetry.

[115] H. C. Hamaker, “Formation of a deposit by electrophoresis,” *Trans. Faraday Soc.*, vol. 35, no. 0, pp. 279–287, Jan. 1940, doi: 10.1039/tf9403500279.

[116] P. Sarkar and P. S. Nicholson, “Electrophoretic deposition (EPD): Mechanisms, kinetics, and application to ceramics,” *J. Am. Ceram. Soc.*, vol. 79, no. 8, pp. 1987–2002, 1996, doi: 10.1111/j.1151-2916.1996.tb08929.x.

[117] S. Eigler, S. Grimm, F. Hof, and A. Hirsch, “Graphene oxide: A stable carbon framework for functionalization,” *J. Mater. Chem. A*, vol. 1, no. 38, pp. 11559–11562, Oct. 2013, doi: 10.1039/c3ta12975f.

[118] S. Kim *et al.*, “Room-temperature metastability of multilayer graphene oxide films,” *Nat. Mater.*, vol. 11, no. 6, pp. 544–549, May 2012, doi: 10.1038/nmat3316.

[119] S. Kashyap, S. Mishra, and S. K. Behera, “Aqueous Colloidal Stability of Graphene Oxide and Chemically Converted Graphene,” *J. Nanoparticles*, vol. 2014, pp. 1–6, Nov. 2014, doi: 10.1155/2014/640281.

[120] N. V. Mandich, “pH, hydrogen evolution and their significance in electroplating operations,” *Plat. Surf. Finish.*, vol. 89, no. 1, pp. 54–58, 2002.

[121] C. Chen, W. Kong, H.-M. Duan, and J. Zhang, “Theoretical simulation of reduction mechanism of graphene oxide in sodium hydroxide solution,” *Phys. Chem. Chem. Phys.*, vol. 16, no. 25, p. 12858, Jul. 2014, doi: 10.1039/c4cp01031k.

[122] D. Hanaor, M. Michelazzi, C. Leonelli, and C. C. Sorrell, “The effects of carboxylic acids on the aqueous dispersion and electrophoretic deposition of ZrO2,” *J. Eur. Ceram. Soc.*, vol. 32, no. 1, pp. 235–244, Jan. 2012, doi: 10.1016/j.jeurceramsoc.2011.08.015.

[123] T. Kuila, P. Khanra, N. H. Kim, J. K. Lim, and J. H. Lee, “Effects of sodium hydroxide on the yield and electrochemical performance of sulfonated poly(ether-ether-ketone) functionalized graphene,” *J. Mater. Chem. A*, vol. 1, no. 32, pp. 9294–9302, Aug. 2013, doi: 10.1039/c3ta11014a.

[124] V. T. Huong, T. Shimanouchi, D. P. Quan, H. Umakoshi, P. H. Viet, and R. Kuboi, “Polymethylthiophene/Nafion-modified glassy carbon electrode for selective detection of dopamine in the presence of ascorbic acid,” *J. Appl. Electrochem.*, vol. 39, no. 10, pp. 2035–2042, Oct. 2009, doi: 10.1007/s10800-009-9860-z.

[125] S. F. Rahman, K. Min, S. H. Park, J. H. Park, J. C. Yoo, and D. H. Park, “Selective determination of dopamine with an amperometric biosensor using electrochemically pretreated and activated carbon/tyrosinase/Nafion®-modified glassy carbon electrode,” *Biotechnol. Bioprocess Eng.*, vol. 21, no. 5, pp. 627–633, Nov. 2016, doi: 10.1007/s12257-016-0382-3.

[126] P. Xing, G. P. Robertson, M. D. Guiver, S. D. Mikhailenko, K. Wang, and S. Kaliaguine, “Synthesis and characterization of sulfonated poly(ether ether ketone) for proton exchange membranes,” *J. Memb. Sci.*, vol. 229, no. 1–2, pp. 95–106, Feb. 2004, doi: 10.1016/j.memsci.2003.09.019.

[127] R. Yee, K. Zhang, and B. Ladewig, “The Effects of Sulfonated Poly(ether ether ketone) Ion Exchange Preparation Conditions on Membrane Properties,” *Membranes (Basel).*, vol. 3, no. 3, pp. 182–195, Aug. 2013, doi: 10.3390/membranes3030182.

[128] M. R. Abidian, D. H. Kim, and D. C. Martin, “Conducting-polymer nanotubes for controlled drug release,” *Advanced Materials*, vol. 18, no. 4. John Wiley & Sons, Ltd, pp. 405–409, Feb. 17, 2006, doi: 10.1002/adma.200501726.

[129] M. R. Abidian and D. C. Martin, “Experimental and theoretical characterization of implantable neural microelectrodes modified with conducting polymer nanotubes,” *Biomaterials*, vol. 29, no. 9, pp. 1273–1283, Mar. 2008, doi: 10.1016/j.biomaterials.2007.11.022.

[130] D. D. Ateh, A. Waterworth, D. Walker, B. H. Brown, H. Navsaria, and P. Vadgama, “Impedimetric sensing of cells on polypyrrole-based conducting polymers,” *J. Biomed. Mater. Res. - Part A*, vol. 83, no. 2, pp. 391–400, Nov. 2007, doi: 10.1002/jbm.a.31308.

[131] D. H. Kim, S. M. Richardson-Burns, J. L. Hendricks, C. Sequera, and D. C. Martin, “Effect of immobilized nerve growth factor on conductive polymers: Electrical properties and cellular response,” *Adv. Funct. Mater.*, vol. 17, no. 1, pp. 79–86, Jan. 2007, doi: 10.1002/adfm.200500594.

[132] J. M. Fonner *et al.*, “Biocompatibility implications of polypyrrole synthesis techniques,” *Biomed. Mater.*, vol. 3, no. 3, Sep. 2008, doi: 10.1088/1748-6041/3/3/034124.

[133] N. Su, “Improving electrical conductivity, thermal stability, and solubility of polyaniline-polypyrrole nanocomposite by doping with anionic spherical polyelectrolyte brushes,” *Nanoscale Res. Lett.*, vol. 10, no. 1, pp. 1–9, Dec. 2015, doi: 10.1186/s11671-015-0997-x.

[134] J. Stejskal *et al.*, “Polypyrrole salts and bases: Superior conductivity of nanotubes and their stability towards the loss of conductivity by deprotonation,” *RSC Adv.*, vol. 6, no. 91, pp. 88382–88391, Sep. 2016, doi: 10.1039/c6ra19461c.

APPENDIX A

The results from the FSCV system were collect as .csv files and plotted using MATLAB. There are 3 types of data from the system:

a) Raw data – Contains the baseline from saline and the DA signal.
b) Subtracted data – Contains the unfiltered data of the DA signal.
c) DA signal's filtered data.

FSCV analysis shown above focuses on the data type (c) where filtration was done by using a moving average 2D filter. Below are the two codes used for plotting (1) MATLAB code to check stability (2) MATLAB filtered DA signal from the raw data.

(1)

```
clear all
close all

no_dopa = csvread ('Bashir electrode #Au no dopamine.csv'); %data 1
dopa = csvread ('Bashir electrode #Au with dopamine.csv'); %data 2

num_of_sample_per_scan = 3600;
sampling_rate = 200000;
feedback_resistor = 1.0*10^6;

no_dopa = reshape(no_dopa,[num_of_sample_per_scan %saline baseline
1length(no_dopa)/num_of_sample_per_scan]);
dopa = reshape(dopa,[num_of_sample_per_scan %after injecting dopamine
1length(dopa)/num_of_sample_per_scan]);
no_dopa = no_dopa(:,50:100);
dopa = dopa(:,50:100);

average_no_dopa = mean (no_dopa,2);
average_dopa = mean (dopa,2);
subtracted_raw = dopa - average_no_dopa;
subtracted_filtered = m2_filter(subtracted_raw, 0, 30);

average_subtracted_raw = average_dopa - average_no_dopa;
average_subtracted_filtered = m2_filter(average_subtracted_raw, 0, 30);
```

```
t=0:1/sampling_rate: (num_of_sample_per_scan-1)/sampling_rate;
t=t';
scan_num_to_plot = 40;

figure,
set(gcf, 'Position', [100, 100, 1600, 900])
plot (t, subtracted_raw(:,scan_num_to_plot), 'g');
hold on
plot (t, subtracted_filtered(:,scan_num_to_plot), 'k');

applied_volt_max = 0.6;
applied_volt_min = -0.2;
applied_voltage_rising = applied_volt_min:(applied_volt_max-
applied_volt_min)/1600:applied_volt_max-(applied_volt_max-applied_volt_min)/1600;
applied_voltage_falling = applied_volt_max:-(applied_volt_max-
applied_volt_min)/1600:applied_volt_min+(applied_volt_max-applied_volt_min)/1600;
applied_voltage = [applied_voltage_rising applied_voltage_falling]';

figure,
plot (applied_voltage,
(subtracted_filtered(1:3200,scan_num_to_plot)/(2.567*feedback_resistor))*10^9, 'k');
xlim([applied_volt_min applied_volt_max]);
ylabel ('Current (nA)');
xlabel ('Applied Voltage (V)');

figure,
set(gcf, 'Position', [100, 100, 1600, 900])
plot (t, average_subtracted_raw, 'g');
hold on
plot (t, average_subtracted_filtered, 'k');

figure,
plot (applied_voltage,
(average_subtracted_raw(1:3200)/(2.567*feedback_resistor))*10^9, 'g');
hold on
plot (applied_voltage,
(average_subtracted_filtered(1:3200)/(2.567*feedback_resistor))*10^9, 'k');
```

```
xlim([applied_volt_min applied_volt_max]);
ylabel ('Current (nA)');
xlabel ('Applied Voltage (V)');

%
>>>>>>>>>>>>>>>>>>>>>>>>>>>>>>>>>>>>>>>>>>>>>>>>>>>>>>>>>>>>>>>>>>>>>>>>>>>>>>>>
```

(2) To plot the DA signal from the raw data directly on MATLAB, a filter was first developed and included in the same folder. That works concurrently when running the main source code.

```
clear all
close all

no_dopa = csvread ('Bashir electrode #Au no dopamine.csv'); %Saline baseline
dopa = csvread ('Bashir electrode #Au with dopamine.csv'); %After adding dopamine

num_of_sample_per_scan = 3600;
sampling_rate = 200000;
feedback_resistor = 1.0*10^6;

no_dopa = reshape(no_dopa,[num_of_sample_per_scan
length(no_dopa)/num_of_sample_per_scan]);
dopa = reshape(dopa,[num_of_sample_per_scan
length(dopa)/num_of_sample_per_scan]);

average_no_dopa = mean (no_dopa,5); %Use 5th scan
subtracted_raw = dopa - average_no_dopa;
subtracted_filtered = m2_filter(subtracted_raw, 0, 300);

t=0:1/sampling_rate: (num_of_sample_per_scan-1)/sampling_rate;
t=t';
scan_num_to_plot = 10;
figure,
set(gcf, 'Position', [100, 100, 1600, 900])
plot (t, subtracted_raw(:,scan_num_to_plot), 'g');
hold on
```

```
plot (t, subtracted_filtered(:,scan_num_to_plot), 'k');


 applied_volt_max = 0.6;
applied_volt_min = -0.2;
applied_voltage_rising = applied_volt_min:(applied_volt_max-
applied_volt_min)/1600:applied_volt_max-(applied_volt_max-applied_volt_min)/1600;
applied_voltage_falling = applied_volt_max:-(applied_volt_max-
applied_volt_min)/1600:applied_volt_min+(applied_volt_max-applied_volt_min)/1600;


applied_voltage = [applied_voltage_rising applied_voltage_falling]';
filtered_subtracted_current =
(subtracted_filtered(1:3200,scan_num_to_plot)/(2.567*feedback_resistor))*10^9;
figure,
plot (applied_voltage, filtered_subtracted_current , 'black','LineWidth',1.9,
'DisplayName', 'Au-ppy');
xlim([applied_volt_min applied_volt_max]);


xlabel('Applied Voltage (V)', 'FontSize', 16, 'FontWeight', 'bold');
ax.XAxis.LineWidth = 5;
ylabel('Current (nA)', 'FontSize', 16, 'FontWeight', 'bold');
ax.YAxis.LineWidth = 5;
legend


%Moving Average 2-D filter
%X contains values to be filtered, HL is horizontal while VL is vertical limit.
%HL adds columns and VL adds rows to padded matrix
function [y]=m2_filter(x,hl,vl)
if nargin<2
   hl=1;
   vl=1;
end
if (vl<0)||(hl<0)
   error('limits must be positive')
end
x=im2double(x);
[row, col, space]=size(x);    %Checking size of input
```

```
y=0*x;     %Output of same size and type as input

for s=1:space   %For computation across all layers
   x_pad=zeros(row+2*vl,col+2*hl); %Padded Matrix (hl increase col)
   x_pad(1+vl:row+vl,1+hl:col+hl)=x(:,:,s);
   for i=1+vl:row+vl     %Going through rows
      for j=1+hl:col+hl     %Going through values one by one
         y(i-vl,j-hl,s)=sum(x_pad(i,j-hl:j+hl))+sum(x_pad(i-vl:i+vl,j));
         %Summing Values around current entry according 2 vl and hl
         y(i-vl,j-hl,s)=y(i-vl,j-hl,s)-x_pad(i,j);%Current Values gets added
         %twice. Once in row and once in Col


      end
   end

end
y=y/(2*hl+2*vl+1);
end
```

APPENDIX B

Table B.1: Feedback resistor values used during FSCV analysis

Electrode	**R_feedback Value**
Bare Au	1 MΩ
Au-GO (DI pH 3.90)	330 kΩ
Au-GO (NaCl pH 7.08)	330 kΩ
Au-GO (PBS pH 9.68)	330 kΩ
Au-GO (0.02 mg/mL)	330 kΩ
Au-GO (0.1 mg/mL)	330 kΩ
Au-GO (0.3 mg/mL)	330 kΩ
Au-GO (7 min)	330 kΩ
Au-GO (15 min)	330 kΩ
Au-GO (30 min)	330 kΩ
Au-GO (60 min)	330 kΩ
Au-GO-SPEEK (10 kDa consecutive)	330 kΩ
Au-GO-SPEEK (100 kDa consecutive)	330 kΩ
Au-GO-SPEEK (10 kDa simultaneous)	330 kΩ
Au-GO-SPEEK (100 kDa consecutive)	330 kΩ
Au-GO-SPEEK (10 kDa 15 min dipcoating)	200 kΩ
Au-GO-SPEEK (100 kDa 15 min dipcoating)	200 kΩ
Au-GO-SPEEK (10 kDa 130 min dipcoating)	200 kΩ
Au-GO-SPEEK (100 kDa 130 min dipcoating)	200 kΩ
Au-GO-SPEEK-ppy	150 kΩ
Au-ppy	150 kΩ
Au-GO-ppy	150 kΩ
Au/GO/SPEEK/ppy	150 kΩ

CURRICULUM VITAE

Name Surname : Bashir Bwogi

EDUCATION:

B.Sc. : 2019, Erciyes University, Engineering, Biomedical Engineering (Cum Laude)

PROFESSIONAL EXPERIENCE AND REWARDS:

- 2019-2021, Research Assistant, Istanbul Medipol University, Turkey
- Spring semester 2021, Teaching Assistant, Istanbul Medipol University, Turkey
- 2019-2021, Research scholarship, Turkish Institute of Science and Technology
- Spring semester 2018, Peer Tutor, Hankuk University of Foreign Studies, South Korea
- Spring semester 2018, Innovative Project of the year, Hankuk University of Foreign Studies, South Korea
- 2017-2018, Finance Minister, Erciyes University African Students' Association, Turkey
- 2016-2018, Humanitarian Official, SENA Turkish Foundation, Uganda
- 2014-2019, Excellence scholarship for Bachelor's, Turkish Government

DESIGN AND OPTIMIZATION OF A DURABLE GOLD-BASED MICROELECTRODE FOR DOPAMINE DETECTION

ORIGINALITY REPORT

9%	6%	6%	2%
SIMILARITY INDEX	INTERNET SOURCES	PUBLICATIONS	STUDENT PAPERS

PRIMARY SOURCES

1	Muhammad Sajid, Nadeem Baig, Khalid Alhooshani. "Chemically modified electrodes for electrochemical detection of dopamine: Challenges and opportunities", TrAC Trends in Analytical Chemistry, 2019 Publication	1%
2	Submitted to RMIT University Student Paper	1%
3	Submitted to Nashville State Community College Student Paper	<1%
4	link.springer.com Internet Source	<1%
5	Submitted to Eastern Mediterranean University Student Paper	<1%
6	acikerisim.tedu.edu.tr Internet Source	<1%
7	www.hindawi.com Internet Source	